1964

Structures and transformation kinetics of phases in the uranium-rhenium alloy system

Ross Jones Jackson
Iowa State University

STRUCTURES AND TRANSFORMATION KINETICS OF PHASES IN THE URANIUM-RHENIUM ALLOY SYSTEM

by

Ross Jones Jackson

A Dissertation Submitted to the
Graduate Faculty in Partial Fulfillment of
The Requirements for the Degree of
DOCTOR OF PHILOSOPHY

Major Subject: Metallurgy

Approved:

Signature was redacted for privacy.

In Charge of Major Work

Signature was redacted for privacy.

Head of Major Department

Signature was redacted for privacy.

Dean of Graduate College

Iowa State University
Of Science and Technology
Ames, Iowa

1964

TABLE OF CONTENTS

INTRODUCTION

General Considerations

The investigation of the structures and transformation kinetics of uranium-rich phases in the uranium-rhenium system was undertaken as part of a general program to increase the knowledge concerning the alloying behavior of uranium.

Constituent Metals

Historical

In 1779, element 92 was discovered by the German chemist, Martin Klaproth, who gave it the name uranium[1] to commemorate the planet Uranus which had been discovered some eight years earlier. In 1841, a French chemist, Eugene Peligot, showed Klaproth's material to be UO_2 and later succeeded in producing elemental uranium. Over a century after Klaproth's discovery, in 1896, Antoine Becqueral discovered that radiation emanating from uranium salts would darken photographic film. This discovery opened the door to radioactive studies, and eventually, to the advent of atomic energy.

During the long period from the discovery of uranium up through the first third of the present century, uranium was of minor commercial importance. With the discovery in 1939

---

[1]The material on which this historical outline of uranium is based is taken from Holden (1).

of the fission of the uranium isotope U-235 and the eventual development in December 1942 of a successful, controlled, chain-reacting pile for uranium fission, the atomic age was born. The military importance of uranium for weapons production and the use of uranium fuel in nuclear power reactors have given considerable impetus to the production and technology of this element.

In the year 1869, the Russian chemist, Dimitri Mendeleef, published his now famous periodic table.[1] Numerous blanks appeared in the original chart, and Mendeleef predicted that these blanks would be filled with then unknown elements; he also predicted the properties these elements would have, and assigned atomic numbers and provisional names. In group VII-b, headed by manganese, there were two unfilled spaces belonging to elements 43 and 75. To these, he assigned the provisional names of eka-manganese and dvi-manganese, respectively.

Despite near completion of the table by the 1920's these two elements were still undiscovered. In 1925, the situation changed markedly, with almost simultaneous claims of discovery of element 75 by three separate groups of workers. Credit for the actual discovery is now generally attributed to Walter Noddack and Ida Tacke, who in 1925 announced they

---

[1]The material on which this historical outline of rhenium is based is taken from Sims *et al.* (2).

had detected the presence of the element in platinum ores and columbite. Although their claim did not go unchallenged, their suggested name of rhenium, after the German province of Rhineland, is still retained.

The high temperatures encountered in certain areas of modern technology has led in recent years to a comprehensive evaluation of the physical and mechanical properties of the refractory metals and their alloys. In this connection, rhenium, because of several unique properties, has received increasing attention.

Atomic and physical properties

Table 1 compares atomic and physical properties of uranium and rhenium that are of interest in this investigation. The values listed are based on the critical evaluations of Klein (3), Laves (4) and Melaven (5) as noted in the table. References to the original work may be found in these compilations. Table 2 lists the structural features of the constituent metals. The uranium structural values are those of Klepfer and Chiotti (6) while those for rhenium are due to Sims *et al.* (7). Table 3 lists features of the phase transformations in uranium. The solid state dimensional changes listed are reported by Klepfer and Chiotti (6) while the remaining data are taken from the critical evaluation of Klein (3).

Table 1. Some properties of the constituent metals[a]

Property	Uranium	Rhenium
Atomic number	92	75
Atomic weight	238.07	186.31
Melting point	1132°C	3180°C
Boiling point	~3800°C	~5600°C
Heat of fusion	4.7 kcal/mole	7.9 kcal/mole
Heat of vaporization	~100 kcal/mole	~152 kcal/mole
Thermal conductivity	0.0645 cal/cm/°C/sec at 25°C	0.17 cal/cm/°C/sec at 20°C
Electrical resistivity	30×10^{-6} ohm-cm at 25°C	19.14×10^{-6} ohm-cm at 20°C
Gaseous electronic configurations	$5f^3 6d 7s^2$	$5d^5 6s^2$
Chemical valence	3,4,5,6	-1,+4,+7
Goldschmidt radii (CN = 12)	1.54 Å	1.37 Å
Goldschmidt radii (CN = 8)	1.51 Å	1.34 Å
Pauling radii (CN = 12)	1.516 Å	1.373 Å
Pauling valence	5.78	5.78

[a]The values listed for uranium are from the critical evaluation of Klein (3); those listed for rhenium are from the critical evaluation of Melaven (4); except for both metals the valence and radius values are taken from Laves (5). References to the original work may be found in these compilations.

Table 2. Structural features of the constituent metals[a]

Structure and phase	Cell dimensions (Å)	Atoms per cell	Space group	X-ray density (g/cm^3)
Orthorhombic α uranium	a = 2.853 b = 5.865 c = 4.954	4	Cmcm	19.07
Tetragonal β uranium at 700°C	a = 10.75 b = 5.65	30	P4/mnm	18.14
BCC γ uranium at 800°C	a = 3.534	2	Im3m	17.91
Hexagonal rhenium	a = 2.760 b = 4.458	2	C6/mmc	21.04

[a]The uranium data are those of Klepfer and Chiotti (6) while those for rhenium are due to Sims et al. (7).

Table 3. Phase transformations in uranium[a]

Transformation	Temperature	$\frac{\Delta V}{V}$	$\frac{\Delta L}{L}$	$\Delta H \left(\frac{kcal}{mole}\right)$
alpha → beta	667°C	+1.06	+0.35	0.7
beta → gamma	775°C	+0.736	+0.245	1.15
gamma → liquid	1132°C	~5		~4.7

[a]The solid state dimensional changes are reported by Klepfer and Chiotti (6) while the remaining data are taken from the critical evaluation of Klein (3).

Uranium-Rhenium Alloys

Technology

Uranium is alloyed to enhance desired properties or to investigate compositions that are interesting from a fundamental or practical viewpoint. The reasons most commonly cited for alloying to enhance desired properties are to confer thermal or irradiation stability and to obtain corrosion resistance. Chiswik (8) points out that the approach in the use of alloying to improve dimensional stability and corrosion resistance has been in two directions: (a) alloy additions in relatively low concentrations designed to modify the kinetics of the β or γ phase decomposition so as to yield a structure combining random orientation and small grain size; and (b) alloy additions in sufficient concentrations to stabilize partially or completely the cubic γ phase, thereby circumventing the intrinsic instability of the orthorhombic α structure. The first group may be referred to as "α-phase" alloys, the second group as "γ-phase" alloys. By restricting the alloy additions to low concentrations and to elements of favorable nuclear properties, the "α-phase" alloys are best suited for the utilization of natural or slightly enriched uranium in thermal reactors. The "γ-phase" alloys are more suitable for fast reactors, since they require higher contents of alloying additions. The "γ-phase" alloys are of considerable

interest in reactor fuel element technology because, as Wilkinson (9, p. 1128) points out, they exhibit, as a class, increased high temperature strength; good resistance to dimensional changes on thermal cycling and, generally, on irradiation; and improved resistance to aqueous corrosion.

Rhenium's relatively high cross section for thermal neutrons (84 barns) as well as price and scarcity dictate that if used as an alloying element, it would have to be used sparingly. However, one should not definitely rule out its use as an "α-phase" or "γ-phase" alloy since improvements in fuel properties could possibly make it economically feasible.

Another aspect of uranium alloys to consider is the compositions that develop in irradiated reactor fuels and the subsequent pyrometallurgical processing of such fuels (10). Attempts often are made to simulate these compositions for convenience in metallurgical investigations by alloying appropriate amounts of the major constituent elements in nonradioactive form, with uranium. Presently in laboratory studies of such alloys, equi-atomic mixtures of stable molybdenum and ruthenium isotopes are being substituted for radioactive technetium (11). Perhaps a better substitute would be rhenium, since similarities of elements in a given group are usually pronounced in the fifth and sixth periods due to the lanthanide contraction and the resulting similar-

ities in radii (4; 12, p. 500 and 533).

Theoretical considerations and predictions

Uranium alloy systems have been classified into three types.[1] One type is the compound-free systems of very low miscibility. This includes the alloys of Ag, Ca, Ce, La, Li, Mg, Na, Nd, Pr, Ta, Th and W. The second type is the low-miscibility systems containing intermetallic compounds and includes the elements Al, Be, Bi, Co, Cu, Fe, Ga, Hg, Mn, Ni, Pb, Si, Sn and Zn. The third classification includes the γ-miscible systems which may or may not form intermediate phases. The group includes elements which are soluble in γ uranium to an extent of greater than 4 a/o and includes the alloys or uranium with Au, Cr, Hf, Mo, Nb, Pd, Pt, Pu, Rh, Ru, Ti, V and Zr.

If the above classification is considered with respect to the periodic table it becomes apparent that all transition elements listed above except Mn, Fe, Co, Ni, Ta and W fall into the γ-miscible classification. In these six exceptions the maximum solubility in γ is about 2-3 a/o. According to Buzzard (13) all the elements from group IV-b of the periodic table through group VIII-b of periods 4, 5 and 6 ionize to

---

[1]This classification is similar to one advanced by Wilkinson (9, p. 858) except the dividing line for γ-miscible systems is 4 a/o rather than 8 a/o. This new lower limit allows a classification that is interpretable in light of the periodic table.

leave vacancies in the outer s-band, except Ta and W, which lose the d-bands; hence their outer bands are the s-bands, which are not favorable to solubility and explains the anomalous behavior of these two elements. In the case of Mn, Fe, Co and Ni the lower solubility can be attributed to their small size and the resulting unfavorable size factor with uranium. Since rhenium is a normal transition element it seems reasonable to expect it to be a γ-miscible alloy and to expect a γ solubility of greater than 4 a/o.

Since the crystal structures of uranium and rhenium are not similar, it is imperative that an intermediate phase or region of immiscibility separate the terminal solid solutions.

Further predictions concerning the phase relationships in the uranium-rhenium system are possible if one considers the Hume-Rothery rules (14, p. 102) and their limitations evidenced by applications to known uranium alloy systems. The limitations undoubtedly arise from the uncertainties in atomic size, valence and bonding types in uranium, especially in the α and β forms, which make it difficult to predict alloying behavior according to the Hume-Rothery rules alone.

The relative valency rule indicates that a disparity in valence is conducive to lower solubility and that this disparity has an especially pronounced effect when the valence of the solute is less than that of the solvent. Valencies of 4, 5 and 6 are generally assigned to uranium in the α,

β and γ forms, respectively (9, p. 878). On this basis, all other things being equal, rhenium with a valence of seven (5, p. 429) would be more soluble in uranium than uranium in rhenium. Also, rhenium would be most soluble in γ uranium and least so in the α form. The latter statement is equivalent to saying that the γ-β and β-α transformation temperatures will both be lowered by the addition of rhenium.

By an examination of the existing phase diagrams of uranium[1] with elements of groups IV-b and V-b, it is found that tetravalent solute elements tend to stabilize tetravalent α uranium relative to pentavalent β, and, conversely, pentavalent solutes tend to stabilize β with respect to α uranium as predicted above. However, a more complete examination[2] reveals that nearly all metals, regardless of valence, tend to stabilize γ relative to β. This is not too surprising, since of the three uranium modifications, γ is the most metallic, and, hence, should be the most compatible with a metallic solute element.

The greater the difference between electronegativities of two metals the greater is the tendency to form compounds

---

[1]See Rough and Bauer's (15) compilation of uranium and thorium phase diagrams.

[2]The only known exception is silicon.

rather than extensive solid solutions. Electronegativity values calculated from Gordy's expression (16, p. 80), assuming a valence of five for uranium, were 1.5 for uranium and 2.3 for rhenium. Pauling's values based on heats of formations and bond strengths agreed very well and were 1.6 and 2.3. Hence, the electronegativity difference is about 0.7 units. One would expect, therefore, a tendency towards compound formation in the uranium-rhenium system since a difference of one-half unit on the electronegativity scale is usually sufficient to hinder extensive primary solid solutions by the tendency towards compound formation even though both the solid solutions and the compound are stabilized by the large difference (16, p. 84).

Alpha uranium has twelve near neighbors, two at 2.762 Å, two at 2.852 Å, four at 3.261 Å and four yet farther at 3.322 Å; hence, a coordination of twelve is assumed (17). The distance of closest approach in the β uranium structure is 2.59 Å and the atoms have either 12, 14 or 15 nearest neighbors (18). For γ uranium, the distance of closest approach is 3.01 Å and there are eight nearest neighbors. Using a coordination number of twelve for the α and β forms and a coordination number of eight for γ, the atomic radius disparity compared to rhenium is -1, +5 and -11% for the α, β and γ forms, respectively. Thus, the size factor appears favorable for solubility in each case. However,

since the size of a metal atom depends on the extent to which it has given up electrons or changed their energy levels, it is obvious that these figures can only serve as a rough guide for predicting solubility of rhenium in uranium. Also, covalent bonding (19, p. 413), which distinguishes α uranium from most other metals, would be expected to restrict the formation of solid solutions in the α form, even when atomic size, valence and structure of the solute elements are favorable.

There are twenty-seven metallic binary uranium phase diagrams listed in Rough and Bauer's compilation (15) that do not show a complete series of solid solutions. Twenty-four of these exhibit eutectic formation of the γ phase and only three a peritectic formation. The three solutes causing peritectic formation of γ are BCC in structure, and, hence compatible with the γ structure, thus, stabilizing it with respect to the liquid. All the known hexagonal solute elements give rise to eutectic formation of γ. Hexagonal rhenium would therefore be expected to stabilize the liquid with respect to γ and to most likely result in the eutectic formation of γ.

On the basis of this simplified semi-theoretical treatment and considering the shape of other binary uranium phase diagrams, one can predict the uranium-rhenium system to contain one or more intermetallic phases and limited terminal solid solutions. The solubility of rhenium in the γ region

should exceed 4 a/o and should be greater than the solubility of uranium in rhenium. In addition, a lowering of the γ-liquid, β-γ, and α-β transformations should occur giving rise to greatest solid solubility in the γ form and least in the α and most likely to a eutectic formation of γ and eutectoid formation of both the α and β forms.

Literature survey

A search of the literature revealed only six research studies dealing with uranium-rhenium alloys. Of the six studies, only three appeared to be of a significant nature. Seybolt (20, 21) determined the hardness and examined the microstructure of a single uranium-rich alloy. Kulin et al. (22) determined the hardness and specific gravity of a few uranium-rich alloys.

The first significant study was that of Hatt (23), who, during a survey of UX_2 compounds, located the URe_2 compound and determined its structure. On the basis of x-ray diffraction studies he reported that above 180°C, URe_2 has a C14 Laves structure whereas below this temperature a lower symmetry orthorhombic structure is observed. Some of Hatt's findings are summarized in Table 4.

The next significant study is that of phase relationship studies conducted at Fulmer Research Institute in England and reported by Rough and Bauer (15) in their compilation of uranium and thorium phase studies. In addition to the URe_2

Table 4. Structural features of the URe_2 compound

Structure	Cell dimensions (Å)	Atoms per cell	Space group	Remarks
Orthorhombic	a = 5.600 b = 9.178 c = 8.463	8	Cmcm	dimensions at 20°C
Hexagonal	a = 5.433 c = 8.561	4	$P6_3/mmc$	C14-type; dimensions at 213°C

compound they reported an ordered structure containing 8 to 10 a/o Re which formed at about 800°C on cooling. This phase was tentatively assigned a tetragonal structure with c/a = 0.98 and was believed to be similar to U_2Mo. They proposed that the γ phase was formed by a peritectic reaction at a temperature of 1150 to 1200°C in the neighborhood of 16 a/o Re. Below the peritectoid horizontal the solubility was reported to decrease to about 6 a/o Re at 1000°C with little variation in solubility between 1000 and 800°C. The solubility of rhenium in α uranium was listed as about 1 a/o at 650°C and less than 0.5 a/o at 600°C. From this information, Wilkinson (9, p. 1367) has constructed a tentative phase diagram which is reproduced in Figure 1. They also report that the γ phase can be retained in alloys containing 5 a/o Re but that decomposition to a distorted α structure proceeds at room temperature and that a distorted α structure is developed on quenching alloys containing

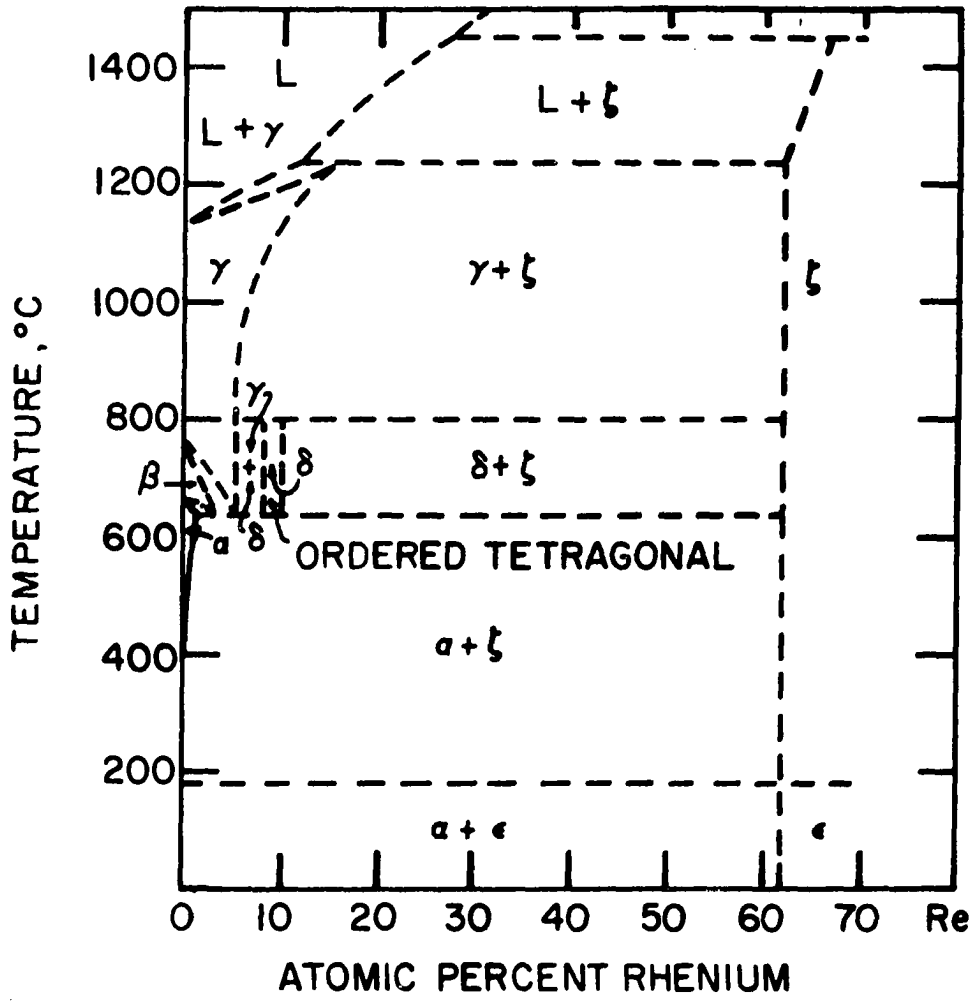

Figure 1. The uranium-rhenium phase diagram as taken from Wilkinson (9, p. 1367)

4 a/o Re.

In work which preceded and laid the groundwork for the present investigation (24), the phase diagram of the uranium-rhenium system and the kinetics of transformation of some uranium solid solutions were studied. The phase diagram is presented in Figure 2 and an enlarged portion of particular interest in the present investigation is shown in Figure 3. This diagram differs from its English counterpart; however, the latter is based on a limited number of observations of a tentative nature, and undoubtedly were not meant to be construed as sufficient evidence to construct a total or partial phase diagram. Also, the diagram presented in Figure 2 is in slightly better agreement with the semi-theoretical predictions outlined earlier, the major difference being in the manner of formation of the γ phase from the liquid.

Nonequilibrium alloys

During the course of the phase diagram studies, nonequilibrium alloys were often observed on the uranium side of the URe_2 phase. This phenomenon led to the present investigation of the reaction kinetics of these alloys.

The appearance of nonequilibrium alloys in the uranium-rhenium system is not too surprising, since highly γ-miscible alloy systems, as a class, are characterized by sluggish transformations and stable or metastable γ or α structures in the relatively highly alloyed compositions.

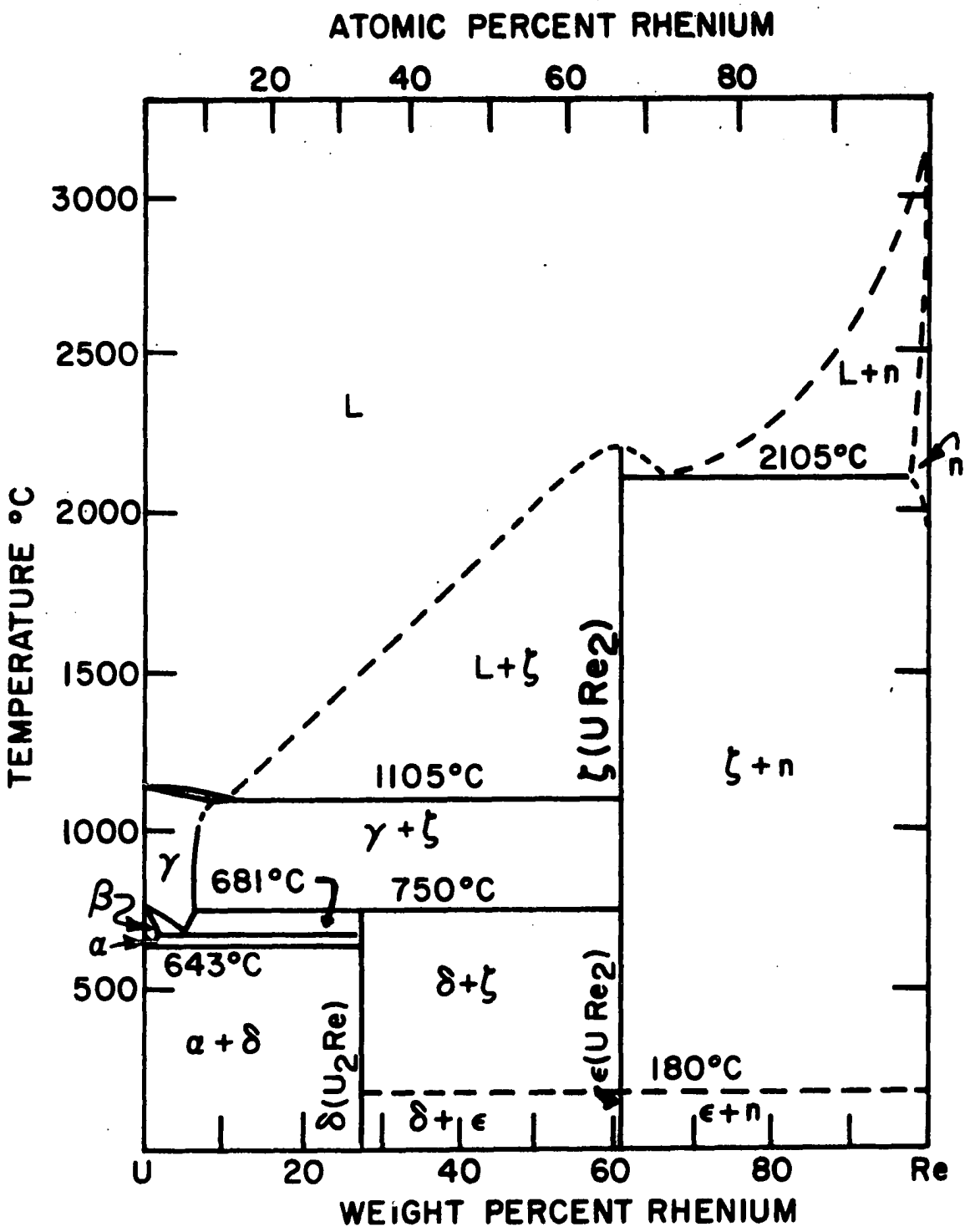

Figure 2. The uranium-rhenium phase diagram according to Jackson et al. (24)

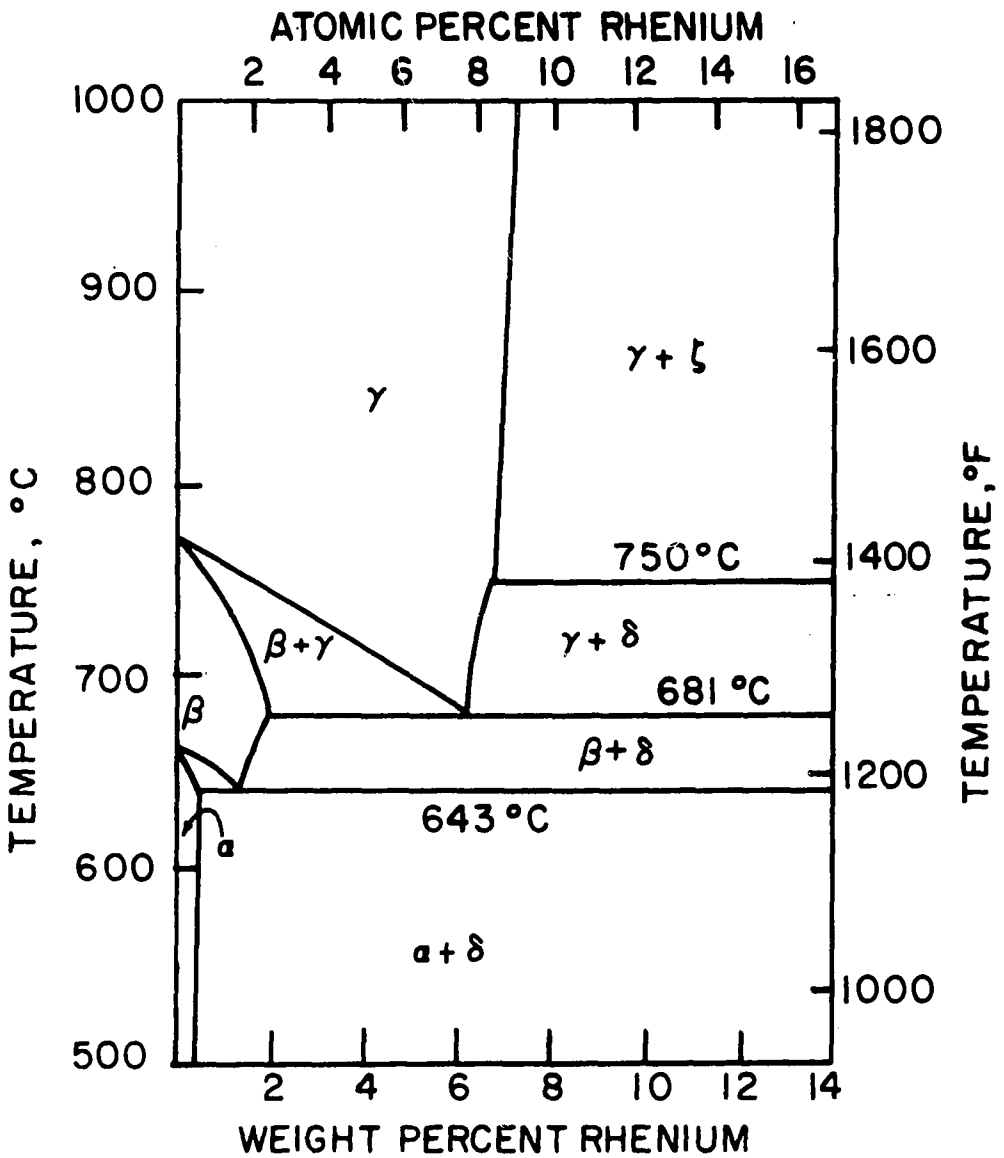

Figure 3. The eutectoid regions according to Jackson et al. (24)

Metastable phases of the martensitic α type have been reported in the uranium-molybdenum (25, 26), uranium-niobium (27, 28), uranium-titanium (29), uranium-vanadium (28), and uranium-zirconium (30) systems. In addition to the variations of the α-uranium phase, a metastable phase based on the cubic γ structure has been reported in the uranium-molybdenum (31), uranium-niobium (32), and uranium-titanium (33) systems.

In evaluating the properties of highly γ-miscible systems, the nature of these metastable states must be considered. The changes in properties brought about by alloying and subsequent thermal treatments are the results of changes in crystal structure or microstructure. Often the wanted crystal structure and microstructure is brought about through a nonequilibrium solid-state transformation as witnessed by the formation of the tempered martensite microstructure in steels. Thus, if uranium alloys are to be used to their full potential a knowledge of their nonequilibrium transformations will be necessary. It is towards an understanding of these nonequilibrium transformations, metastable states, and resulting microstructures that this research is directed.

Research Objectives

The work reported herewith had the following objectives:

1. Determination of the compositional limits within which the stable and metastable phases are produced, the

cooling rate being constant.

2. Investigation of the effect of different cooling rates in producing alternative structures.
3. Investigation of any relationships existing between the observed phases and determination of the sequence of phase changes.
4. Development of a crystallographic and microstructural model to explain the observed behavior.
5. Determination of any relationship existing between metastability in uranium-rhenium alloys and other systems in which metastable states are observed.

To achieve these objectives, a study was made of the time-temperature-composition dependency of crystal structure and microstructure under nonequilibrium cooling conditions.

EXPERIMENTAL PROCEDURE

Alloy Preparation

The uranium used in this investigation was from a direct cast ingot produced at the Hanford Works of the General Electric Company. The supplier's chemical analysis of this material is shown in Table 5. The rhenium was first grade metal purchased from the Chase Brass and Copper Company in the form of 0.040 in. rhenium strip. The major impurities present in this metal as determined by the analytical groups at this laboratory are given in Table 5.

All the alloys were prepared by melting under a helium atmosphere in a nonconsumable tungsten electrode arc furnace similar to that of Geach and Summers-Smith (34). The melting procedure has been discussed by Williams (35).

Two different sets of alloys were used during the course of the investigation. The early kinetic studies used alloys which were initially prepared for the phase diagram studies. These alloys were made by melting small rhenium chunks with massive uranium metal. Difficulty in making alloys was anticipated because the melting point of rhenium exceeds that of uranium by 2050°C. However, since uranium has a high boiling point and consequently a low vapor pressure, loss of uranium by vaporization did not occur. Difficulty did arise in dissolving the rhenium particles in uranium-rich liquid during melting. Reasonable homogeneity was achieved by

Table 5. Chemical analysis of the constituent metals

Impurity atom	Amount present[a] Uranium	Rhenium
Al	20 ppm	not detected
C	36 ppm[b]	150 ppm[b]
Ca		trace
Cr	2 ppm[b]	trace
Cu		trace
Fe	18 ppm	not detected
H	4 ppm	not determined
Mg	3 ppm	trace
Mn	5 ppm	not detected
Ni	10 ppm	not detected
Pb	5 ppm	not detected
Si	22 ppm	not detected

[a]Spectrographic analysis unless indicated otherwise.

[b]Gravimetric analysis.

reducing the size of the rhenium particles and by keeping uranium-rich alloys molten for approximately one hour. These alloys were then homogenized under vacuum at 925°C for one week in a tantalum container.

The kinetic studies, for the most part, utilized a series of alloys that were prepared in a somewhat different manner. Initially, a master alloy of composition URe_2 was prepared. This alloy was then crushed and chunks approximately 1-2 mm in diameter were used as the source of rhenium in preparing the uranium-rich alloys. The use of a lower melting rhenium source (the melting point of URe_2 is 2200°C while that of rhenium is 3180°C), in addition to the small particle size, reduced the probability of occurrence of

residual unreacted rhenium and shortened the required melting time.

The constituents were weighed to ± 0.0005 g on an analytical balance. Prior to weighing, the massive uranium was cleaned electrolytically in a chromic-acetic acid bath and except for the weighing operation was thereafter kept under vacuum. The expression derived to determine the weight of URe_2 required was

$$\text{Weight of } URe_2 = \frac{(\text{w/o Re})\ (\text{weight of massive U})}{(61.02 - \text{w/o Re})}.$$

The melting procedure consisted of first purifying the helium by melting a getter of crystal bar zirconium whose hardness was approximately R_A30. Two alloy charges were then melted at a current of 280 amperes for two minutes each, then inverted and again melted for two minutes. This sequence was subsequently repeated at currents of 320, 360 and 400 amperes. Between melting sequences the button was cut in two and recombined in an effort to obtain a more homogeneous alloy. Also, between melting sequences and after the last one the getter was remelted for one minute at a current of 280 amperes. After the melting operation the hardness of the getter was checked and if the hardness exceeded R_A40 the alloys were discarded. Four ingots were discarded due to this arbitrary maximum.

The compositions of the alloys prepared in this manner and their weight changes on melting, etc. are listed in

Table 6. Data concerning alloy preparation

Composition a/o	Composition w/o	Weight of U (g)	Weight of URe_2 (g)	Weight of button (g)	Change in weight on melting (g)	Probable error in composition (%)
0.00	0.00	30.515	---	30.515	+0.001	0.003
1.00	0.78	29.454	0.383	29.837	+0.001	0.003
2.00	1.57	32.817	0.867	33.684	+0.012	0.036
3.00	2.36	25.929	1.044	26.973	-0.003	0.011
4.00	3.16	27.154	1.481	28.635	-0.016	0.056
5.00	3.95	25.124	1.741	26.865	-0.020	0.074
6.00	4.76	25.057	2.118	27.175	-0.006	0.022
7.00	5.56	26.766	2.683	29.449	-0.004	0.014
8.00	6.37	26.907	3.136	30.043	-0.003	0.010
9.00	7.18	25.270	3.370	28.640	-0.008	0.028
10.00	8.00	23.913	3.606	27.519	-0.008	0.029
12.00	9.64	23.351	4.381	27.732	-0.002	0.007
14.00	11.30	21.065	4.785	25.850	-0.022	0.085

Table 6. The change in weight on melting is attributed to a competition between weight gain due to pickup of copper and tungsten from the hearth and electrode, respectively, plus reaction with atmospheric contaminants to form involatile products; and weight loss due to "spitting" of URe_2 when struck by the arc, and volatilization. Since spectrographic analysis indicated no contamination from the copper hearth and tungsten electrode, and since the alloys for the most part had a high metallic luster; one has some basis for assuming the probable error in over-all composition is given approximately by the change in weight divided by the total weight of the alloy. This probable error is tabulated in Table 6 and averages about 0.03%. Since the apparent uncertainty in composition is thus about 3 parts in 10,000, the

intended composition is assumed to be the actual composition.

The uranium-rhenium phase studies by Jackson *et al.* (24) followed the ASM procedure of listing compositions in terms of weight percent. The present work utilizes an atom percent notation, since most kinetic studies of this type are reported on this basis. As an aid in cross interpreting these two reports, an atom to weight percent conversion chart is shown in Figure 4. This figure also shows the various compositions used in this investigation and their method of preparation.

All the as-cast alloys were heat treated under vacuum in a tantalum container to improve the degree of homogeneity. Prior to homogenization, a small portion (approximately 2 grams) was cut from one side of each button and used for evaluating the properties of the as-cast structures. The major portion of the button was then cleaned electrolytically, and, without further reduction in size, homogenized.

The homogenizing treatment consisted of heating at 25°C/hr to 825°C, followed by holding at this temperature for four days, and then cooling to room temperature at 25°C/hr. The selected soaking temperature of 825°C was the result of a compromise between excessive grain growth and low rate of homogenization.

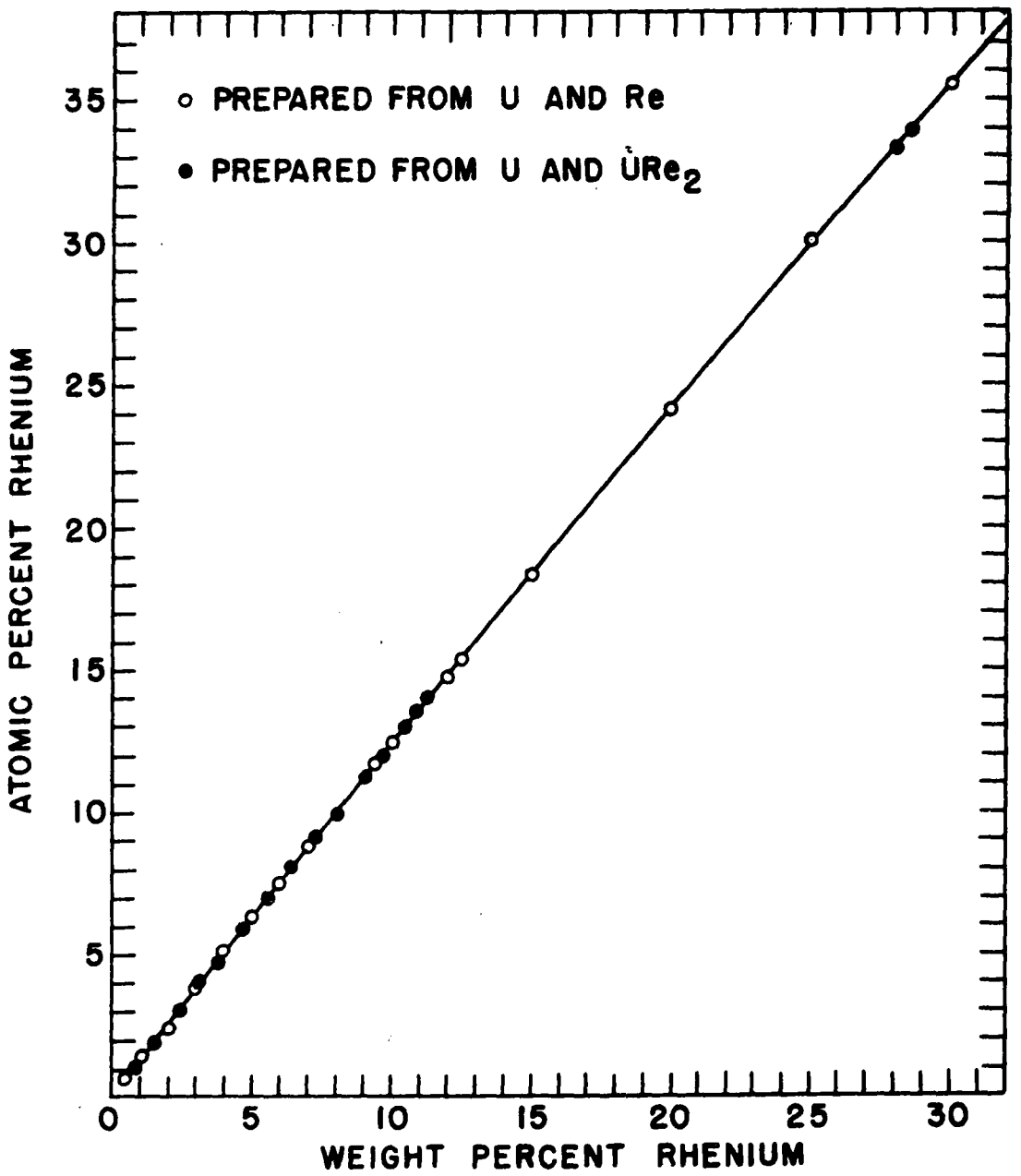

Figure 4. Atom to weight percent conversion chart for uranium-rhenium alloys

Alloy Examination

General considerations

The homogenized alloys were subjected to various heat treatments and examined by various standard techniques. All the experiments which required heating of the specimens were conducted at pressures less than 1×10^{-5} mm of mercury and when necessary a tantalum holder or shield was used to protect the specimen.

Thermal analysis

Direct thermal analysis and differential thermal analysis were used to locate phase transformations. Specimens varied in size from 1 to 20 grams, generally being 1-3 grams for fast cooling rates and considerably larger for the slower rates. Heating and cooling rates for the larger specimens, while linear during a given run, were varied from 10° to 100°C/hr. For faster cooling rates, the rate was not linear and depended on the furnace characteristics or the quenching medium. For differential thermal analysis, nickel or tantalum was used as the neutral body and alumina as the insulation. Pt/Pt-Rh thermocouples were pressed into holes drilled in the center of the neutral body and test specimen. Temperatures were read directly with manually operated high precision potentiometers or automatically recorded with a Moseley "Autograf" x-y recorder.

Specimen preparation

To determine the effect of cooling rate on the structure produced, series of alloys were equilibrated at various temperatures followed by cooling to room temperature at various rates. For comparative purposes it was desirable to have a standard specimen size. Sheet specimens approximately 1/16 in. thick by 3/16 in. wide by 3/8 in. long were machined from the homogenized buttons. These specimens were large enough that after heat treating, they could be readily examined for density, grain size, hardness, microstructure and crystal structure; and were small enough that the thermal gradient developed on cooling did not noticeably change the value of the measured property from one region of the specimen to another.

Quenching methods

Specimens were quenched by two methods: (a) water quenching, where rates of approximately 1000°C/sec were attained, and (b) vacuum quenching where the cooling rate was approximately 10°C/sec.

To water quench alloys, three specimens were equally positioned on a small perforated 2-mil tantalum holder which was itself joined to a Pt/Pt-Rh thermocouple bead. The perforated holder weighed 0.8 g and served to support the specimens upright and to protect them from contamination resulting from accidentally touching the hot fused silica

furnace tube. The assembled unit was then suspended in a vertical fused silica tube which was surrounded by a vertical tube furnace. The head through which the thermocouple wires passed was provided with a thin glass window sealed on with a vacuum sealing wax. Above this was a reservoir that could be filled with water. When the specimens were ready to be quenched, the reservoir was filled with ice water and the cover glass broken allowing the evacuated silica tube to be filled with water almost instantaneously. At the same time, the furnace was lowered rapidly away from the tube. Cooling rates of approximately 1000°C/sec were attained in this manner.

Vacuum quenching refers to removal of the furnace from around an evacuated fused silica tube containing the specimen. This was accomplished by using a sample arrangement similar to that used in water quenching except the holder-thermocouple unit was placed in a horizontal furnace tube and a removable track-type horizontal furnace heated the specimen. As soon as the furnace was removed, a stream of cool air was passed across the furnace tube. Cooling rates of approximately 10°C/sec were achieved in this manner.

Metallography

Prior to polishing, the specimens were mounted for ease of handling. The as-cast alloys were mounted in a cold-setting epoxy resin and the homogenized alloys in a thermo-

setting plastic. The specimens to be quenched were first mounted in a thermosetting plastic and then removed by a hook placed in a small hole drilled at the side of the specimen. The specimens after being heat treated and quenched could then be pressed back into the existing hole and polished immediately. This technique eliminated the time loss (12-hour curing periods) and slight heating effect associated with cold-setting mounting materials.

After mounting, the specimens were subjected to one minute each on 320, 400, 500 and 600 grit Si-C paper. The intermediate polishing operation consisted of three steps of five minutes each on rotary laps of 600 grit Si-C on 10 ounce canvas duck followed by an oil lapped #6 diamond paste on 70 denier nylon cloth without nap and #3 diamond paste on a medium nap synthetic rayon polishing cloth. The worked surface was then removed by electropolishing in a chromic-acetic acid bath composed of 1 part CrO_3, 1 part H_2O and 4 parts CH_3COOH (glacial acetic acid, HAc). A periodic potential was used and consisted of twelve cycles of $2\frac{1}{2}$ seconds at 40 volts dc followed by $2\frac{1}{2}$ seconds at zero volts. Use of a constant voltage resulted in surface irregularities. The periodic method yielded a smooth surface free of disturbed metal as revealed by examination under polarized light. Surface irregularities also occurred on electropolishing when the surface was not cleaned properly after mechanically

polishing. A rinse in glacial acetic acid provided a clean surface.

Since polarized light examination loses some of its effectiveness at high magnification, a need was found to etch the polished surfaces. Also, a check on the structures revealed by polarized illumination was desirable. A satisfactory electrolytic etch was obtained by lowering the voltage of the chromic-acetic acid bath to 25 volts. A chemical etchant consisting of a 1:1 mixture of nitric and acetic acid was found to work well on all the alloys. Approximate etching times for the as-cast and homogenized alloys are shown in Figure 5. Generally, the higher the rhenium content the shorter the etching time.

Other etchants or techniques also gave satisfactory results, and were used nearly exclusively during the early stages of the investigation. The $\epsilon(URe_2)$ phase could be selectively etched with a mixture composed of 6 parts by weight of $K_3Fe(CN)_6$, 2 parts KOH, and 92 parts H_2O. The $\delta(U_2Re)$ phase was revealed by extended polishing and could be further delineated by ion bombardment etching (36). The α-phase alloys could generally be satisfactorily etched with an electrolyte containing 36 parts by weight of HNO_3 (70%), 1 part citric acid, and 63 parts H_2O. Etching by ion bombardment was used for the γ-phase and β-phase alloys and for the α-phase alloys which were difficult to etch.

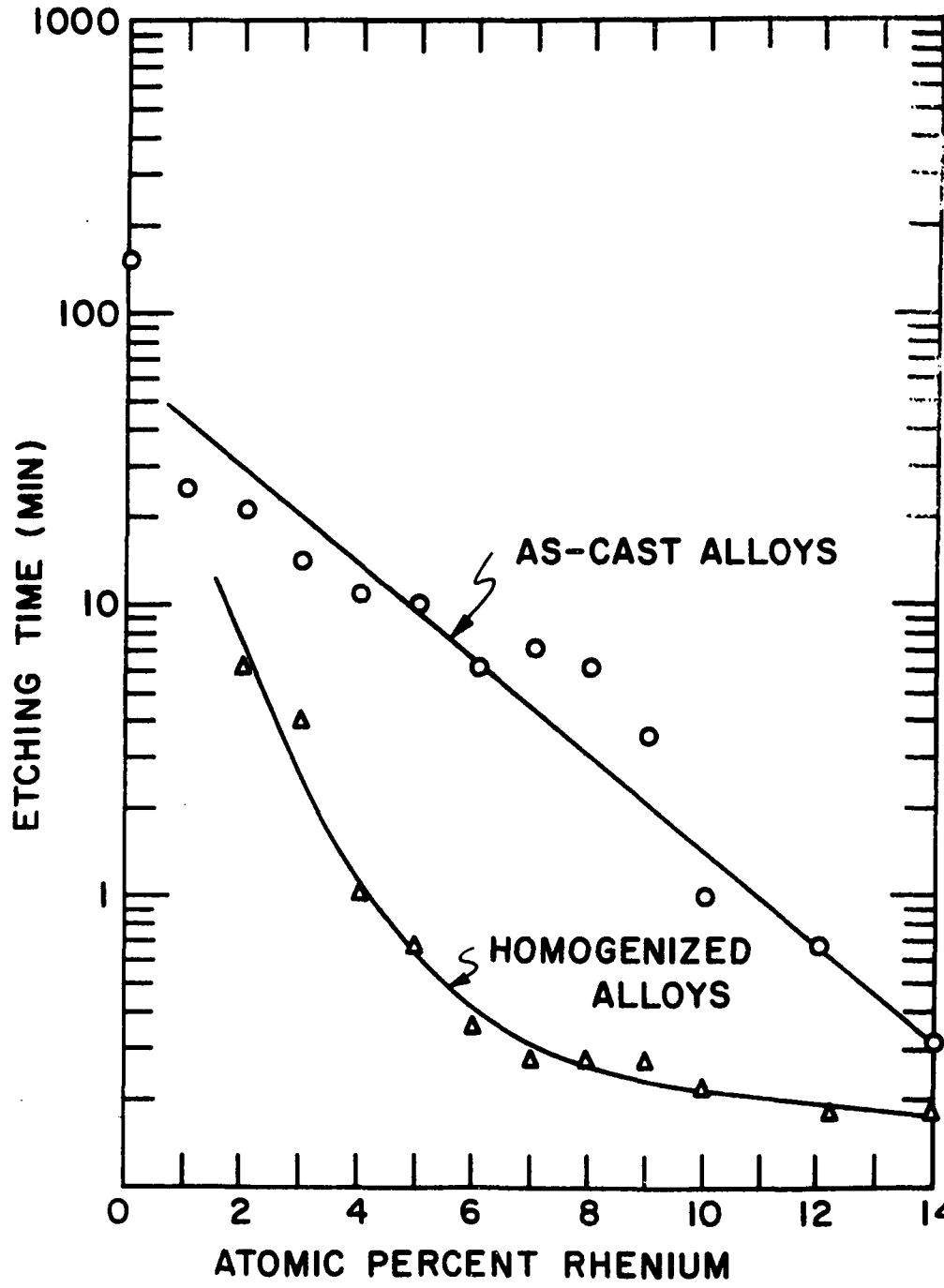

Figure 5. Etching times for a 1:1 mixture of nitric and acetic acid

Etching times of six minutes at an argon pressure of fifteen microns and a potential of six kilovolts were common.

In some instances, the microstructure could not be resolved using an optical microscope. To discern the fine detail, replicas of etched surfaces were examined in a RCA EMU-1 electron microscope. The replicating process consisted of first coating the etched surface with a parting layer of sodium metaphosphate followed by shadowing with chromium and finally coating with carbon. The composite coating was then floated off the substrate giving rise to a chromium-shadowed carbon replica.

Hardness measurements

For this investigation an indentation tester of the Armstrong-Vickers type was employed. To minimize non-metallurgical variables a constant preset load of 10 kg was used and all measurements were made on flat electropolished surfaces. In addition, all reported hardness values are averages of at least four representative readings.

Density measurements

The density measurements used a volume calculation based on an apparent loss in weight method. The alloy was weighed in air and then in a liquid of known density. The expression used to calculate density was

$$\rho = \rho_1 \left(\frac{W_a}{W_a - W_1} \right),$$

where W_a is the weight in air, W_l the weight when submerged, and ρ_l the density of the liquid.

Distilled water was initially chosen as the liquid due to its known temperature dependency. However, this was a poor choice due to the low wetability between water and metal. Later, bromobenzene was used as the displaced liquid and a marked increase in ease of weight determination was noticed. All the reported densities were with bromobenzene as the displaced liquid. A value of 1.4878 g/cm^3 was used for its density at 28°C, the temperature of the readings. A 10 mil nichrome wire was used to suspend the samples. Its presence was corrected for by subtracting its weight in air and its weight when submerged from the corresponding readings. Balance readings were made to ± 0.0002 grams.

Grain size determinations

The grain size of each specimen was estimated using the ASTM comparative method (37, p. 283). The procedure followed was to chemically etch the specimen and project its image on a ground-glass screen at 100 magnifications. The projected image was compared with a series of graded standard ASTM grain-size charts until a suitable match was obtained. An alternative approach, used nearly exclusively during the late stages of the investigation, was to compare the image revealed by polarized illumination with a standard grain-size measuring eyepiece.

Large grain sizes not covered by the ASTM system were encountered. In these instances the grain size is listed as the average diameter of the grains in inches. This method coupled with the ASTM method worked well for determining the grain size of the β and γ phases and for some α-phase alloys. Often, however, the α phase was present as platelets and its grain size is reported as plate width in millimeters as determined by a stage micrometer.

The shape of the grains for each specimen was also recorded. In some instances, mixtures of grain shapes were encountered. However, one of the grain shapes usually predominated and it is listed as the grain shape of the sample.

X-ray methods

Phase identification was made by x-ray diffraction methods using copper radiation with a Norelco diffractometer and a 114.6 mm Debye-Scherrer camera. The high temperature x-ray work was performed with equipment similar to that described by Chiotti (38).

To obtain Debye-Scherrer photographs of the quenched specimens they were first machined on a cut-off wheel to a cylindrical shape having a diameter of about 0.5 mm followed by electrolytically thinning in a chromic-acetic acid bath to a diameter of about 0.15 mm. Debye-Scherrer photographs were made from the reduced sections with filtered copper Kα radiation in a 114.6 mm diameter camera.

Originally, filtered chromium Kα radiation was used in an effort to better resolve any line splitting that occurred and to reduce the number of reflections. However, extraneous reflections were detected and for the high uranium alloys they were often of higher intensity than the known reflections. The presence of the extraneous reflections was attributed to a surface film as their intensity was considerably reduced when the more penetrating and intense copper radiation was used. Efforts to prevent the formation of or to remove the surface film by using different electropolishing solutions and acid rinses did not prove successful. The early work performed with chromium radiation was later duplicated with copper radiation and no changes in lattice parameters were noted. However, the standard error decreased noticeably.

It is well known that metallurgical specimens strongly absorb x-rays and hence the diffracted beam must originate from a thin surface layer. An approximate calculation for the effective depth of penetration for a diffracted beam for uranium using copper radiation at $45^{\circ}\theta$ yielded values of 0.00015 cm (15,000 Å) for 95% contribution and 0.000035 cm (3,500 Å) for 50% contribution. For chromium radiation the effective penetration is less than half the above value. Thus, one can guess that the surface layer is in the neighborhood of a thousand angstroms thick. For a discussion of

this calculation see Cullity (39, p. 269).

Immediately after each heat treatment, a diffractometer pattern was obtained. These patterns served as a quick means of phase identification and also were more sensitive in detecting line splitting than were Debye-Scherrer photographs. The sample size and shape was that of the flat bars described earlier. To obtain high quality diffractometer patterns it was often necessary to electropolish the surface rather than mechanically polish it as the latter tended to flatten the diffraction peaks, especially for the soft alloys. A Norelco diffractometer with copper $K\alpha$ radiation was used at a chart speed of $1^{o}(2\theta)$ per minute.

In some instances the x-ray specimens were in the form of fine powders. To prepare powder specimens, alloys containing more that 45 a/o Re were readily crushed while alloys containing less were reduced to powder by filing. Only material passing a 200 mesh screen was used. The powder was treated magnetically to remove any iron contamination and was then given a stress-relief anneal. Surface contamination during annealing was a problem for powders containing a uranium phase. When this happened, the powders were used in the as-filed condition. To produce the specimens for the Debye-Scherrer camera a glass fiber coated with a hydrocarbon grease was rolled in the powder. For use in the diffractometer the powder was spread on a transparent sheet and

affixed to it with transparent tape or a cement-acetone mixture.

To assign Miller indices to the β-phase reflections, it was first necessary to correct the lattice parameters to room temperature and to then calculate the theta values for the various reflections. The β-uranium structure at 720°C as proposed by Thewlis (40) is tetragonal with a_o = 10.759 Å and c_o = 5.656 Å. Correcting these values to room temperature using the linear coefficient of expansion determined by Klepfer and Chiotti (6) of α[100], α[010] = 23.4 ± 1.5 x 10^{-6} per °C and α[001] = 6.0 ± 2 x 10^{-6} per °C yielded lattice parameters at 23°C of a_o = 5.632 Å and c_o = 10.584 Å. The theta values for the various reflections were calculated with the aid of a computer. Mueller *et al.* (41) developed a computer program from which d spacings and theta values are obtained after an input of only the space group and lattice constants. The results of this program for the β-uranium structure at 23°C are given in Table 7.

To assign Miller indices to the α-phase reflections the results of LaPlaca as listed in the ASTM diffraction data card file were used (42). There were a number of readable reflections in the α-uranium pattern for d spacings smaller than those listed by LaPlaca (the lower limit of his d spacings was d = 0.923 Å). To assign indices to these reflections it was necessary to calculate the possible reflections at these higher theta values from the known lattice parameters

Table 7. Interplanar spacings and diffraction angles of α uranium at 23°C

hkl	d (Å)	θ (CuKα$_1$)	hkl	d (Å)	θ (CuKα$_1$)
002	2.8162	15.873	305	1.0731	45.872
400	2.6460	16.924	315	1.0676	46.175
112	2.6358	16.992	762,922	1.0631	46.432
410	2.5670	17.461	823	1.0596	46.632
330	2.4947	17.985	941	1.0556	46.860
202	2.4861	18.049	663	1.0390	47.849
212	2.4202	18.558	932	1.0372	47.954
411	2.3358	19.254	10.1.1	1.0352	48.078
331	2.2810	19.736	415	1.0315	48.306
222	2.2502	20.018	554,714	1.0256	48.679
312	2.1549	20.944	10.2.1	1.0207	48.996
322	2.0322	22.273	724	1.0115	49.599
431,501	1.9815	22.875	913	0.99224	50.421
511	1.9476	23.296	862,10.0.2	0.99074	51.028
432	1.6921	27.078	960	0.97849	51.923
223	1.6781	27.323	952	0.96568	52.904
512	1.6709	27.451	961	0.96405	53.033
522	1.6117	28.549	804	0.96418	53.022
621	1.6042	28.696	10.5.0	0.94666	54.455
541	1.5860	29.055	664	0.93369	55.584
532	1.5257	30.322	10.5.1	0.93357	55.595
631	1.5193	30.463	545	0.93087	55.839
413	1.5154	30.550	970	0.92828	56.075
333	1.5001	30.895	962	0.92429	56.444
602	1.4949	31.014	216	0.92080	56.773
612	1.4802	31.356	635	0.91679	57.157
720	1.4538	31.993	10.2.3	0.90831	57.996
551,711	1.4466	32.172	844	0.90591	58.239
622	1.4386	32.371	705	0.90334	58.504
542	1.4255	32.706	10.5.2	0.89732	59.137
641	1.4203	32.841	10.6.1	0.89601	59.277
004	1.4081	33.163	645	0.89362	59.536
730	1.3898	33.658	882	0.88780	60.181
314	1.2979	36.403	972	0.88162	60.889
820	1.2835	36.879	10.7.0	0.86708	62.665
613	1.2762	37.125	10.7.1	0.85698	64.001
414	1.2345	38.603	516	0.85533	64.229
802	1.1974	40.034	526	0.84707	65.411
742,812	1.1899	40.342	825	0.84664	65.474
703	1.1776	40.851	864,10.0.4	0.84605	65.562
553,713	1.1704	41.157	10.5.3	0.84529	65.676
822	1.1679	41.262	10.1.4	0.84336	65.968
841	1.1580	41.693	982	0.83904	66.639
723	1.1495	42.074	835	0.83342	67.550
911	1.1444	42.303	973	0.83212	67.767
851	1.1003	44.431	10.7.2	0.82869	68.355

and space group. Use was made of the computer program described above. Using LaPlaca's values of a_o = 2.858 Å, b_o = 5.877 Å and c_o = 4.955 Å the possible higher order reflections were calculated and are listed in Table 8.

Table 8. High-angle reflections for α uranium

hkl	d (Å)	$\sin^2\theta$ (CuKα_1)	θ (CuKα_1)
062	0.91089	0.71505	57.737
153	0.90804	0.71955	58.023
224	0.89186	0.74588	59.728
312	0.87919	0.76755	61.175
243	0.87055	0.78286	62.226
330	0.85673	0.80831	64.035
135	0.84478	0.83135	65.753
331	0.84421	0.83247	65.839
063	0.84249	0.83587	66.101
006	0.82583	0.86993	68.858
045	0.82158	0.87896	69.640
313	0.81722	0.88837	70.482
154	0.81706	0.88870	70.512
332	0.80969	0.90497	72.045
260	0.80792	0.90893	72.435
170	0.80553	0.91433	72.980
261	0.79739	0.93309	75.009
171	0.79510	0.93849	75.640
026	0.79503	0.93864	75.658
244	0.78943	0.95201	77.346
116	0.78624	0.95974	78.425
225	0.78476	0.96337	78.966

Lattice parameters were determined with the aid of an IBM 7074 computer. The computer program was worked out by Mueller and Heaton (43) and permits the determination of lattice parameters and standard errors for systems of orthorhombic symmetry and higher. It utilizes an extrapolation carried out analytically by the method of least squares, and

has provisions for using as many as three separate correction terms for eccentricity, absorption, divergence, etc. However, generally only the Nelson-Riley function was used. Provisions are also made for weighting each reflection. Use was made of an observation weight or a trignometric function ($1/\sin^2 2\Theta$) depending on the nature of the pattern. A computer program developed by Hansen (44) was used to determine lattice constants for a monoclinic structure. This program yielded extrapolated monoclinic lattice constants by the method of least squares using the Nelson-Riley function. To avoid duplication, the reader is referred to the original articles (41, 43, 44) for the particulars of the computer programs.

RESULTS AND DISCUSSION

Results of Core Experiments

The purpose and objectives of this research were discussed in the introductory chapter. The experimental techniques used to achieve these objectives were presented in the preceding chapter. The core experiments were basically those in which series of alloys were water quenched, vacuum quenched and slow cooled from the γ and β phase fields. More specifically, they were: (1) series of alloys water quenched from 975° and 850°C after 1/2 and 4 hours at temperature, respectively; (2) series of alloys water quenched and vacuum quenched from 975, 850 and 642°C after 1/2, 4 and 6 hours at temperature, respectively; and, (3) a series of alloys cooled at 25°C/hr from 825°C after four days at temperature. For the sake of conciseness and comparative purposes, the results of these core experiments are presented in tabular form in Tables 9 through 15. The significance of these data is discussed later under the appropriate heading along with results from supplementary experiments.

The grain size listed in Tables 9 through 15 is preceded by a Greek symbol which represents the phase to which the measurement refers. For example, a γ-quenched alloy may have two grain sizes listed. The grain size preceded by an α would refer to the size of the α grains developed on

quenching. The grain size preceded by a γ would refer to the prior γ grains which were readily visible and measurable in the quenched microstructure.

Table 9. Results from examination of as-cast alloys

Composition a/o Re	Hardness VHN	Density g/cm^3	ASTM grain size		Structure
0	236	19.13		00-1	α
1	293	18.79[a]	γ β	00-1 6	$\alpha + \beta$
2	319	18.57[a]	γ β	00-1 4-5	β
3	406	18.02[a]	β	4	β
4	395	19.00	γ	1-2	α'_b
5	329	19.04	γ	1-2	α'_b
6	284	18.99	γ	2	α'_b
7	251	18.99	γ	00	α'_b
8	188	18.91	γ	1-3	α''_b
9	96	18.90	γ	2-3	$\alpha'' + \gamma^\circ$
10	150	19.03	γ	5-6	γ°
12	197	19.02	γ	6-7	γ°
14	258	19.03	γ	6-7	γ°

[a]Sample contained numerous cracks and voids.

Table 10. Results from examination of alloys cooled at 25°C/hr after four days at 825°C

Composition a/o Re	Hardness VHN	Density g/cm^3	ASTM grain size	Structure[a]
0	161	19.06		α
1	235	18.96	α 00-8	α
2	376	18.65	γ 00-1 α 7	β+α(W)
3	397	18.85	2 micron[b]	β+α
4	405	18.91	γ 1-2	α+β+δ
5	380	19.04	γ 00-1	α+δ(S)+β(?)
6	351	19.15	γ 00-1	α+δ(W)
7	401	19.09	γ 00-0	α+δ(T)
8	437	19.16	γ 00-3	α+δ(M)
9	464	19.19	γ 1-3	α+δ(M$^+$)
10	493	19.21	γ 4-5	α+δ
12	488	19.20	γ 6-7	α+δ
14	483	19.21	γ 6-7	α+δ

[a]The letters in parenthesis show relative amounts of secondary phases present as indicated by x-ray line intensities (S=strong, M=medium, W=weak, T=trace, ?=positive identification not made). This procedure is followed in subsequent tables.

[b]Approximate distance between δ platelets.

Table 11. Results from examination of alloys vacuum quenched after six hours at 662°C

a/o Re	Hardness VHN	Microstructure[a]	ASTM grain size[b]	X-ray phases	Lattice constants Å
0	172	lightly twinned, equi-axed G., regular G.B.	α 1-2 (0.03in.-6)	α[c]	
1	251	heavily twinned, irregular G. and G.B.	α 5(1-9)	α	
2	363	equi-axed β G., irregular β G.B., discontinuous δ	β 0(00-3)	β	
3	387	equi-axed β G., irregular β G.B., continuous δ, regular γ G.B.	β 2(1-6) γ 2-3(1-6)	β+δ(T)	
4	405	same as above	β 3 γ 2-3	β+δ(M)	
6	405	same as above	β 3(2-7) γ 0(00-1)	β+δ(M)	a_o=10.645 c_o= 5.628 c/a=0.529
8	442	equi-axed β G., irregular β G.B., fine δ	β 4	β+δ(M)	a_o=10.649 c_o= 5.625 c/a=0.528
10	468	equi-axed γ G., proeutectoid and fine δ	β ? γ 4-5	β+δ(M)	a_o=10.644 c_o= 5.625 c/a=0.528
14	464	same as above	β ? γ 7-8	β+δ(S)	

[a]Abbreviations used are G. for grains and G.B. for grain boundaries. This procedure is followed in subsequent tables.

[b]A.S.T.M. number used unless length unit follows number. This procedure is followed in subsequent tables.

[c]Strong preferred orientation. Other alloys in this table had random orientation of grains.

Table 12. Results from examination of alloys water quenched after four hours at 850°C

a/o Re	Hardness VHN	Microstructure	ASTM grain size	X-ray phases	Lattice constants Å
0	181	twinned α G.	α 4-5(3-6)	α	a_o=2.854 b_o=5.868 c_o=4.954
1	330	equi-axed β G., some α plates	β 0-00 (0.03in.-2)	β+α(T)	
2	339	equi-axed β G.	β 1-2	β	
3	387	equi-axed β G.	β 6(4-8)	β	
4	373	banded α G., equi-axed γ G.	α <0.004mm[a] γ 0.05 in.	α'	a_o=2.860 b_o=5.809 c_o=4.956
5	319	banded α G., equi-axed γ G.	α γ 0.04 in.	α'	a_o=2.872 b_o=5.817 c_o=4.969
6	276	banded and acicular α, equi-axed γ G.	α <0.007mm γ 0.04 in.	α'	a_o=2.869 b_o=5.806 c_o=4.973
7	235	banded and acicular α, equi-axed γ G.	α <0.02mm γ 0.047 in.	α''	a_o=2.877 b_o=5.797 c_o=4.977 γ=90.78
8	192	banded and acicular α, equi-axed γ G.	α <0.005mm γ 0-00	α''	a_o=2.871 b_o=5.768 c_o=4.978 γ=91.49
9	150	banded and acicular α.	α <0.005mm γ 1-2	α''	a_o=2.875 b_o=5.755 c_o=4.959 γ=92.22
10	108	equi-axed γ G., fine ε network	γ 4-5	γ'	a_o=3.452
12	150	equi-axed γ G., fine ε network	γ 6	γ'	a_o=3.448
14	161	equi-axed γ G., fine ε network	γ 7	γ'	a_o=3.448

[a] Plate width of α phase.

Table 13. Results from examination of alloys vacuum quenched after four hours at 850°C

a/o Re	Hardness VHN	Microstructure	ASTM grain size	X-ray phases
1	240	highly twinned α, irregular α G. and G.B.	α 2(00-9)	α'
2	357	equi-axed β G., irregular β G.B., discontinuous δ	β 1(00-8)	β
3	394	equi-axed β G., irregular β G.B., continuous δ, regular γ G.B.	β 00(0.03 in.-3)	β
4	390	granular α, equi-axed γ G., discontinuous δ'(W)	α un-resolved γ 0.04 in.	$\alpha' + \delta'$(W)
5	478	granular α, equi-axed γ G.	α un-resolved γ 0.04 in.	$\alpha'' + \delta'$(W)
6	292	granular plus banded α, equi-axed γ G.	α un-resolved γ 0.04 in.	α''
7	242	banded α G., equi-axed γ G.	α un-resolved (max. α size) γ 0.04 in.	α''
8	167	banded α G., equi-axed γ G.	α un-resolved γ 0.04 in. (0.1 in.-6)	α''
9	103	equi-axed γ G., discontinuous grain growth	γ 1(0.04 in.-6)	γ^o
10	149	equi-axed γ G.	γ 4	γ^o
12	167	equi-axed γ G.	γ 7	γ^o
14	176	equi-axed γ G.	γ 8(7-8)	γ^o

Table 14. Results from examination of alloys water quenched after one-half hour at 975°C

a/o Re	Hardness VHN	Microstructure	ASTM grain size	X-ray phases
1	351	equi-axed β G., some α plates	β 1(00-2)	$\beta + \alpha$(W)
2	373	equi-axed β G., irregular β G.B., discontinuous δ	β 2(0-4)	β
3	409	equi-axed β G., irregular β G.B., continuous δ	β 5(2-7)	β
4	370	banded α G., equi-axed γ G.	γ 0.03in.(0.043 in.-2)	α'
5	322	banded and acicular α, equi-axed γ G.	α <0.006mm α bands <0.02mm γ 0.04 in.	α'
6	289	banded and acicular α, equi-axed γ G.	α <0.006mm α bands <0.02mm γ 0.05 in. (0.16 in.-1)	α'
7	238	banded and acicular α, equi-axed γ G.	α <0.012mm γ 0.04 in.	α'
8	183	banded and acicular α, equi-axed γ G.	α <0.02mm γ 0.043 in.	α''
9	149	banded and acicular α, equi-axed γ G.	α <0.06mm γ 0.04 in.	α''
10	141	equi-axed γ G.	γ 0.12 in.	diffuse γ°
12	161	equi-axed γ G.	γ 6(5)	γ°
14	170	equi-axed γ G.	γ 7	γ°

Table 15. Results from examination of alloys vacuum quenched after one-half hour at 975°C

a/o Re	Hardness VHN	Microstructure		ASTM grain size	X-ray phases
1	236	highly twinned α, irregular α G. and G.B.	α	1-2(0.05 in.-8)	α′
2	373	equi-axed β G., irregular β G.B., discontinuous δ	β	0-1(0.03 in.-8)	β
3	390	equi-axed β G., irregular β G.B., discontinuous δ, regular γ G.B.	β	00(0.04 in.-5)	β
4	380	granular α G., equi-axed γ G., discontinuous β	α γ	un-resolved 0.03 in.	α′+β(T)
5	448	granular α G., equi-axed γ G.	α γ	un-resolved 0.04 in.	α′
6	280	granular plus banded α G., equi-axed γ G.	α γ	un-resolved 0.05 in.	α″
7	242	banded α G., equi-axed γ G.	α γ	un-resolved 0.05 in.	α″
8	160	banded α G., equi-axed γ G.	α γ	un-resolved 0.08 in.	α″
9	117	equi-axed γ G.	γ	0.05 in.	γ°
10	157	equi-axed γ G., discontinuous grain growth	γ	2(0.04 in.-4)	γ°
12	177	equi-axed γ G.	γ	7	γ°
14	185	equi-axed γ G.	γ	7	γ°

Incomplete $\delta(U_2Re)$ Formation

The slow rate of formation of $\delta(U_2Re)$ led to alloys containing nonequilibrium quantities of U, $\delta(U_2Re)$ and $\epsilon(URe_2)$. Various stages in the growth of this phase are illustrated in Figures 6, 7 and 8. Figure 6 shows the nonequilibrium structure produced by equilibrating the 29.9 a/o Re alloy above the peritectoid reaction isotherm and then slow cooling to room temperature. The dendrites are ϵ and the matrix consists of the unetched α-δ eutectoid structure.

Figure 7 shows a 24.2 a/o Re alloy heated for three weeks slightly below the peritectoid reaction isotherm. The gray matrix in this nonequilibrium three-phase alloy is α uranium, the white phase is both rimmed peritectoid and coalesced eutectoid δ, and the dark material which is enclosed by the white envelope is primary ϵ. The equilibrium microstructure for a 33.8 a/o Re alloy heated slightly below the peritectoid reaction isotherm for six months is shown in Figure 8, and consists of small, anisotropic grains of δ having an ASTM grain size of ten.

Actually the above mentioned extended heat treatment did not convert the near-stoichiometric alloys to equilibrium configurations due to segregation of reaction constituents on a microscale, the results being small random pockets of uranium solid solution and $\epsilon(URe_2)$ separated from one another by diffusion distances in the neighborhood of 0.1 to 0.5 mm,

Figure 6. The 29.9 a/o Re alloy heated one week at 900°C and slow cooled showing primary URe_2 in unetched eutectoid matrix. Etchant: $K_3Fe(CN)_6$, KOH, H_2O. X500.

Figure 7. The 24.2 a/o Re alloy heated 3 weeks at 700°C and furnace cooled showing primary URe_2(dark) with eutectoid and peritectoid δ (white) in α uranium matrix(gray). Etchant: $K_3Fe(CN)_6$, KOH, H_2O. X250.

Figure 8. The 33.8 a/o Re alloy heat treated for 6 months at 710°C showing the small (ASTM No. 10), anisotropic grains of the δ phase. Polarized illumination. X150.

Figure 9. The 24.2 a/o Re alloy shown above after heating at 30°C/hr to 850°C and furnace cooling showing decomposition of the δ peritectoid rim. Etchant: $K_3Fe(CN)_6$, KOH, H_2O. X1400.

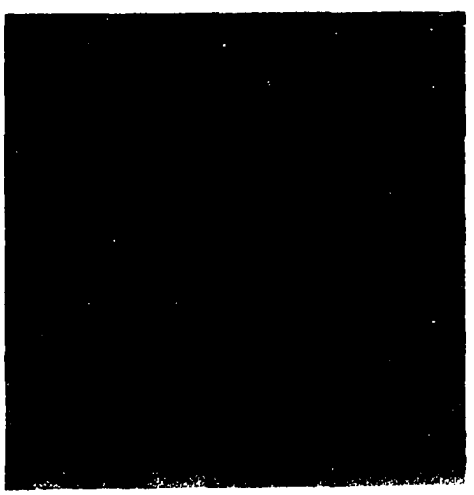

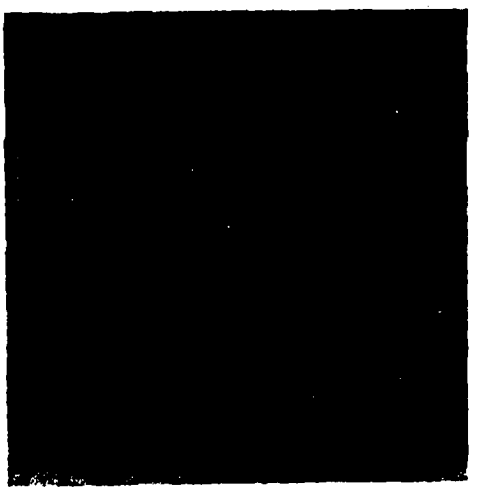

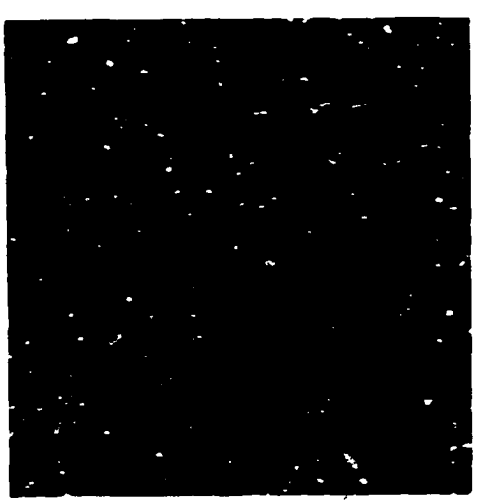

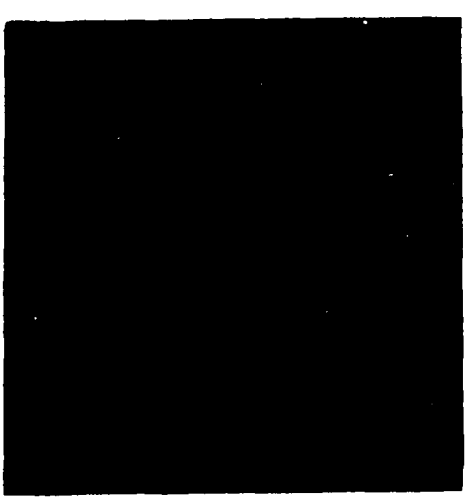

which on a microscale are rather large.

DTA heating curves of alloys not previously heat treated to grow δ showed no evidence of the peritectoid reaction isotherm. This is illustrated by the values shown in parenthesis in Table 16. These alloys initially had eutectoidally formed δ present, but this was consumed in the $\alpha \rightarrow \beta$ and $\beta \rightarrow \gamma$ transformations. The heating rates for values shown in Table 16 varied from 10° to 60°C/hr, generally being 30°C/hr.

DTA heating curves of alloys given an extended heat treatment to grow δ showed a temperature range of decomposition for δ rather than a relatively sharp transformation temperature as was the case for the $\alpha \rightarrow \beta$ and $\beta \rightarrow \gamma$ transformations. This behavior is illustrated in Figure 10 which shows some typical differential heating curves. The temperature range of the $\delta \rightarrow \gamma + \zeta$ reaction could be partly due to a composition gradient across the peritectoid rim, but is more likely mainly due to the diffusion-controlled slow growth of the γ and ζ phases. The microstructural change accompanying this transformation is shown in Figure 9.

An effort was made to determine the crystal structure and solubility limits of the δ phase. The results of these studies will soon be made available in a separate report.

A word is in order concerning the naming of intermediate phases in the U-Re alloy system. The U_2Re phase and the low

Table 16. Results from differential heating curves

Composition (a/o Re)	Temperature of $\alpha - \beta$ transformation (°C)	Temperature of $\beta - \gamma$ transformation (°C)	Temperature of U_2Re decomposition (°C)
0.0	663	771	
0.6	644-652	761	
	646-654		
	645-654	761	
1.3	644	740-765	
1.9	643		
	644	717-746	
	632	721-747	
2.5	642	684-745	
	648	682-730	
3.8	644	680-728	
	644	682-730	
5.1	644	683-698	
	642	682-705	
12.4	642	679	
	642	679	
15.4	646	683	752
24.2	643	679	
	645	680	752
	644	685	745
35.4	(643)	(678)	
	(644)	(680)	753
46.0	(644)	(679)	
			750
56.1	(644)	(678)	
	(642)	(679)	
			748

and high temperature forms of URe_2 are referred to as δ, ϵ and ζ, respectively. This follows the terminology of Rough and Bauer (15) who call the first intermediate phase in every uranium system δ. In the remainder of this paper, the distinction between the low and high temperature forms of the second intermediate phase is often not necessary and both are

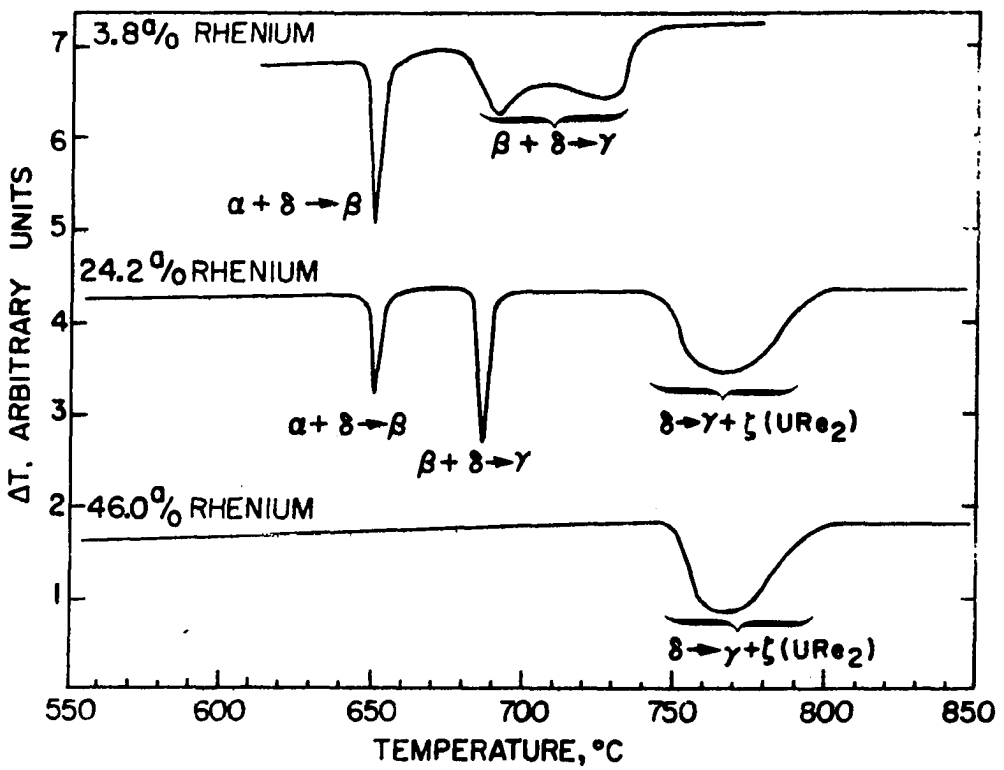

Figure 10. Some typical differential heating curves

referred to as URe_2.

An alternative approach in naming the first intermediate phase would be to label U_2Re as γ' since it appears to be an ordered form of γ uranium. The precedent for the alternative approach is the U_2Mo intermediate phase which is an ordered form of γ (45) and which is often referred to as γ'. Another approach is used in the U-Zr system where the only stable intermediate phase, UZr_2, is often labeled ϵ. This phase is also an ordered form of γ (46), and hence, sets another precedent.

Beta Phase Reaction Kinetics

Retention conditions

The β solid solution containing sufficient rhenium could be readily supercooled to room temperature. The results of a series of vacuum quenches from the β region (662°C) are tabulated in Table 11 and shown graphically in Figure 11. It is readily seen that under these conditions about 1.5 a/o Re is sufficient to permit the capture of the β phase.

Faster quenching rates (water quenching) resulted in retention of the β phase in the 1 a/o Re alloy. However, at these low rhenium contents, isothermal decomposition of the β phase occurred at room temperature by the growth of α plates in the β matrix. The β phase has been retained with as little as 0.6 a/o Re by water quenching from higher in the β field (710°C).

Figure 11. Some results from examination of alloys vacuum quenched after six hours at 662°C

(a). Phases present as a function of composition

(b). Vickers hardness as a function of composition

(c). Lattice constants of β phase as a function of composition

(d). Grain size as a function of composition

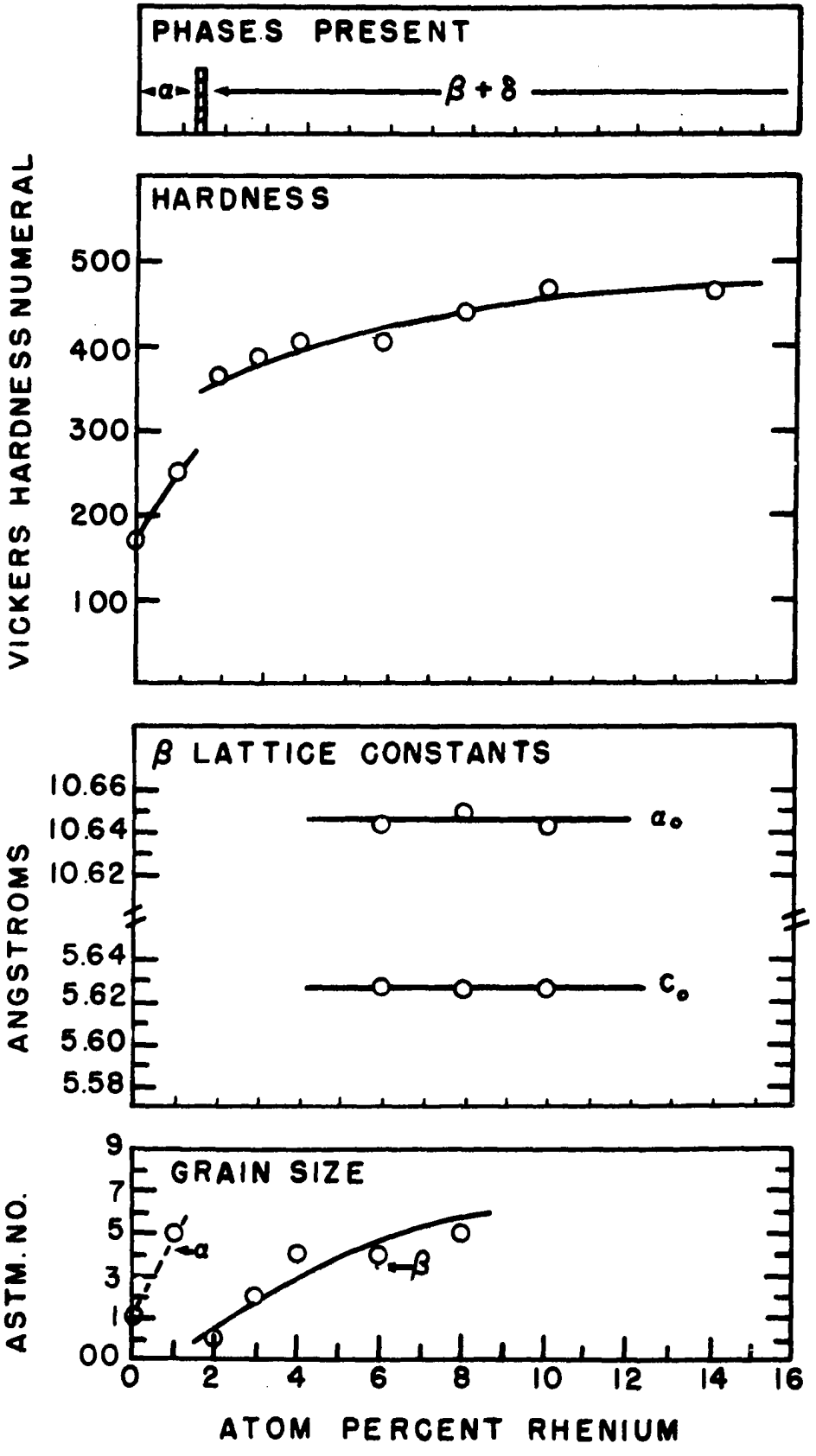
PHASES PRESENT
α
β + δ
HARDNESS
VICKERS HARDNESS NUMERAL
500
400
300
200
100
β LATTICE CONSTANTS
ANGSTROMS
10.66
10.64
10.62
5.64
5.62
5.60
5.58
a_o
c_o
GRAIN SIZE
ASTM. NO.
9
7
5
3
1
00
α
β
0
2
4
6
8
10
12
14
16
ATOM PERCENT RHENIUM

The β phase is easily retained at higher rhenium contents in that the 1.9 and 2 a/o Re alloys furnace cooled from 662°C were retained β. Furnace cooling refers to a nonlinear rate of approximately 200°C/hr at 600°C, 100°C/hr at 400°C and 50°C/hr at 200°C.

Differential thermal analysis of the 0.6 and 1.9 a/o Re alloys cooled at 45°C/hr from the γ region showed only slight undercooling of the $\gamma \rightarrow \beta$ transformation while the $\beta \rightarrow \alpha$ transformation was depressed considerably. The $\beta \rightarrow \alpha$ transformation occurred at 432°C for the 0.6 a/o alloy and did not occur in the 1.9 a/o alloy, indicating a retention of the β phase in the latter case. Hence, it appears that small amounts of rhenium retard the $\beta \rightarrow \alpha$ transformation markedly, while the $\gamma \rightarrow \beta$ transformation is hardly affected.

Identical behavior was observed on rapidly cooling from the γ region for compositions less than 3.5 a/o Re. That is, β was obtained on water quenching the 1 a/o alloy from 975° and 850°C, while α was obtained on vacuum quenching. In either vacuum or water quenching, a stable β phase was formed at the 2 and 3 a/o compositions. Even at cooling rates of 25°C/hr starting from the γ field, β was the principal phase present in the 2 and 3 a/o alloys and indicates the ease with which β is retained.

A change in transformation characteristics occurs between 3 and 4 a/o Re on cooling from the γ region. Alloys

of composition 1.9, 3.8 and 5.1 were heat treated at 850°C and cooled at approximately 400°C/hr. X-ray analyses of these alloys showed the 1.9 and 3.8 a/o alloys to be β phase, while the 5.1 a/o alloy was principally α'(a supersaturated α uranium structure) with some δ (U_2Re) present. Differential thermal cooling curves of the 1.9 and 3.8 a/o alloys showed only the $\gamma \rightarrow \beta$ transformation. This occurred at 730-700°C at 48°C/hr for the 1.9 a/o alloy and at 677-630°C for the 3.8 a/o alloy at 100°C/hr. A cooling curve showed a very broad anomaly at 614-535°C (possibly two overlapping transformations) for the 5.1 a/o Re alloy. A possible explanation for these happenings is that in the 1.9 and 3.8 a/o Re alloys the sequence of phase changes at these cooling rates is normal (i.e., $\gamma \rightarrow \beta \rightarrow \alpha$), whereas in the 5.1 a/o alloy the sequence is $\gamma \rightarrow \alpha' \rightarrow \alpha$. This possibility is discussed later.

Martensitic $\beta \rightarrow \alpha$ transformation

As mentioned earlier, the $\beta \rightarrow \alpha$ transformation occurred isothermally at room temperature for low rhenium contents. Some observed characteristics of this low temperature transformation are: (1) the transformation occurs by the growth of plates of α on preferred habit planes in the β matrix; (2) the rate of growth of the α plates under isothermal conditions is slow, yet much too rapid to be governed by normal diffusion, thus pointing to a shear mechanism; (3) the transformation goes to completion isothermally at room

temperature; and (4) plates already formed seem to catalyze the formation of others in the regions between existing plates since some grains were heavily transformed while others were still free of α.

Figure 12 shows the formation of α plates about 3 hours after quenching. At this time most of the grains were free of α. Judging from this photomicrograph, most of the plates nucleate at or near grain boundaries. Figure 13 shows a region after four days at room temperature. At this time the sample was predominantly α.

The behavior observed for these low rhenium alloys was very similar to that observed for dilute U-Cr alloys. White (47) studied four low-chromium alloys and found the time-transformation diagrams to consist of two separate "C" curves. He concluded that the transformation occurring at the higher temperatures was diffusion controlled, while the other, at lower temperatures, was martensitic in nature. Holden (48) studied a similar composition in the U-Cr system and found the habit plane in the β matrix for the α plates to be the {321} plane. He also found that the partially transformed α phase may be reversed to untransformed β by rapidly "quenching up" to temperatures above the nose of the lower "C" curve. One might surmise that U-Re alloys would behave in a similar manner.

Figure 12. The 1 a/o Re alloy water quenched from 850°C and aged 3 hrs showing α plates in the untransformed β matrix. At this time most of the grains were free of α. Polarized illumination. X150.

Figure 13. The above alloy after aging for 4 days at 23°C showing α plates in untransformed β matrix. At this time many of the grains had completely transformed to α. Etchant: HNO_3, HAc. X275.

Figure 14. The 2 a/o Re alloy heated 1 hr at 600°C showing formation of pearlite-like colonies of $\alpha + \delta$ in a predominantly α matrix. Etchant: HNO_3, HAc. X750.

Diffusion controlled $\beta \rightarrow \alpha$ transformation

The 2 and 3 a/o retained β alloys contained sufficient rhenium to stabilize the β phase and no isothermal decomposition was detected at room temperature for periods up to six months. Neither was decomposition detected after pressing at 16,000 psi (1.9 a/o alloy) nor after immersion in liquid nitrogen for 30 minutes (3.8 a/o Re alloy).

The stability of retained β alloys is illustrated by the following series of experiments. Retained β alloys of compositions 2 and 3 a/o Re were heated at 175°C for one hour, then vacuum quenched and later examined. This procedure was repeated at temperatures of 250, 325, 400, 450, 500, 550 and 600°C. The results are shown in Table 17 and Figure 15. Table 17 shows the phases detected by x-ray analyses. Figure 15 shows the hardness as a function of heat-treating temperature.

A general interpretation of these results is that β transforms to α above 500°C but it does so in a very sluggish manner and that a decrease in hardness accompanies the transformation. The small differences in decomposition rates for the three alloys may be due to the number of δ phase particles present, which could possibly serve as nucleation sites for the $\beta \rightarrow \alpha$ transformation.

The only significant metallographic changes observed under bright field illumination was the formation of regions

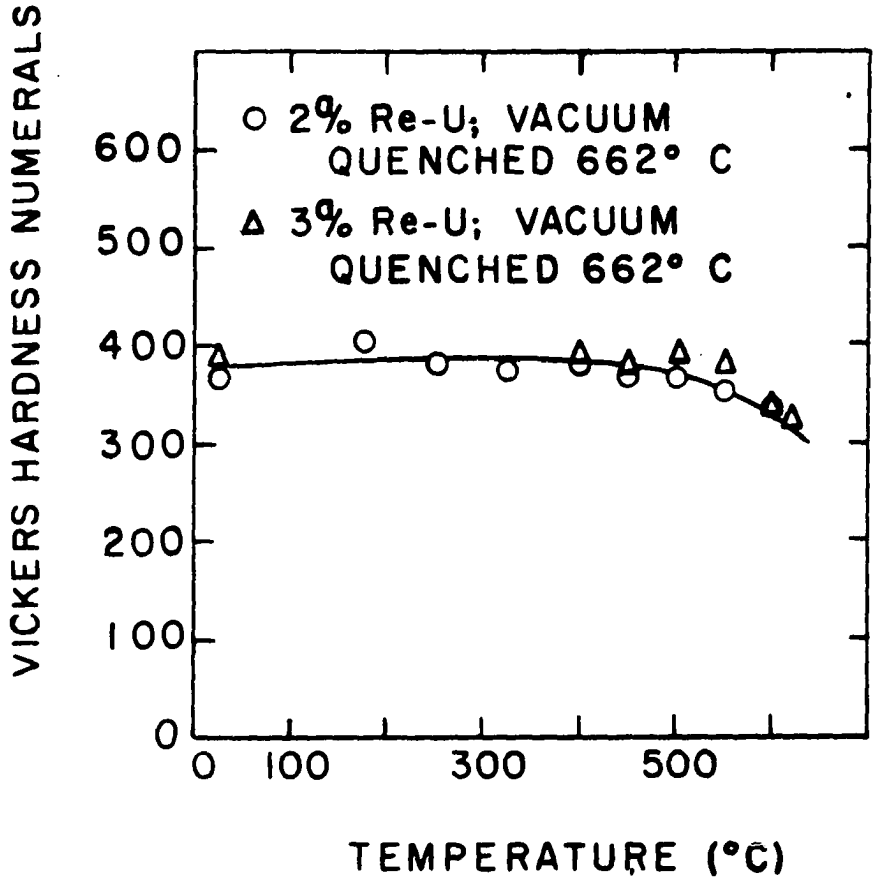

Figure 15. Hardness changes of retained β alloys after aging for one hour at temperature shown

Table 17. Phases detected by x-ray analyses during the aging of retained β

Heat-treating temperature	Composition and thermal history		
	2 a/o Re-U Vacuum Q. 662°C	3 a/o Re-U Vacuum Q. 662°C	3 a/o Re-U Vacuum Q. 850°C
23°C	β	$\beta + \delta(T)$[a]	β
175°C	β	$\beta + \delta(T)$	β
250°C	β	$\beta + \delta(T)$	β
325°C	β	$\beta + \delta(T)$	β
400°C	β	$\beta + \delta(T)$	β
450°C	β	$\beta + \delta(T)$	β
500°C	β	$\beta + \alpha(T) + \delta(T)$	β
550°C	$\beta + \alpha$	$\beta + \alpha + \delta(T)$	$\alpha + \beta + \delta(T)$
600°C	$\alpha + \beta + \delta(T)$	$\alpha + \delta(T)$	$\alpha + \delta(T) + \beta(T)$
620°C		$\alpha + \delta(T)$[b]	

[a]The letter "T" denotes a small but readily detectable amount.

[b]The amount of δ phase present increased slightly.

resembling pearlite colonies. Figure 14 shows these colonies in the 2 a/o alloy heated at 600°C. The colonies undoubtedly consist of $\alpha + \delta$; however, they may be due to an $\alpha' \rightarrow \alpha + \delta$ reaction rather than a $\beta \rightarrow \alpha + \delta$ reaction since their appearance coincided with the first appearance of δ in the x-ray patterns and not with the first appearance of β.

During the earlier stages of the investigation, certain extraneous x-ray reflections were often observed from the β

and α phase alloys. It was originally thought these might be due to an intermediate $\beta \rightarrow \alpha$ transition state. However, subsequent studies showed the additional reflections to be due to a tenacious surface film of β-UH_3 resulting from improper electropolishing.

Metallographic observations

Microstructures representative of the series of alloys vacuum quenched from 662°C are shown in Figure 16. These microstructures are interpreted in the following manner. The large grain size and relatively smooth grain boundaries of the pure uranium alloy shown in Figure 16a are due to being held high in the α region. Had this alloy been in the β range, large grain size, feathery structure and many elongated plate-like grains would have been expected (1, p. 136). The 1 a/o Re alloy shown in Figure 16b had the microstructure of the dilute U-Cr alloys known to have undergone a martensitic $\beta \rightarrow \alpha$ transformation, i.e. elongated, feathery and highly twinned grains (1, p. 137).

The 2 a/o alloy in Figure 16c shows large β grains[1] under polarized illumination. The bright streamers are microcracks which are a carry-over from the cast structure.

---

[1]The terms grain size and grain boundaries for the β phase is used loosely in that regions that respond similarly to polarized light (i.e., have similar orientations) are considered as grains even though the γ phase platelets are interspersed throughout these regions.

Figure 16. Representative microstructures of the series of alloys vacuum quenched after six hours at 662°C

(a). Pure uranium showing large α grains and subgrains with smooth grain boundaries. The dark striations are twins. Polarized illumination. X150.

(b). The 1 a/o Re alloy showing elongated, feathery and highly twinned α grains. Polarized illumination. X150.

(c). The 2 a/o Re alloy showing large β grains with typical ragged boundaries. The bright streamers are microcracks. Polarized illumination. X150

(d). The 4 a/o Re alloy showing retained β (light) and δ (dark). The prior γ grain boundaries are outlined by the continuous β network. Electrolytic etch. X150.

(e). The 6 a/o Re alloy showing extent of β grains. The δ platelets are barely visible. Note absence of prior γ grain boundaries. Compare with next photomicrograph. Polarized illumination. X150.

(f). The same 6 a/o Re alloy as in (e) under bright field illumination showing retained β (light) and δ (dark). The extent of the β grains is not visible. Electrolytic etch. X150.

(g). The 8 a/o Re alloy showing the fine distribution of δ in the β matrix. Electrolytic etch. X150.

(h). The 14 a/o Re alloy showing network of URe_2 outlining previous γ grain boundaries and fine unresolved distribution of δ in β matrix. Polarized illumination. X150.

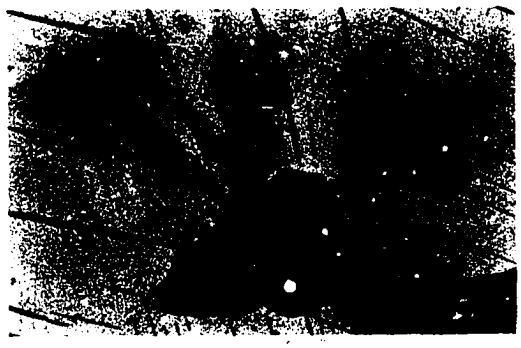

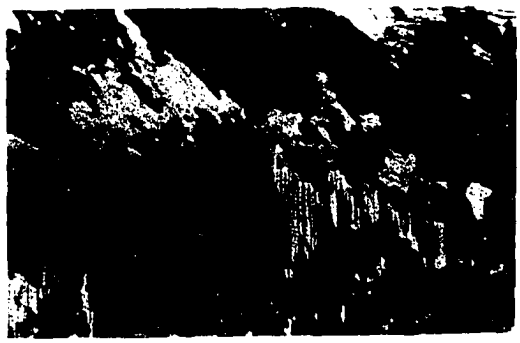

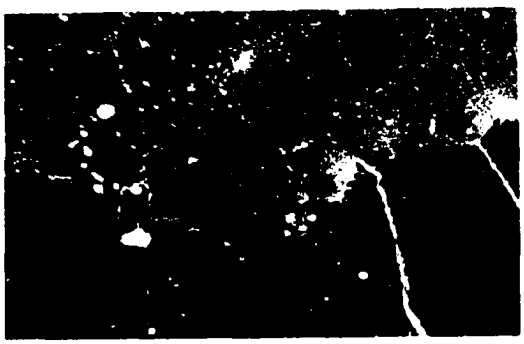

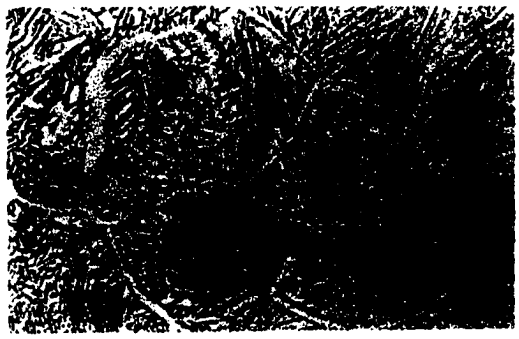

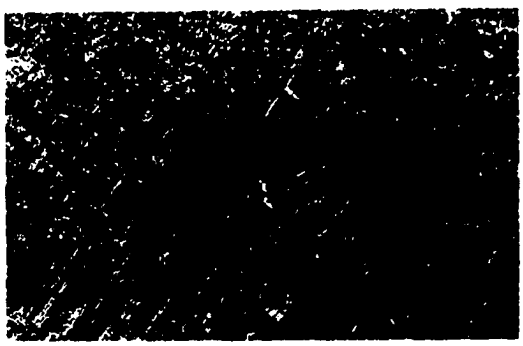

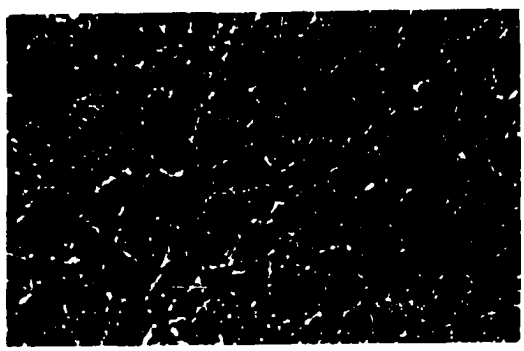

Chemical and electrolytic etching did not reveal the β grain boundaries but did show a very fine, slightly elongated discontinuous δ phase constituent. Similar behavior was observed in the 3 and 4 a/o alloys but in these alloys the δ phase was present in the form of platelets (often parallel) which were nearly continuous as shown in Figure 16d. This micrograph also shows a continuous β network outlining the prior γ grain boundaries.

At higher rhenium contents the β grain size decreased, and here again polarized light was necessary to distinguish the β grains. Figure 16e and 16f contrast the different structures obtained under polarized and bright field illumination for the 6 a/o Re alloy. The etched structure is that of the homogenized alloy. Presumably, the $\alpha \rightarrow \beta$ transformation and holding for six hours at 662°C does little to change the δ phase distribution which initially formed during the $\gamma \rightarrow \beta + \delta$ transformation.

The δ phase distribution became finer as the rhenium content increased (Figure 16g). At the higher rhenium contents it was difficult to electropolish without some etching of the specimen. This resulted in an inability to see the β grains at compositions of 10 a/o Re and higher. Figure 16h shows the 14 a/o alloy under polarized light. This micrograph shows a network of URe_2 outlining prior γ grains and a fine distribution of unresolved δ in the β matrix.

The hardness of the alloys vacuum quenched from 662°C is shown in Figure 11b. The increase in α hardness is due to solid solution strengthening, smaller grain size and transformation strains accompanying the martensitic $\beta \rightarrow \alpha$ transformation. The inherent hardness difference of the α and β forms results in the discontinuity between 1 and 2 a/o Re. The increase in hardness of the β phase with composition is due to the smaller grain size of the β phase and to the amount and distribution of the δ phase.

The effect of rhenium content on the retained β lattice parameters is shown in Figure 11c. Values of a_o = 10.64 Å and c_o = 5.63 Å were found for the $\beta + \delta$ two phase region. These compare with calculated values of a_o = 10.584 Å and c_o = 5.632 Å for pure β uranium at 23°C. This calculation was described earlier. This indicates an expansion along the [100] and [010] direction with little change in the [001] direction. The expansion of the β lattice might be expected since one interatomic distance in the β lattice is 2.59 Å (1, p. 31) which is unusually close compared to other uranium phases.

Figure 11d shows the effect of rhenium content on grain size for the series of alloys vacuum quenched from 662°C. It is seen that the grain size of both the α and β forms are refined by increasing the rhenium content.

Gamma Phase Reaction Kinetics

Nature of retained γ

Inspection of Tables 13 and 15 shows that 8.5 a/o Re was sufficient to cause capture of the γ phase on vacuum quenching from either 850° or 975°C. Similarly, as shown in Table 12, about 9.5 a/o Re was sufficient to retain the γ phase on water quenching from 850°C.

X-ray examination of the retained γ alloys showed the structure to be essentially body-centered cubic. Lattice parameters of 3.452, 3.448 and 3.448 Å were obtained for the 10, 12 and 14 a/o Re alloys, respectively, which were water quenched from 850°C. Klepfer and Chiotti (6) report a value of a_o = 3.538 Å for pure uranium at 800°C. Correcting this value to room temperature using the linear coefficient of thermal expansion determined by Klepfer and Chiotti (6) of $\alpha\langle 001\rangle = 22.5 \times 10^{-6}$ per °C yielded an a_o at 23°C of 3.476 Å. Hence, the addition of rhenium atoms causes a contraction of the BCC γ cell. This contraction would be expected on the basis of size considerations.

Some extraneous weak reflections were observed in the x-ray patterns of the γ alloys. Some of these could be accounted for on the basis of a surface film. Debye-Scherrer patterns were obtained with both CrKα and CuKα radiation. The reflections that lost intensity or disappeared in going from CrKα to CuKα radiation were assumed to be those of a

surface film. The reflections that gained intensity in changing from CrKα to CuKα radiation were assumed to be those of the base metal. The reflections attributed to the surface film could for the most part be accounted for on the basis of the β-UH_3 structure discussed earlier. The remaining weak reflections could be indexed on the basis of Kβ reflections of the normal γ-uranium cell.

The retained γ was found to respond actively to polarized light. The optical activity could be due to an epitaxial surface film, but the epitaxial nature would have to depend strongly on film thickness since the best response was obtained with a freshly polished surface. Another possibility is that the optical activity is due to a stable surface film that is itself anisotropic. Such anisotropic films have been known for many years and they make possible, for example, the study of aluminum with polarized light. However, the surface films observed by x-ray techniques, i.e., UC, UO_2 and β-UH_3 are cubic in structure and should not respond to polarized light.

Another interpretation is that the structure is not cubic, but that the presence of rhenium has reduced the symmetry of the γ structure. The only x-ray evidence for line splitting was in the back reflection region of some diffractometer patterns where unresolved humps were observed. These unresolved lines could be construed as due to a tetragonal

cell with a c/a ratio of approximately 0.999. However, in Debye-Scherrer patterns no evidence for line splitting or ordering could be found.

The retained γ structure showing anisotropic behavior with respect to polarized light, and inconclusive evidence for tetragonality is hereafter referred to as γ°. A photomicrograph of this structure is shown in Figure 17.

Additional quenches were made in an effort to obtain a γ-like structure showing definite tetragonality. Compositions of interest were vacuum quenched from 700 and 775°C after 12 and 8 hours at temperature, respectively; and water quenched from 775°C after 8 hours at temperature. The results of these heat treatments are listed in Table 18.

Vacuum quenching did yield structures in which definite broadening of γ° peaks occurred and in which banded microstructures were observed. Careful scrutiny of these x-ray diffraction patterns showed some weak reflections and that the broadening of the fundamental reflections was probably due to unresolved line splitting. This structure is hereafter referred to as γ°_{b} where the subscript indicates the metallographically identified bands and the corresponding alteration in crystal structure.

Tangri (49) determined the structure of a tetragonal ordered phase observed under somewhat similar conditions in the U-Mo system. His proposed structure is based on a block

Figure 17. The 10 a/o Re alloy water quenched from 850°C showing retained γ° microstructure. Polarized illumination. X150.

Figure 18. The 9 a/o Re alloy vacuum quenched from 775°C showing coarse banded γ_b° microstructure. Polarized illumination. X150.

Figure 19. The 9 a/o Re alloy vacuum quenched from 700°C showing the crosshatch γ_b° microstructure. Polarized illumination. X100.

Table 18. Results from examination of alloys quenched from 700 and 775°C after 12 and 8 hours at temperature respectively

a/o Re	Heat treatment[a]	Hardness VHN	Microstructure	ASTM grain size	X-ray phases
8	V.Q. 700°C	170	crosshatch	γ 0.043 in.	α''_b
9	V.Q. 700°C	109	crosshatch	γ 0.04 in.-3	γ°_b
10	V.Q. 700°C	161	crosshatch	γ 4	$\gamma^\circ_b+\delta$(VW)
9	V.Q. 775°C	101	deformation bands and crosshatch	γ 0.04 in.-2	γ°_b
10	V.Q. 775°C	143	normal	γ 4	γ°
12	V.Q. 775°C	173	normal	γ 6	γ°
8	W.Q. 775°C	192	banded	γ 0.04 in.-1	α''_b
9	W.Q. 775°C	151	banded	γ 0-1	α''_b
10	W.Q. 775°C	102	normal	γ 4-5	γ°

[a]The abbreviations V.Q. and W.Q. stand for vacuum quenched and water quenched, respectively.

of 2 x 2 x 1 γ cells and is shown in Figure 20. The results of his structure determination for a cell with a_o = 6.92 Å and c_o = 3.38 Å is shown in Table 19. The γ°_b x-ray patterns observed in the U-Re system agreed with the fundamental and superlattice reflections shown in Table 19. Hence, it is concluded that the γ°_b structure is isomorphous with the tetragonal ordered phase observed by Tangri in the U-Mo system. The γ° structure can be considered as due to a similar cell, except that the alloy is disordered and has a

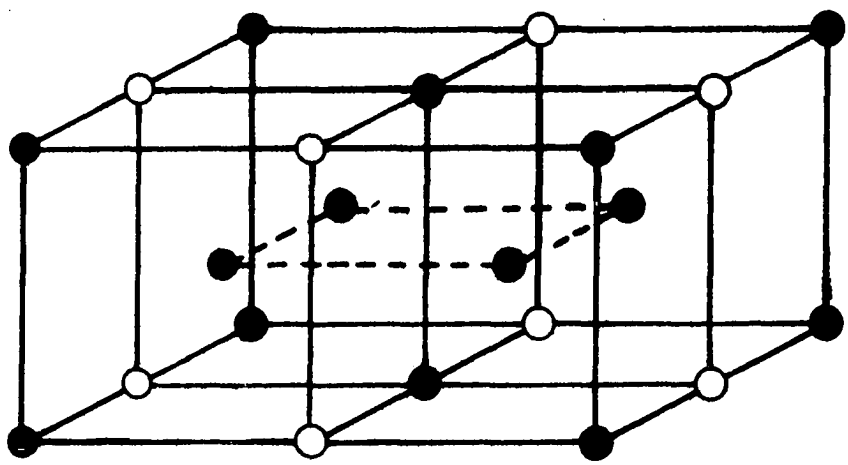

● Uranium atoms

○ Sites occupied statistically by U and Re atoms to different degrees

Figure 20. Proposed structure of γ_b°

Table 19. Values calculated by Tangri (49) for the metastable tetragonal phase in the U-Mo system with lattice constants of a_o = 6.92 Å, c_o = 3.38 Å and c/a = 0.488

hkl	Multiplicity p	Calculated intensity	Calculated d(Å)	Calculated θ ($CuK\alpha_1$)
111	8	<1	2.806	15.93
220	4	40	2.449	18.33
201	8	80	2.442	13.39
311	16	<1	1.840	24.75
400	4	31	1.732	26.40
002	2	13	1.694	27.04
112	8	<1	1.610	28.58
331	8	<1	1.467	31.67
421	16	100	1.409	33.14
222	8	49	1.394	33.54
312	16	<1	1.339	35.12
440	4	21	1.225	38.96
402	8	41	1.210	39.54
332	8	<1	1.176	40.92
531	16	<1	1.121	43.40
620	8	35	1.093	44.80
203	8	34	1.068	46.15
512	16	<1	1.060	45.60
223	8	<1	1.026	48.65
313	16	<1	1.004	50.10
442	8	29	0.992	50.94
532	16	<1	0.973	52.34
403	8	<1	0.942	54.85
641	16	52	0.924	56.47
622	16	51	0.920	56.85
423	16	50	0.913	57.53
800	4	11	0.866	62.80
004	2	5	0.842	66.17
443	8	<1	0.830	68.13
660	4	10	0.816	70.72
603	8	20	0.807	72.64
623	16	<1	0.787	78.16

c/a ratio $\simeq$ 0.5.

A high temperature diffractometer pattern of a 12.4 a/o Re alloy taken after one hour at 685°C showed the γ'_b structure (plus UO_2 and UC as surface contaminants). This indicates the γ solid solution orders at temperature and not on quenching.

As mentioned earlier, banding accompanied the alteration in crystal structure. These bands were of two types. Figure 18 shows the coarse type observed in the 9 a/o Re alloy vacuum quenched from 775°C. These bands were similar to those observed next to hardness indentions in γ' alloys and are referred to as "deformation bands". The other type of banded microstructure consisted of fine woven bands hereafter referred to as the crosshatch structure. An example of this microstructural type is shown in Figure 19. Presumably both types of banding are due to self deformation caused by the removal of ordering or transformation stresses (50, p. 83).

Stability and decomposition modes

The retained γ' phase showed considerable stability. For example, no decomposition of the retained γ' phase in a 12.4 a/o Re alloy was detected after aging at room temperature for 18 months. Similarly, a 10 a/o alloy composed of retained γ' when heated at 95°C/hr underwent an exothermic reaction between 484°-550°C and an endothermic reaction at 648°C. The first inflection was due to the decomposition of

γ to α while the second was the result of the equilibrium $\alpha \rightarrow \beta$ transformation.

Some information regarding the decomposition of the rhenium-saturated γ phase at slow cooling rates was obtained. Differential thermal cooling curves from alloys of composition 15.4, 24.2, 35.4, 46.0 and 56.1 a/o Re showed an anomaly at about 570°-490°C on cooling from 900°C at approximately 90°C/hr. This transformation temperature could apparently be raised by starting at a lower temperature and cooling at a lower rate. For example, the 35.4 and 46.0 a/o alloys cooled at 50°C/hr from 780° and 720°C, respectively, showed one inflection each at 585°-500°C and 652°-570°C, respectively. Diffraction patterns showed the uranium phase present at room temperature to be α uranium. It is concluded that for these alloys the transformations on cooling are not well defined and that the thermal curves show considerable undercooling and possible overlapping of two transformations. If two transformations occur they are possibly due to a $\gamma \rightarrow \alpha' \rightarrow \alpha$ sequence rather than to the equilibrium $\gamma \rightarrow \beta \rightarrow \alpha$ sequence. This possibility is discussed later.

The stability and mode of decomposition of retained γ° alloys are illustrated by the following series of aging experiments. A 10 a/o retained γ° alloy initially water quenched from 850°C was heated for one hour at 175°C, then vacuum quenched and later examined. This procedure was

Table 20. Phases detected by x-ray analyses and microstructures observed after heat treating the γ° and "diffuse γ°" alloys for one hour at temperatures shown

Heat-treating temperature	Composition and Thermal History	
	10 a/o Re-U Vacuum Q. 850°C	10 a/o Re-U Water Q. 975°C
23°C	γ°(sharp) clean equi-axed grains	diffuse γ° clean equi-axed grains
175°C	γ°(sharp) clean equi-axed grains	diffuse γ° clean equi-axed grains
250°C	γ°(sharp) clean equi-axed grains	diffuse γ° clean equi-axed grains
325°C	γ_b°(broadening)	diffuse γ° clean equi-axed grains
400°C	γ_b°(increased broadening)	α
450°C	$\delta' + \alpha$ banded microstructure	α granular
500°C	$\alpha + \delta'$	α granular
550°C	$\alpha + \delta$ granular (loss of anisotropy)	α granular
600°C	$\alpha + \delta$ granular + localized precipitation	α granular

repeated at temperatures of 250, 325, 400, 450, 500, 550 and 600°C. The results are shown in Table 20 and Figure 21. Table 20 lists the phases detected by x-ray analyses as well as the microstructural appearance. Figure 21 shows the hardness as a function of heat treating temperature.

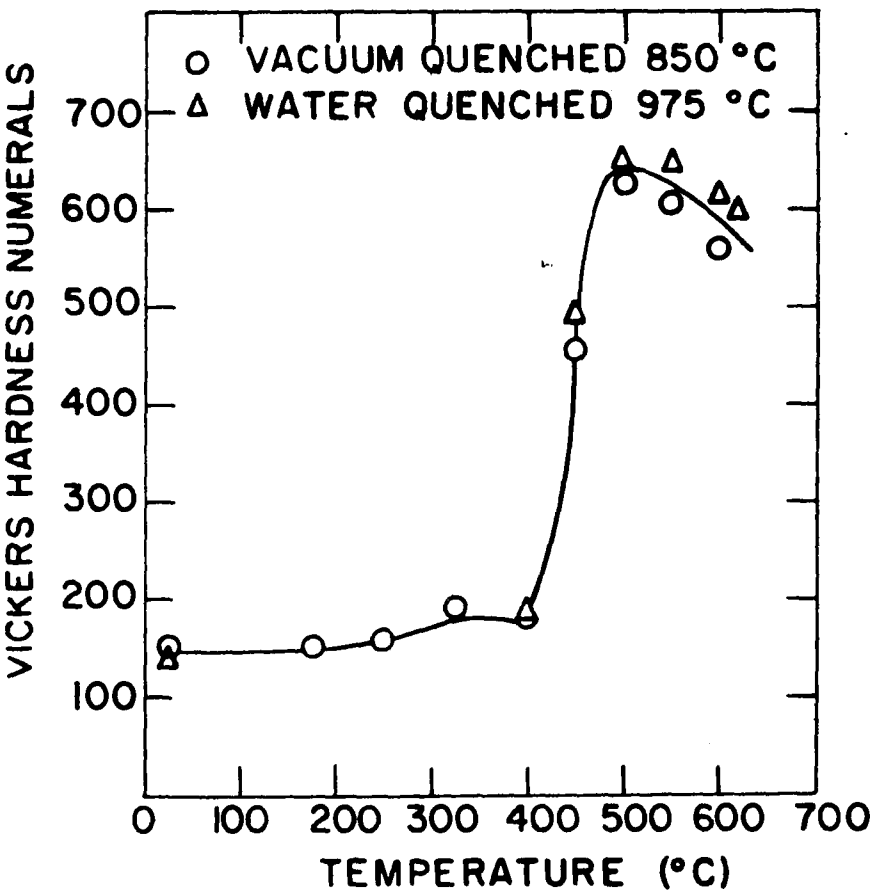

Figure 21. Hardness changes accompanying the heat treating of the 10 a/o Re retained γ° and "diffuse γ°" alloys after one hour at temperatures shown

The x-ray diffractometer patterns that accompanied this series of heat treatments yielded a possible relationship between the ordered tetragonal phase, γ_b°, and the $\delta(U_2Re)$ intermediate phase. Figures 22a and 22b show the gradual broadening of the γ° phase reflections. This broadening is due to the formation of the ordered tetragonal phase.

Further heating resulted in the appearance of a supersaturated α and what is postulated to be a transition phase labeled δ' which is intermediate to γ_b° and $\delta(U_2Re)$. Continued heating results in the rhenium-poor δ' transition lattice acquiring rhenium atoms at the expense of the supersaturated α. This process continues until at 550°C the transitional δ' phase achieves its equilibrium configuration.

Figures 22c, 22d, 22e and 22f show the δ' transition reflections shifting from γ-like positions to equilibrium δ positions. One can argue that the γ line broadening and δ' peaks are merely the resultant of the γ and δ phase reflections. However, the broadened (200) γ peak at 325°C has zero intensity at 27.3°Θ, which is the equilibrium position of the closest δ phase reflection. Furthermore, at 500°C the δ' reflection has a maximum at 27.0°Θ and zero intensity at 26.6°Θ, the equilibrium position of the (200) γ reflection.

The assumption that there is a gradual transition from the γ phase to the δ phase is not too absurd if one looks closer at the δ phase structure. The Debye-Scherrer pattern

Figure 22. Room temperature x-ray diffractometer patterns showing stages in the $\gamma^{\circ} \rightarrow \alpha + \delta$ transformation

(a). After 1 hr at 325°C

(b). After 1 hr at 400°C

(c). After 1 hr at 450°C

(d). After 1 hr at 500°C

(e). After 1 hr at 550°C

(f). After 1 hr at 600°C

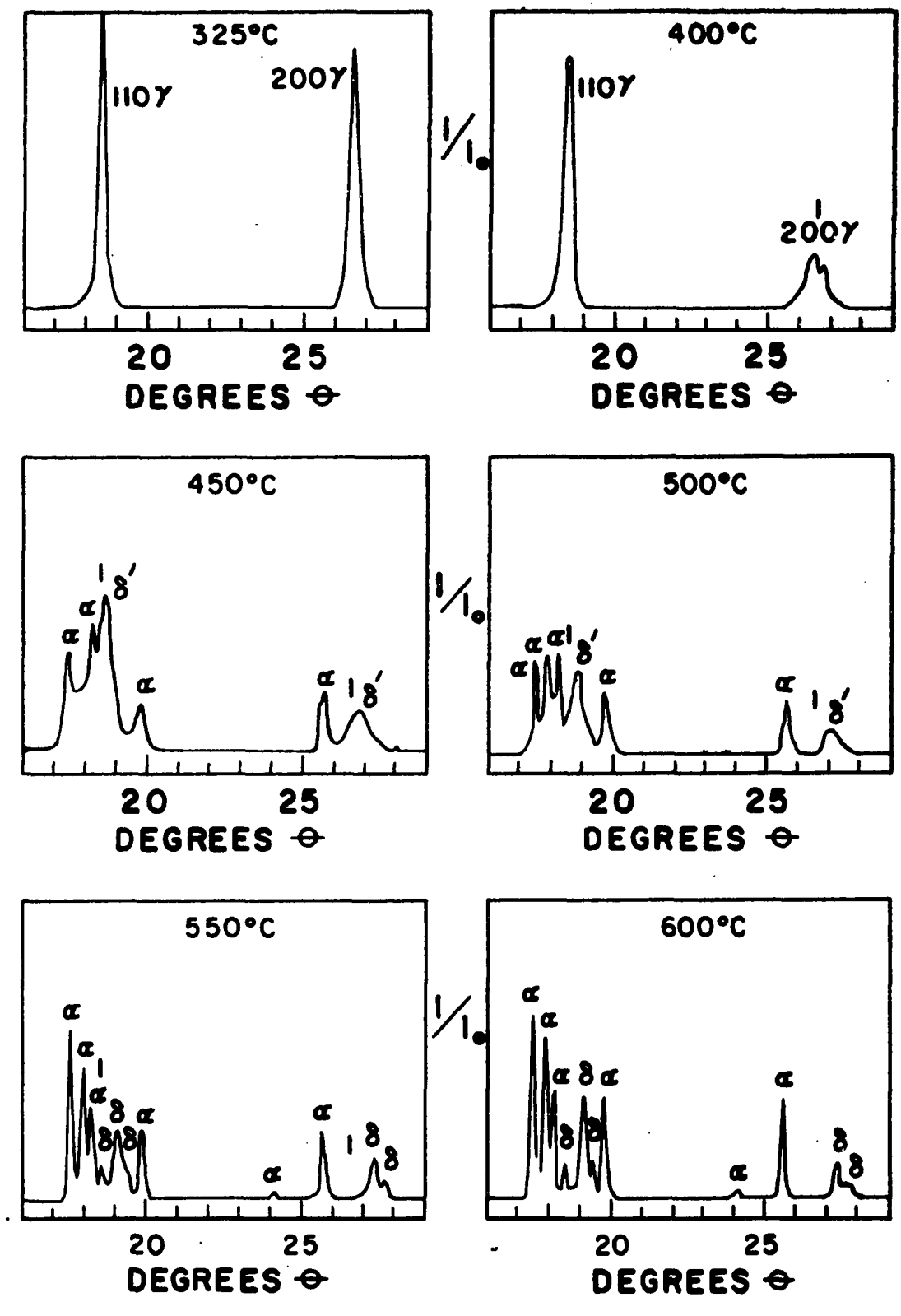
325°C
110γ
200γ
400°C
110γ
200γ
I/I₀
20
25
DEGREES θ
450°C
500°C
550°C
600°C
α
δ
δ'

of δ shows a relation to γ in that each γ reflection is displaced towards higher theta values (contraction of unit cell) and has apparently split into two or three reflections. A possible δ (U_2Re) structure based on three side-by-side BCC cells is shown in Figure 23. By measuring the principal lines in the δ pattern and assuming the 3 x 1 x 1 structure one can obtain experimental lattice parameters of a = 3.30 Å, b = 3.35 Å and c = 10.03 Å.

A calculation based on a hard sphere model gave similar results. Table 1 lists atomic radii of 1.51 Å for uranium and 1.34 Å for rhenium at a coordination of eight. By using these values and the possible 3 x 1 x 1 unit cell one obtains a tetragonal unit cell of a = 3.35 Å and c = 10.05 Å. These values agree well with the experimental values listed above. It should be emphasized that the δ (U_2Re) phase could not be indexed on the basis of the 3 x 1 x 1 unit cell shown in Figure 23. However, it does account for some of the principal lines. The argument is presented only to show a possible relation between the γ uranium cell and the δ (U_2Re) intermediate phase, and the plausibility of the γ_b° and δ′ transition states being intermediate to the two.

The microstructural changes accompanying the γ° decomposition were the appearance of a crosshatch structure followed by a granular structure and later by localized precipitation. The crosshatch structure is shown in Figure 24 and is seen to

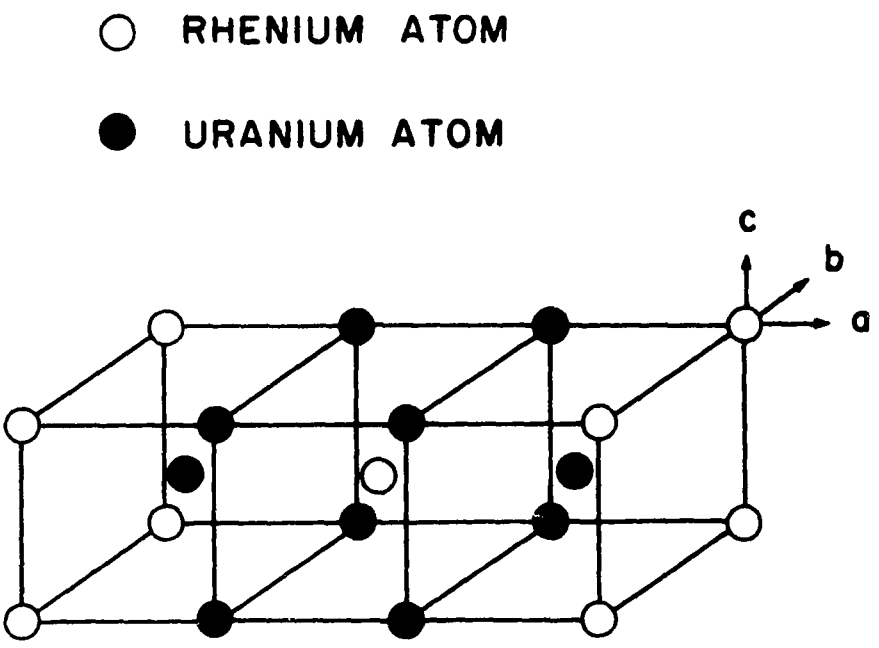

Figure 23. Possible unit cell for δ (U_2Re)

Figure 24. The 10 a/o Re retained γ' alloy vacuum quenched after 1 hr at 450°C showing microstructure similar to crosshatch γ'_b microstructure. Polarized illumination. X100.

Figure 25. Electron micrograph of the replicated granular microstructure of a decomposed 10 a/o Re retained γ' alloy. The two large particles are carbide inclusions. Etchant: HNO_3, HAc. X2800.

Figure 26. The 10 a/o Re retained γ' alloy vacuum quenched after 1 hr at 600°C showing localized precipitation at grain boundaries and inclusions in granular matrix. Etchant: HNO_3, HAc. X250.

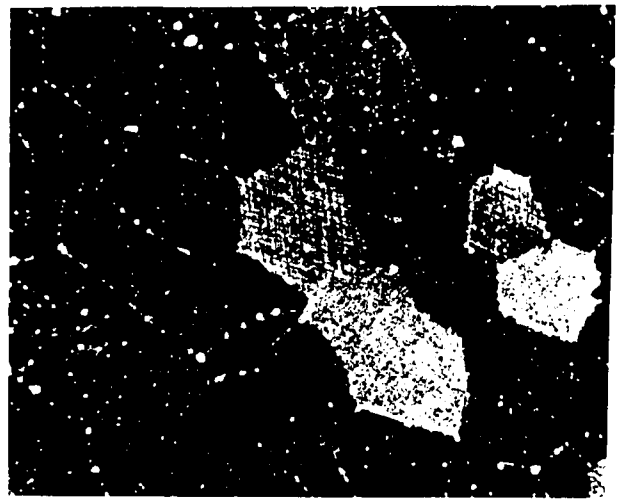

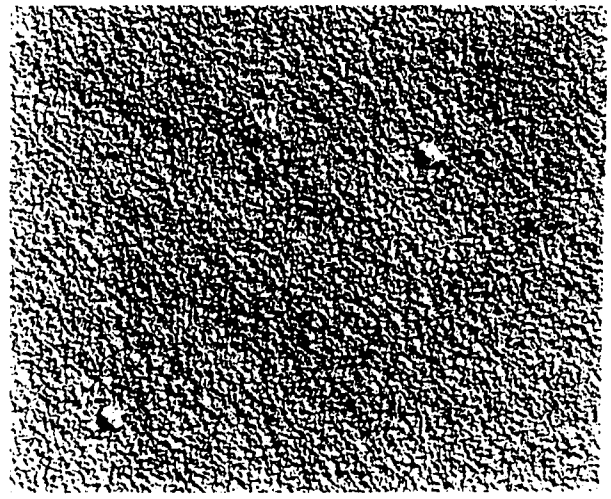

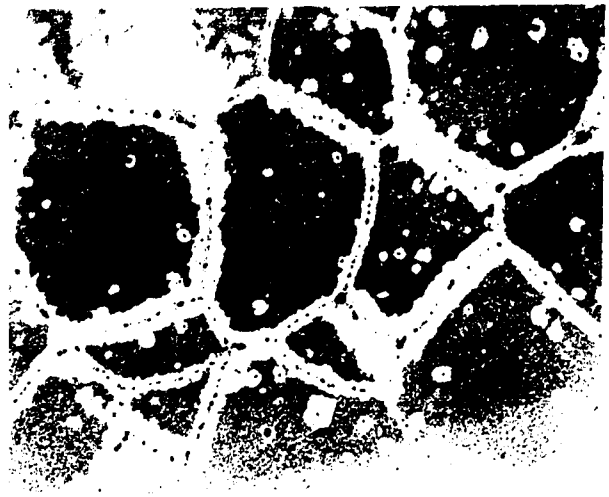

be identical to that of the γ_b° phase obtained on vacuum quenching (Figure 19) from 700°C. The appearance of an unresolved granular structure at higher temperature and the subsequent loss in anisotropy is probably due to the growth of δ. An electron micrograph of the granular structure is shown in Figure 25. The two large particles present have the morphology of carbide particles (51). At 600°C, the remaining supersaturated α decomposes to equilibrium $\alpha + \delta$ via a reaction which nucleates at grain boundaries and inclusions. Figure 26 shows the nature of this localized precipitation. If given time, it would eventually consume the whole grain.

The tremendous increase in hardness (Figure 21) accompanying the γ° decomposition is probably associated with coherency strains between the δ' structure and the matrix from which it grows and the fine dispersion of the resulting δ phase.

An interesting diffraction pattern was obtained from the 10 a/o Re alloy water quenched from 975°C. This pattern consisted of one very broad and flat peak of width 4°Θ centered near the (110) γ peak. The microstructure showed no evidence of decomposition. The stability and decomposition mode of this structure are shown in Figure 21 and Table 20. It is seen that its behavior is quite similar to the retained γ° alloy indicating the structure is very "γ-like". The reason for the "diffuse γ°" structure was not ascertained. It could

be due to an orientation effect since the γ grain size was the largest encountered (average diameter = 0.12 in.). It could also be the result of a heavily faulted structure in which the glide components have been severely restricted as may be the case for the diffuse ω structure observed in Nb-Zr and U-Zr alloys (52). It is interesting to note that unannealed filings taken from retained γ° alloys resulted in diffractometer patterns that were identical to the "diffuse γ°" structure.

Distorted α Structures

Two metastable modifications of the normal orthorhombic α-uranium structure were observed for rapidly cooled γ alloys containing between 3.5 and 9 a/o Re. Figure 27 is a schematic diagram showing the crystallographic differences in x-ray patterns between the stable and metastable α phases. Figure 28 shows Debye-Scherrer photographs of normal α uranium and the two observed metastable modifications.

The α-phase modifications are designated α' and α", the superscripts indicating a departure from the equilibrium structure as determined by x-ray diffraction techniques. The α' modification is a result of a relative contraction of the b parameter with slight expansions along the a and c axes of the normal α-uranium structure. The α" modification occurs at higher rhenium content and is due to a relative contraction

Figure 27. Schematic diagram showing the crystallographic differences between the stable α phase and the metastable α' and α'' phases in the uranium-rhenium system

Figure 28. Debye-Scherrer photographs showing the crystallographic differences between the stable α phase and the metastable α' and α'' phases in the uranium-rhenium system: (a). equilibrium α pattern from 100% U alloy water quenched from 850°C, (b). metastable α' pattern from 5 a/o alloy water quenched from 850°C, (c). metastable α'' pattern from 9 a/o Re alloy water quenched from 850°C.

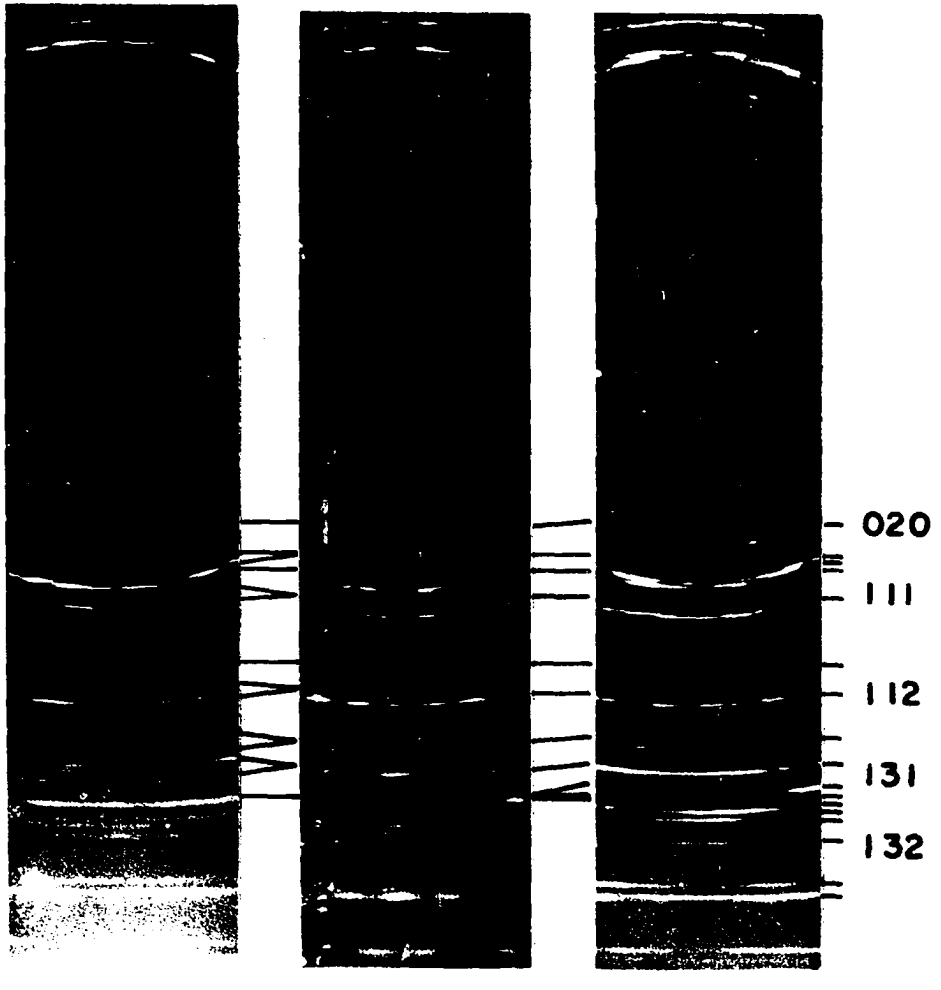
(c)
(b)
(a)
020
111
112
131
132

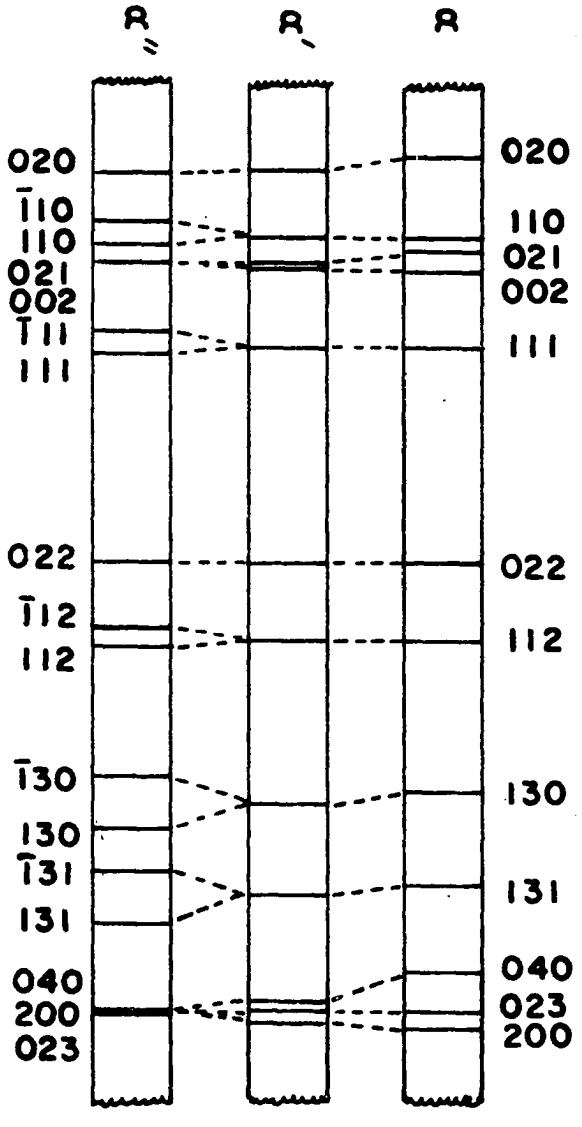
R
R
R
020
$\bar{1}10$
110
021
002
$\bar{1}11$
111
022
$\bar{1}12$
112
$\bar{1}30$
130
$\bar{1}31$
131
040
200
023
020
110
021
002
111
022
112
130
131
040
023
200

of the b parameter, together with a change from an orthorhombic α structure to a monoclinic structure. Similar metastable structures are observed in the U-Mo system (53).

As in the case of the metastable γ structures, subscripts are used to indicate metallographic identification. Acicular, banded and nucleation and growth structures are designated by the subscripts "a", "b" and "n", respectively. Thus, an alloy exhibiting a banded microstructure and which was found by x-ray analysis to have undergone a contraction in the b parameter of the normal orthorhombic structure is designated α'_b. This follows the nomenclature proposed by Lehmann and Hills (54) for metastable U-Mo alloys.

Metallographic structures associated with the α' and α'' phases are shown in Figures 29 through 32. The observed structures varied from granular to very-fine crossed bands (crosshatch structure) to mixtures of fine and coarse bands which often were very acicular in nature. The type of microstructure obtained appeared to be directly associated with cooling rate and composition and not with the crystallographic phase present, i.e., orthorhombic α' or monoclinic α''.

Vacuum quenching yielded microstructures which at low rhenium compositions were granular and which with increasing rhenium content developed a crosshatch structure (compare Figures 29 and 32). Water quenching yielded much coarser structures which at all compositions were considered banded.

Figure 29. The 6 a/o Re alloy vacuum quenched from 850°C showing crosshatch and granular appearing α" microstructure. Polarized illumination. X100.

Figure 30. The 6 a/o Re alloy water water quenched from 850°C showing α' microstructure consisting of coarse and fine bands. Polarized illumination. X100.

Figure 31. The 7 a/o Re alloy water quenched from 850°C showing α" microstructure consisting of coarse and fine bands. Polarized illumination. X150.

Figure 32. The 8 a/o Re alloy vacuum quenched from 975°C showing crosshatch α" microstructure. Note cruciforms around carbide particles. Polarized illumination. X160.

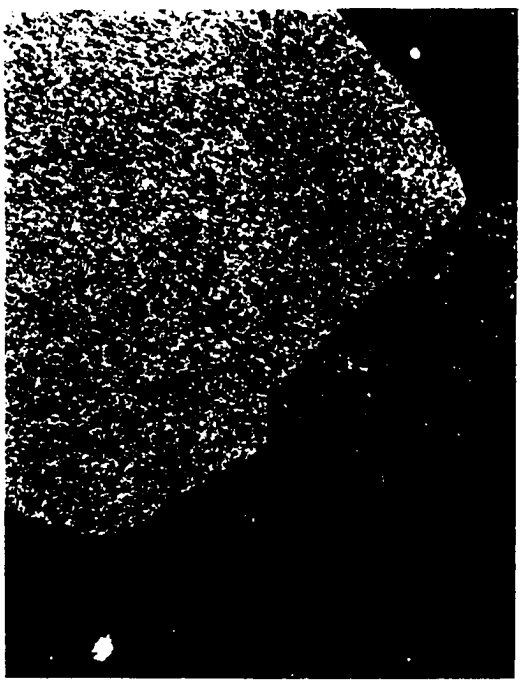

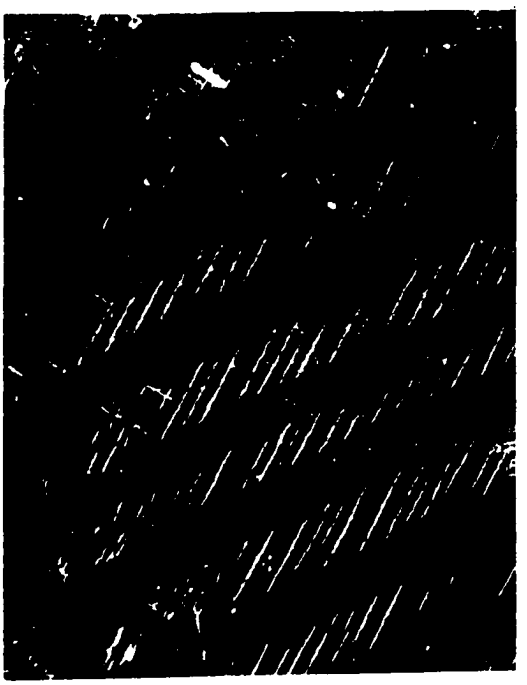

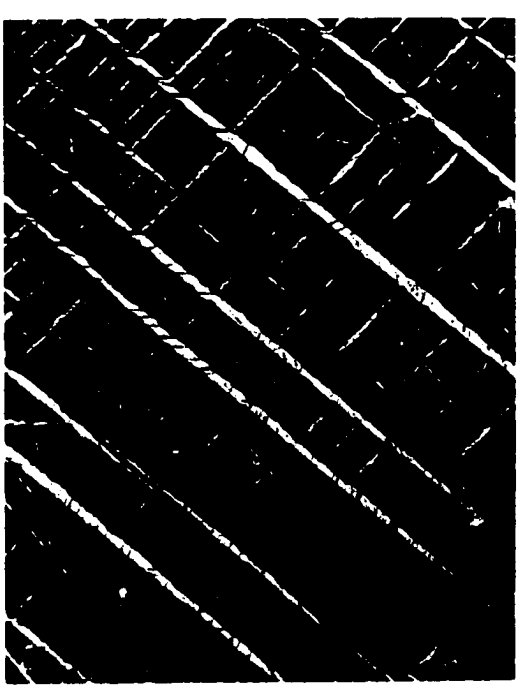

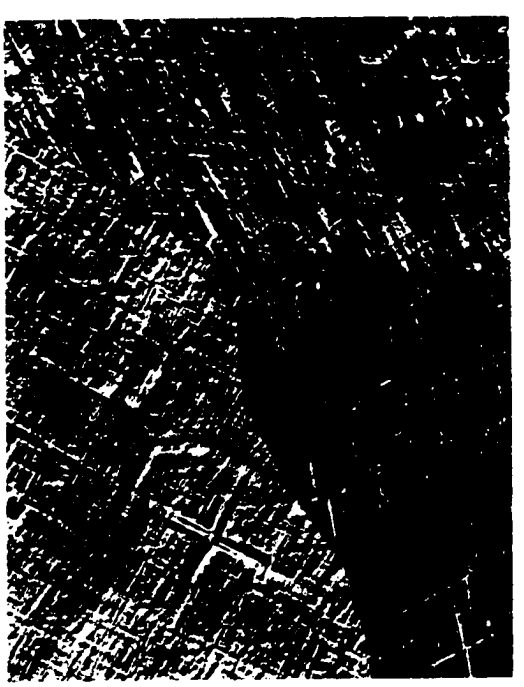

At the higher rhenium contents it was often difficult to say whether the structure should be termed banded or acicular (see Figures 30 and 31). In Figure 30 the large light and dark regions are undoubtedly twin bands. It is difficult to say whether the material perpendicular to the dark bands and at 45° angles to the light bands is due to twin bands or precipitate platelets. The same problem arises in identifying the "fine bands" that are perpendicular to the medium size "bands" and so on. The nature of the α′ and α″ microstructures is further discussed in a later chapter.

Lattice parameters a_o, b_o, c_o and angle γ of the α′ and α″ structures[1] were determined using specimens water quenched from 850°C. The results are represented by solid lines in Figure 33. The main features are:

(1) The values of a_o and c_o increase slightly with increasing rhenium content.

(2) The value of b_o decreases markedly with increasing rhenium content.

(3) A gradual increase in angle γ from 90.0° at 6 a/o Re to 92.2° at 9 a/o Re.

---

[1]Indices were assigned to the α″ reflections by making rough lattice parameter measurements and from these calculating line positions, assuming a monoclinic structure, by use of the computer program described earlier.

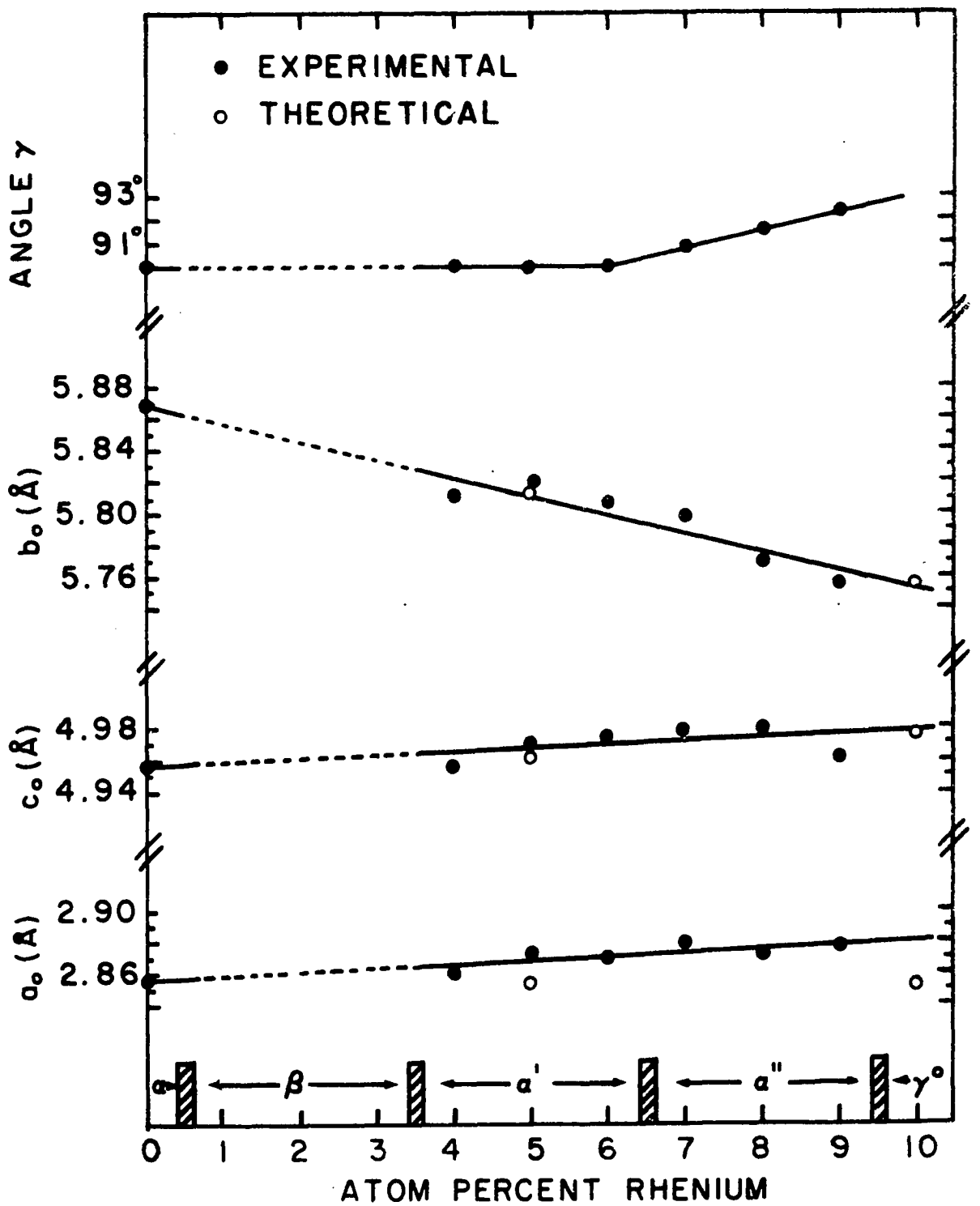

Figure 33. Lattice parameters of the α' and α'' structures developed on water quenching from 850°C

The effect of introducing rhenium atoms into the α-uranium lattice may be explained in the following manner. Figure 34, which is due to Holden (1, p. 27), shows the atomic distances in α uranium. The unequal distances give an ellipsoidal shape to each uranium atom rather than a spherical shape. Assuming that each atom behaves as a hard particle, the rhenium atoms may be represented as hard spheres of radius 1.380 Å when in a coordination of twelve, and uranium atoms may be represented as hard ellipsoids having the dimensions of 1.381, 1.426, 1.630 and 1.660 Å along the directions shown in Figure 34. The substitution of rhenium spheres into the lattice of ellipsoids results in the calculated changes shown as open circles in Figure 33. These calculations were based on geometric reasoning and assuming the solution process can be represented as the substitution of incompressible spherical rhenium atoms into a lattice of incompressible ellipsoidal uranium atoms. Replacement of some of the ellipsoidal uranium atoms by rhenium atoms resulted in a notable contraction of the b_o parameter with a slight increase in the c_o parameter while the a_o value remained nearly constant. The deviation in experimental and calculated lattice parameters may be ascribed to the electronic interaction which was ignored for the purpose of this rough calculation.

The layered corrugated structure of α uranium results

BOND	INTERATOMIC DISTANCE
AB, CD, GH, IJ,	2.852 Å
AC, BD, EF, GI, HJ	2.762 Å
GF, HF, CE, DE	3.322 Å
CF, DF, IF, JF GE, HE, AE, BE	3.261 Å

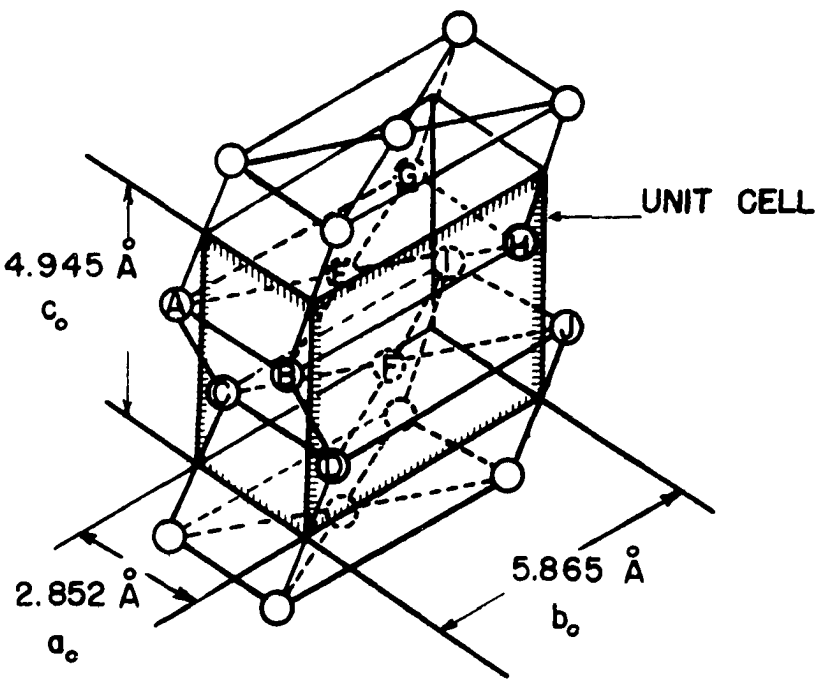

Figure 34. Interatomic distances in the α-uranium structure as taken from Holden (1, p. 27)

from a combination of metallic bonding and hybridization of atomic orbitals to form covalent bonds. The uranium configuration has been likened to a trigonal bypyramid as in PCl_5 by Pauling (19, p. 413), the big difference being the absence of an atom in α uranium at one of the corners of the equatorial triangle. Pauling suggests that this position is occupied by two 7s electrons. The location of the electrons is in the <010> direction which is the direction of weak bonding in the crystal. This b_o parameter decreased as the rhenium content increased, the shorter bond being an indication of strengthing in this direction. In addition, the bond angle within the corrugated layers increased with increasing rhenium content, tending to smooth out the layers.

Direct γ→α Transformation

Duwez (55) has shown that rates of cooling up to 10,000°C/sec from the γ phase do not prevent the formation, in order, of β and α in pure uranium. This sequence of phase changes at fast cooling rates is also observed for U-Re alloys containing less than about 3.5 a/o Re. Some observations supporting this sequence of phase changes are:

(1) For alloys containing less than 3.5 a/o Re which were α at room temperature, two thermal arrests were detected on cooling.

(2) Irregular α grains, similar to those obtained on

quenching pure uranium, were observed on vacuum quenching the 1 a/o Re alloy.

(3) Duplicate alloy specimens, with the same thermal and mechanical histories, containing 1 a/o Re were vacuum quenched from within the β and γ fields, respectively. The microstructures as well as the hardness were nearly identical in both the β and γ quenched specimens.

Thus, it would seem that under these conditions the formation of intermediate β is not suppressed.

In the section on β phase retention it was shown that as the rhenium content increased the $\beta \rightarrow \alpha$ transformation temperature was lowered and that the stability of the β phase increased with increasing rhenium content. Inspection of Tables 12 through 15 show that on either water quenching or vacuum quenching from the γ region the 3 a/o alloy was β while the 4 a/o alloy was α'. If the β phase had formed in the 4 a/o alloy, one would expect it to be present at room temperature. The absence of the β phase suggests a direct $\gamma \rightarrow \alpha'$ transformation at fast cooling rates.

This viewpoint is further supported by the following observations:

(1) A 3.8 a/o Re alloy water quenched from the γ region had an α' structure while one cooled at a slower rate (400°C/hr) had a β structure.

(2) The 4 a/o Re alloy cooled at 25°C/hr had retained β present, while as mentioned above the rapidly cooled alloys were completely converted to α'.

(3) The microstructure of the α' or α'' alloys all showed straight grain boundaries (Figure 35) which were those of the original γ grains. All the retained β alloys showed very irregular grain boundaries (Figure 36). Likewise, any α formed from β had highly irregular grain boundaries (Figure 37). Had the α' or α'' formed via a double transformation, i.e., $\gamma \rightarrow \beta \rightarrow \alpha'$, the microstructure would be expected to be irregular.

Thus, at fast cooling rates, the postulation of a direct $\gamma \rightarrow \alpha'$ transformation is necessary to explain the observed behavior.

This behavior along with certain other aspects of the reaction kinetics observed in U-Re alloys can be rationalized by considering the hypothetical continuous cooling diagram shown in Figure 38. In this it is imagined the alloy is cooled at varying rates from a chosen temperature in the γ range to some lower temperature. The start of transformation from one phase to another is then plotted as a function of time and temperature. If the alloy is cooled from the γ range at various rates, various transformations may occur. At rate 1, γ will transform to β which will transform to α. At rate 2, γ will transform to β, which would be retained to

Figure 35. The 4 a/o Re alloy water quenched from 850°C showing the banded microstructure of the α' state amidst prior γ grain boundaries. Polarized illumination. X100.

Figure 36. The 4 a/o Re alloy vacuum quenched from 662°C showing highly irregular β grains. Polarized illumination. X150.

Figure 37. The 1 a/o Re alloy vacuum quenched from 662°C showing highly irregular α grains. Polarized illumination. X150.

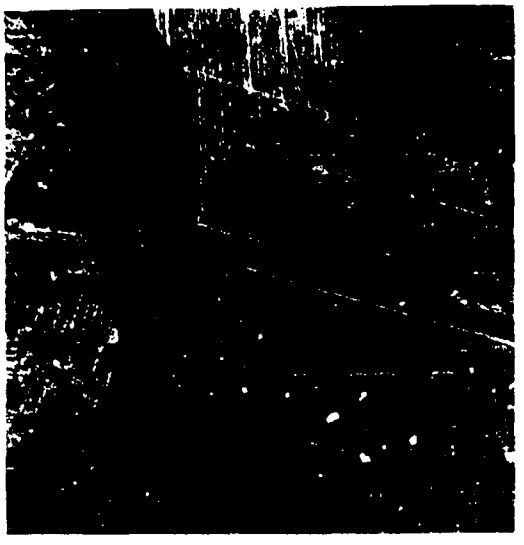

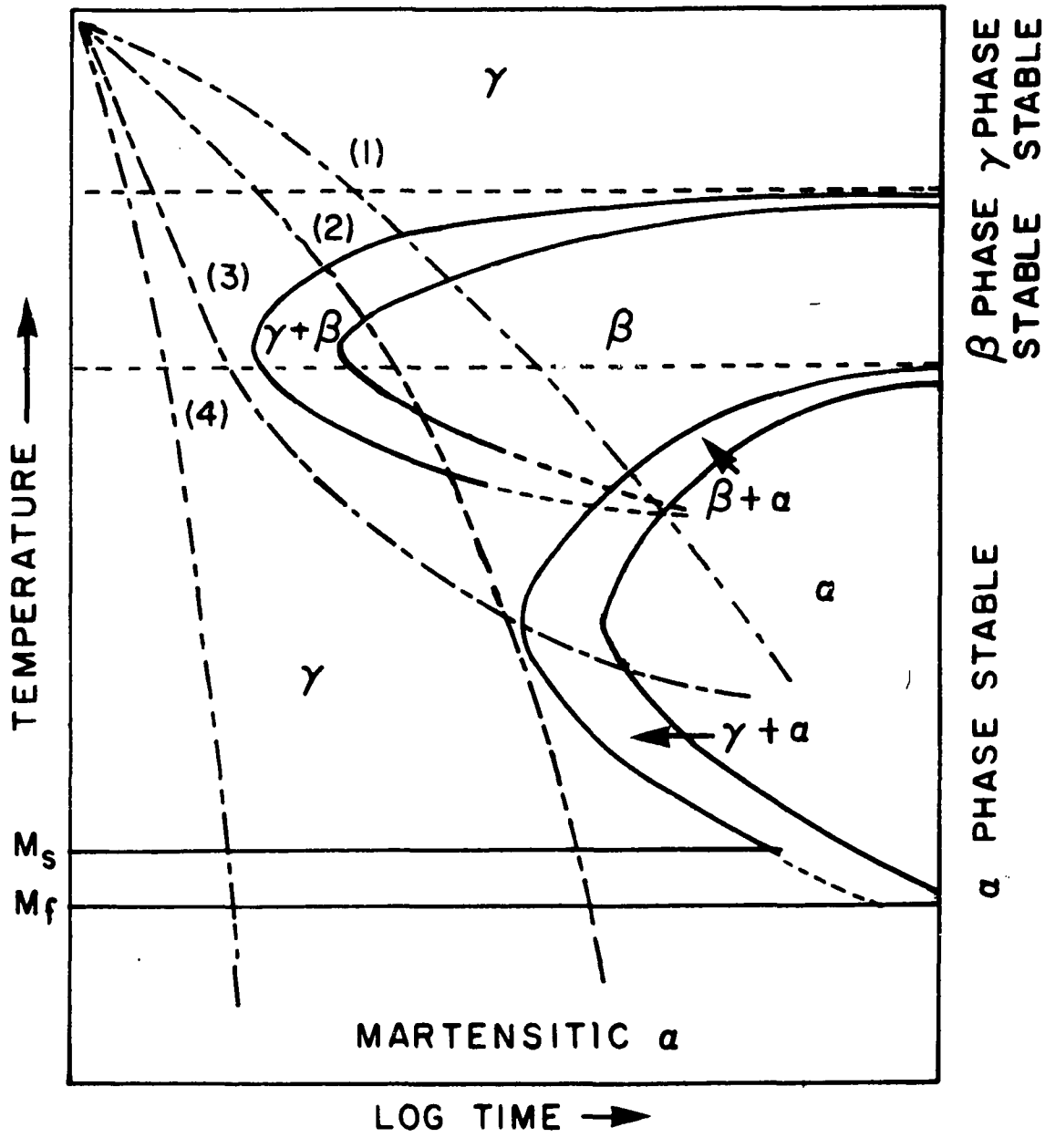

Figure 38. Hypothetical CCT diagram for a γ-uranium alloy

room temperature, or transformed to martensitic α depending on the M_s and M_f temperatures. At rate 3, γ will transform directly to α by diffusion controlled nucleation and growth, and at rate 4 depending whether M_s is above or below room temperature, γ would be retained or transformed to martensitic α. All of these reactions are found in the U-Re system.

Sequence of Phase Changes

In the preceding sections it has been shown that during the transformation of γ to α, the transition structures α', α'', γ_b^* or γ^* may be rendered metastable. Figure 39 summarizes the effect of composition, cooling rate and quenching temperature in producing these metastable structures. The mode of formation of these structures, and their relationship to cooling rates may be explained in the following manner.

It has been proposed by others (56) that increasing additions of molybdenum progressively stiffen the uranium lattice, thus making it more and more resistant to shear, and that the effect of increased cooling rate is to favor the shear process. This presumably arises from increased hydrostatic pressures caused by faster cooling rates and also from increased transformation stresses due to faster rates of transformation, once shear has started. Tangri also proposed that an optimum value of the ratio of quenching stresses to

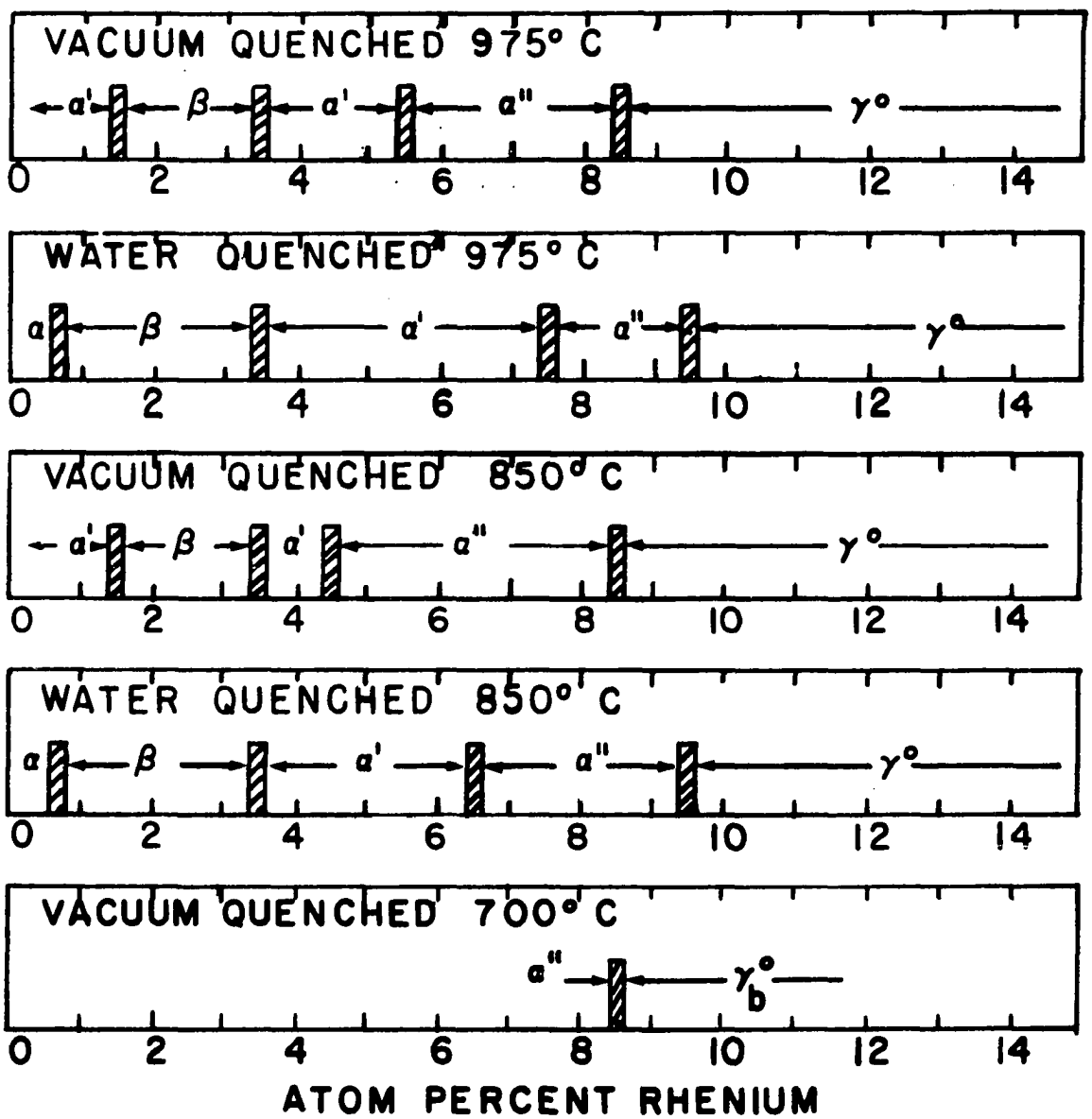

Figure 39. Effect of cooling rate and quenching temperature on the structures produced in the uranium-rhenium system

lattice stiffening, which for convenience of discussion was called the "stress/stiffening ratio", is required to generate any given martensitic phase.

Hatt and Roberts (52) have shown from x-ray diffraction work on a 50 a/o U-Zr single crystal that the α structure can be generated from a BCC γ structure by a shear on $\{112\}_\gamma$ planes in a $\langle 111\rangle_\gamma$ direction. They furthermore, developed a crystallographic model which explains the generation of the α', α'' and γ° structures in the uranium-molybdenum system by progressively restricting the amount of shear. Whereas shear on only one set of $\{112\}_\gamma$ planes is required to generate the α' and α'' structures, two sets of $\{112\}_\gamma$ planes are involved in the generation of γ° structure.

In the light of these observations the following argument may be developed. Consider the projection of atoms in the BCC γ structure onto a $(110)_\gamma$ plane (Figure 40). It may be seen that a critical amount of shear AC is required to change the value of angle γ to 90° and thus generate an orthorhombic structure. On water quenching alloys containing 3.5 to 6.5 a/o Re, the optimum stress/stiffening ratio is realized, thus producing the critical amount of shear required to generate the α' structure. With increasing rhenium additions, the lattice is steadily stiffened until with 7.0 a/o Re content the lattice is too stiff to permit the critical amount of shear. Only a limited shear AB is produced resulting in an

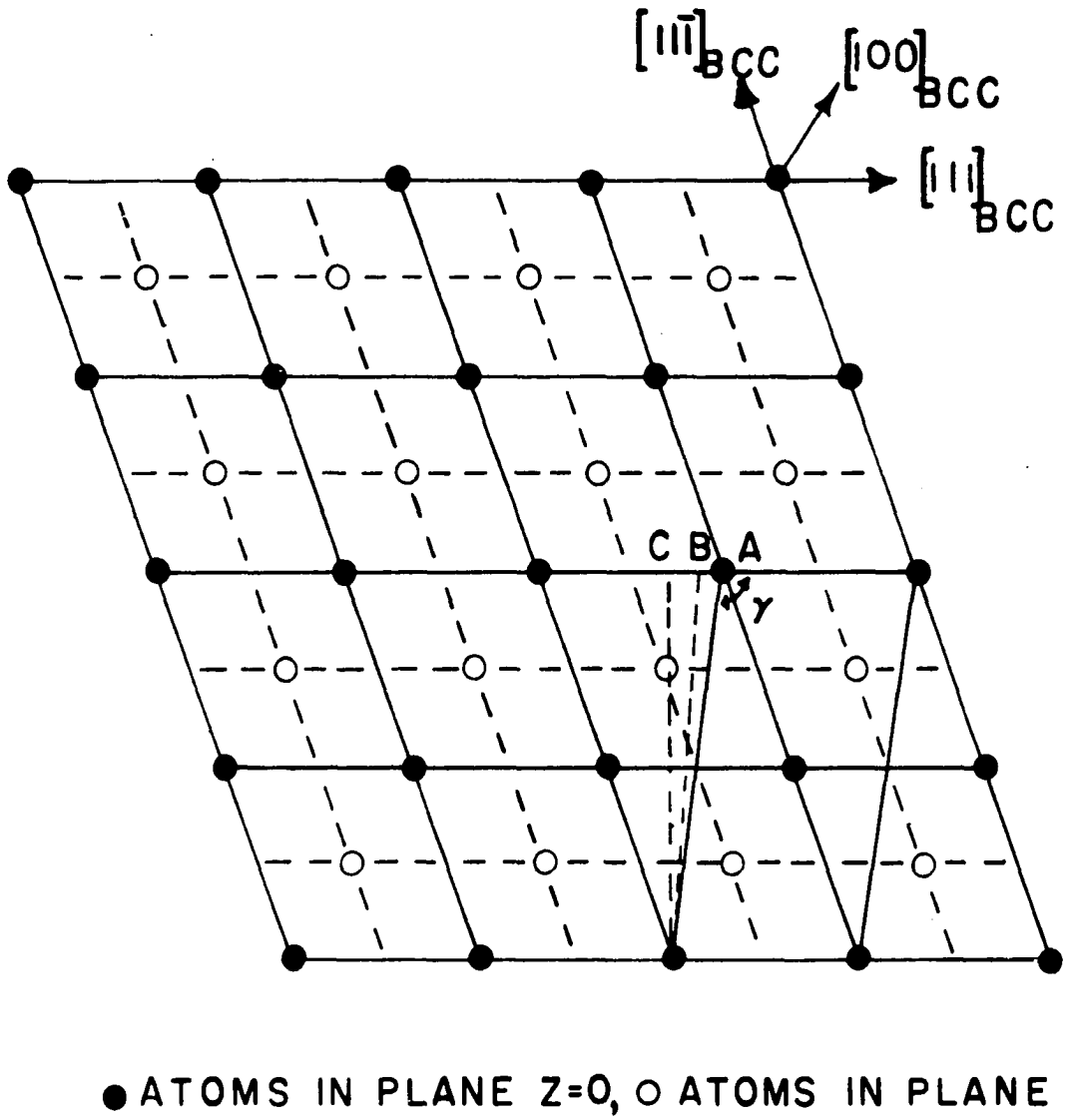

Figure 40. Projection of atoms in BCC structure onto a (110) BCC plane showing the sequence of {112} BCC planes

angle γ of 90.8°, thus yielding a monoclinic α'' structure. Further additions of rhenium progressively restrict the amount of shear, thus causing angle γ to steadily increase to a value of 92.2°, as observed in the 9 a/o alloy. In highly stiffened lattices, as for example in alloys containing 10, 12 and 14 a/o Re only a very limited amount of shear takes place resulting in the generation of the γ° structure.

During the development of this argument, the author's attention was drawn to a similar interpretation explaining the occurrence of metastable phases in the uranium-molybdenum system (56).

The effect of slower cooling rate in a lattice of any given rhenium content and thus of a given stiffness will relatively restrict the amount of shear. This would explain the generation of the α'' structure on water quenching the 9 a/o alloy from 850°C which on vacuum quenching under identical conditions yielded a γ° structure. It can be seen in Figure 39 that, in each case, the effect of rapid quenching is to produce a structure further removed from the parent BCC phase than that obtained with slower cooling, indicating that severe quenching causes the transformation to go towards completion.

This effect is well illustrated by the photomicrographs of a 9 a/o Re alloy vacuum quenched (Figure 41) and water quenched (Figure 42) from 975°C. The rapidly cooled alloy

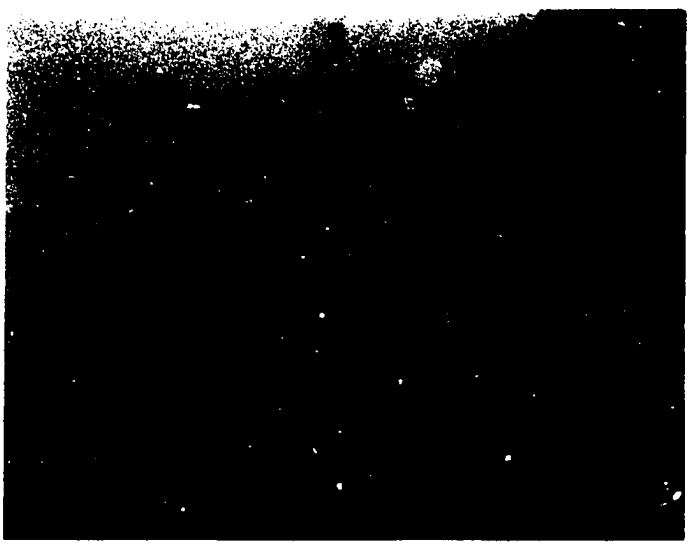

Figure 41. The 9 a/o Re alloy vacuum quenched from 975°C showing clean equi-axed grains of γ° structure. Compare with Figure 42. Polarized illumination. X150.

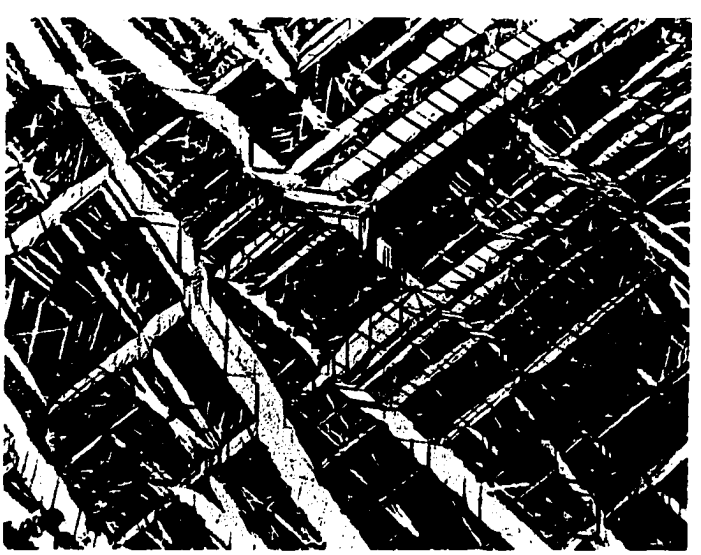

Figure 42. The 9 a/o Re alloy water quenched from 975°C showing single-phase, martensitic-like α'' structure. Compare with Figure 41. Polarized illumination. X100.

has undergone a shear transformation, while the slower cooled alloy appears untransformed. Work by Hills et al. (25) on end quenched U-Mo rods showed similar structural variations. The slow cooled end of a 2.0 a/o molybdenum rod so quenched showed γ° whereas the structure of the rapidly cooled end was α''. An end-quenched 7.5 a/o molybdenum rod had an α'' structure throughout its length but the x-ray pattern of the rapidly quenched region showed only a little line splitting, indicating that its monoclinic angle was very near 90°, i.e., the structure was approaching α'.

Similar observations have been reported for the metastable ω phase in Ti-Zr alloys (57). The ω structure can be regarded as an intermediate between the BCC high temperature phase and the low temperature HCP structure arising from an incomplete shearing of $\{112\}_{\beta}$ planes in $\langle 111\rangle_{\beta}$ directions (58). This structure was obtained by a slower cooling of alloys of composition 40-80 a/o zirconium; rapid quenching caused the transformation to α' to go to completion.

Metallographic Observations

General considerations

Various metallographic observations have been presented in earlier sections to substantiate certain arguments. In this section, metallographic observations not previously discussed are presented and their relationship to earlier

arguments are developed.

After all heat treatments, each of the alloys was examined for hardness, grain size, crystal structure, microstructure and in some instances, density. The results of these examinations are tabulated in Tables 9 through 15. Many of these tabulated results are presented graphically in Figures 43 through 48.

Density measurements

The as-cast and homogenized alloys were examined for density. The results of these examinations are tabulated in Tables 9 and 10.

The 1, 2 and 3 a/o Re alloys contained numerous small cracks and voids that led to the low density values reported for these compositions. At other compositions the density change with composition and structure is small and not regular. This is not surprising since the x-ray densities of the α, β and γ forms at room temperature[1] are 19.07, 18.80 and 18.82 g/cm^3. Likewise, Jackson et al. (24) report gravimetrically determined densities of 18.97 and 18.53 for

---

[1]The x-ray density of α uranium at room temperature is that listed by Klepfer and Chiotti (6). The value for β uranium is calculated from Thewlis' (40) values of a_o and b_o as corrected to room temperature using the coefficients of thermal expansion as determined by Klepfer and Chiotti (6). The value for γ uranium is calculated from the a_o at 800°C and coefficient of thermal expansion as reported by Klepfer and Chiotti (6).

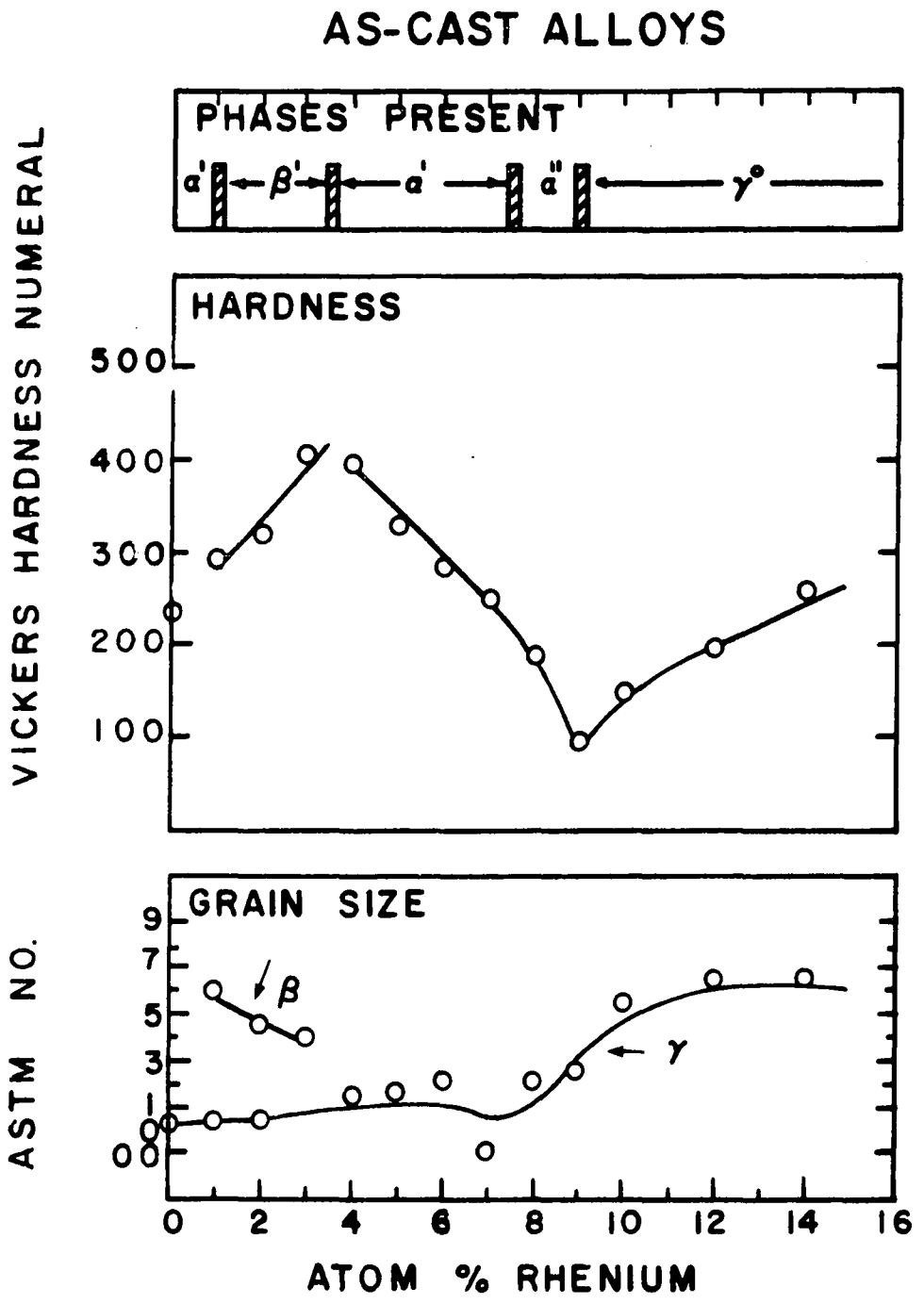

Figure 43. Some results from examination of as-cast alloys

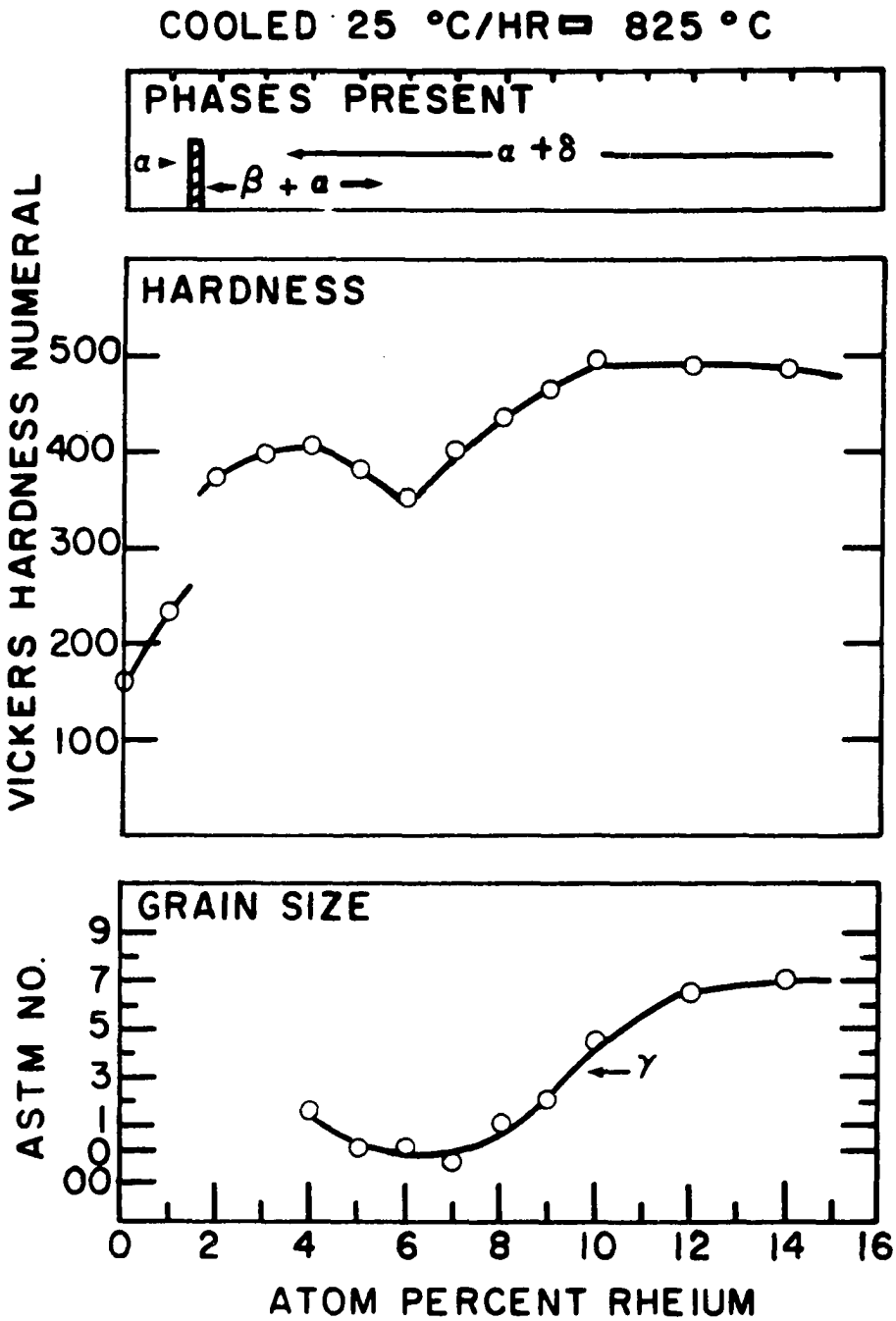

Figure 44. Some results from examination of alloys cooled at 25°C/hr after 4 days at 825°C

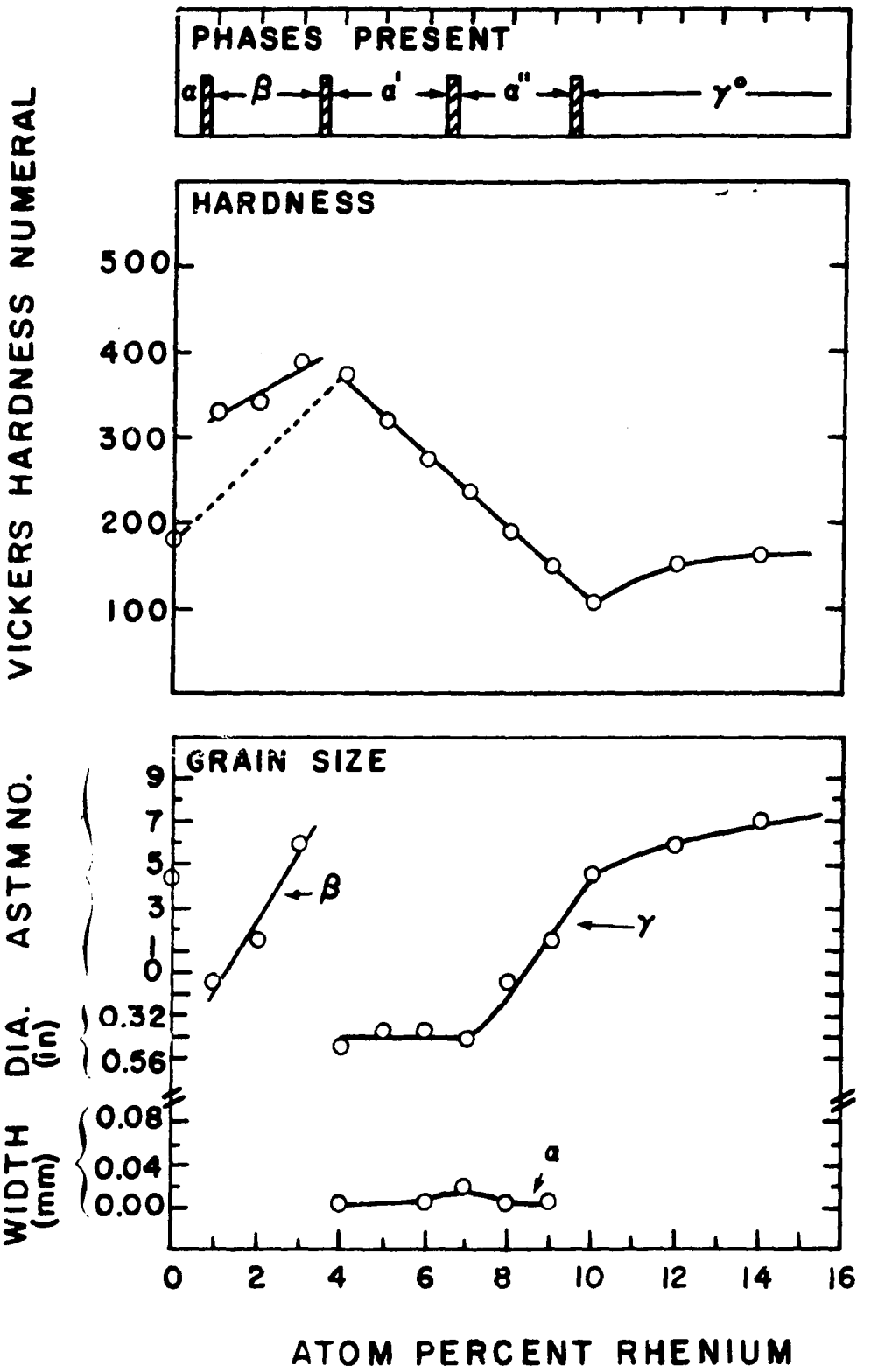

Figure 45. Some results from examination of alloys water quenched after 4 hours at 850°C

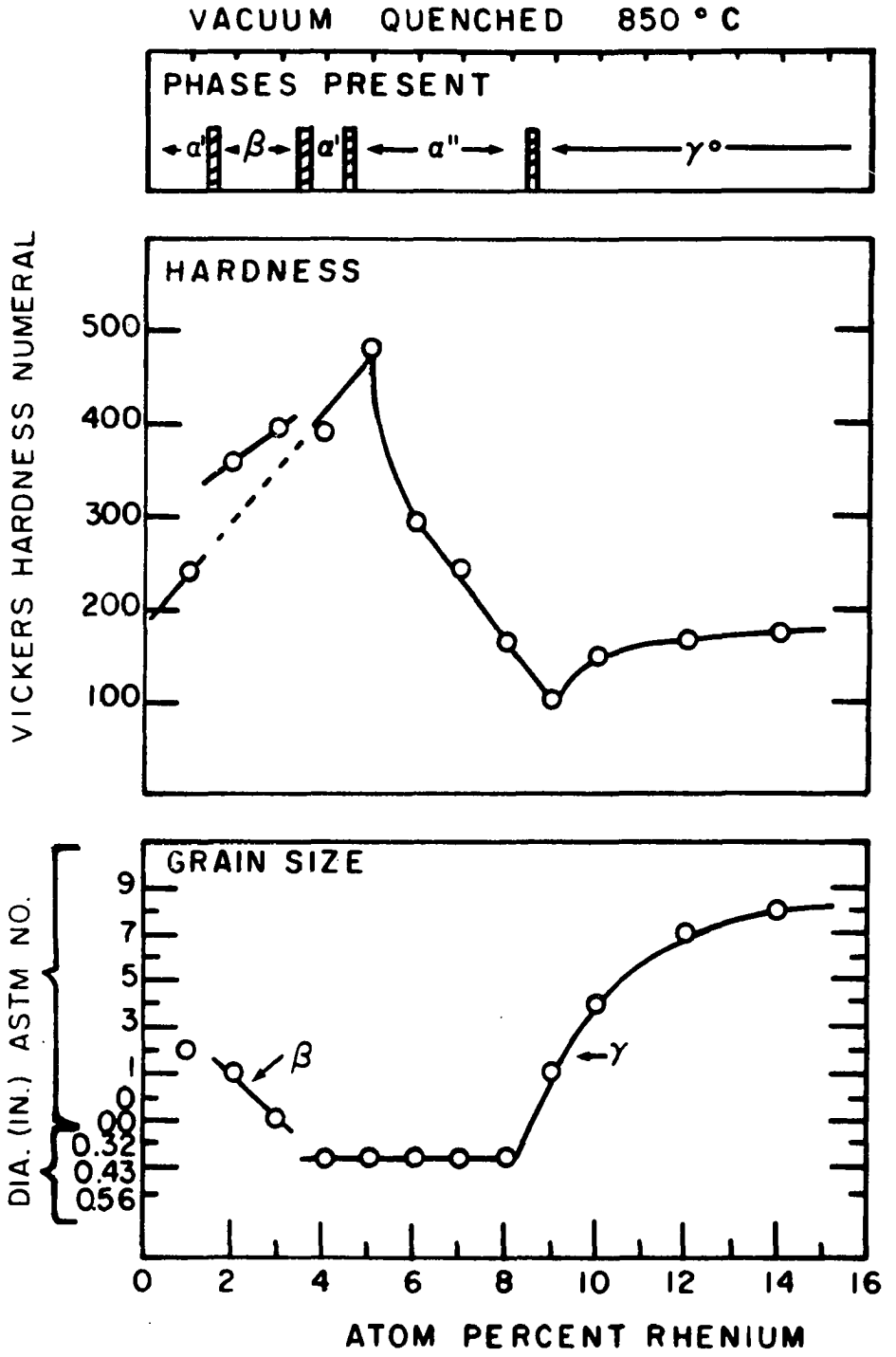

Figure 46. Some results from examination of alloys vacuum quenched after 4 hours at 850°C

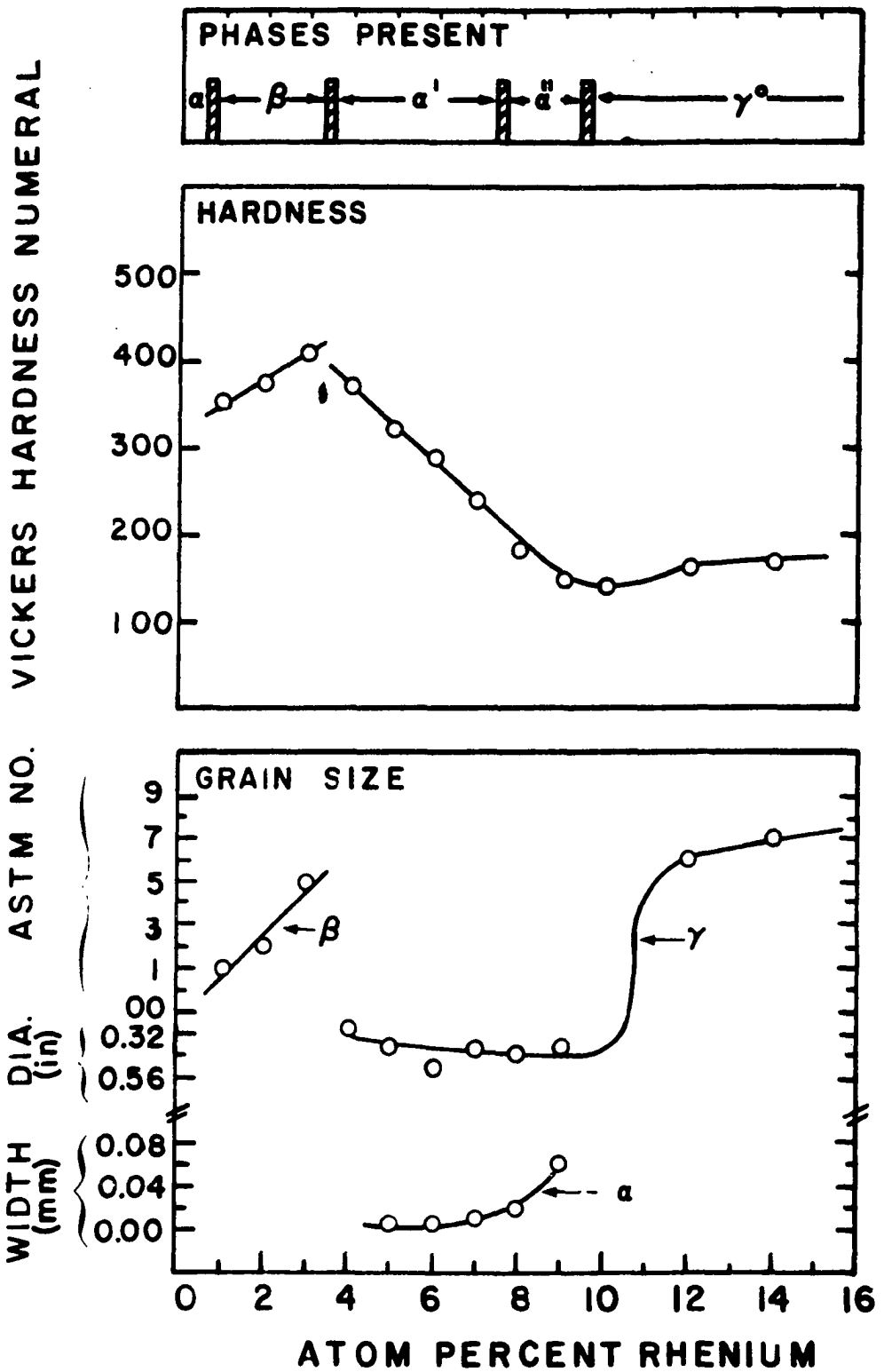

Figure 47. Some results from examination of alloys homogenized for 2 hours at 850°C and then water quenched after 30 minutes at 975°C

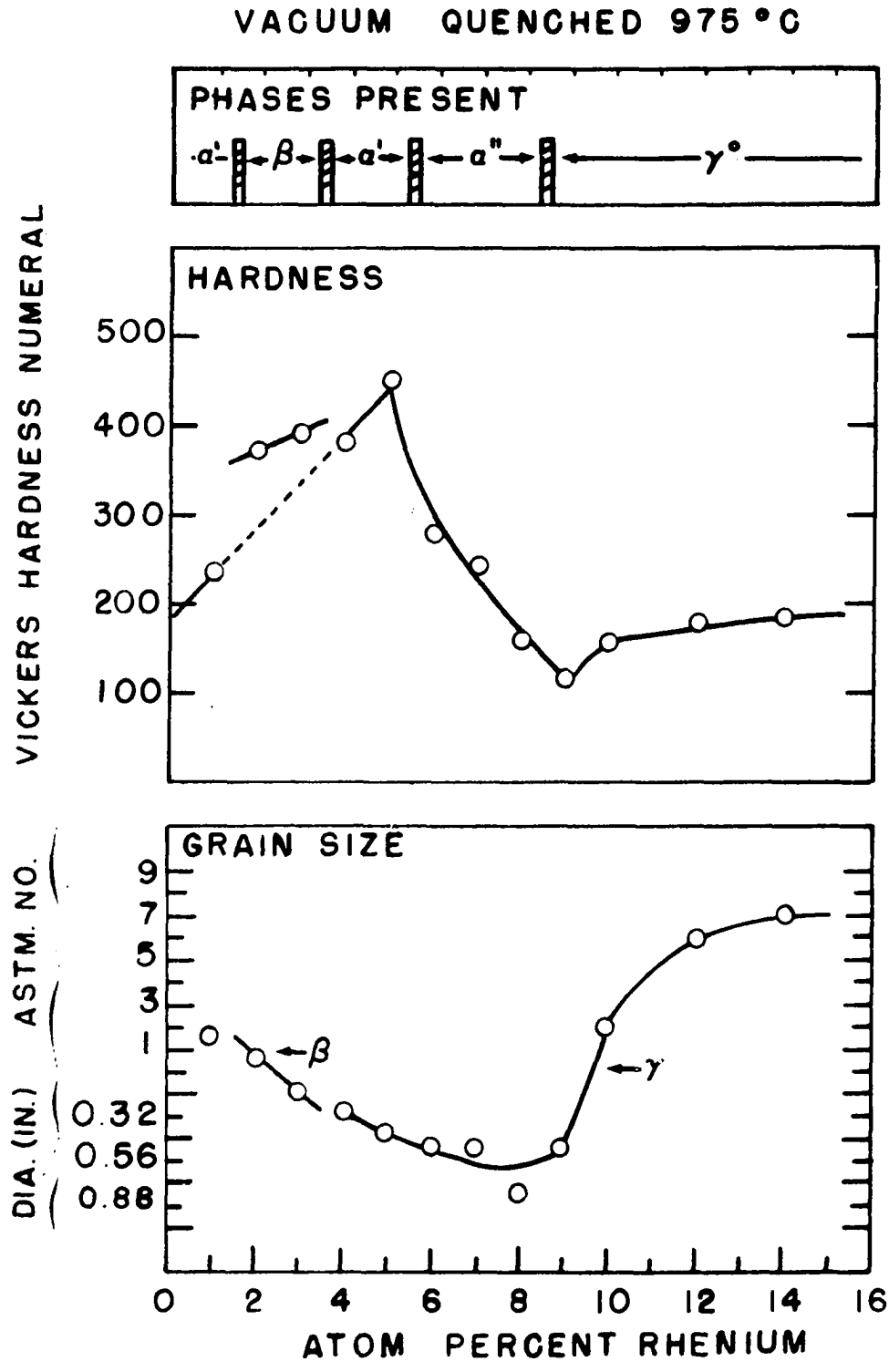

Figure 48. Some results from examination of alloys homogenized for 2 hours at 850°C and then vacuum quenched after 30 minutes at 975°C

the δ (U_2Re) and ϵ (URe_2) intermediate phases, respectively. Also, the samples weighed less than 3 grams, thus magnifying the error in weight measurements; and room temperature fluctuations were difficult to control. Since the density changes were small and the inherent error large for small specimens, the density determinations were discontinued.

The observed density values are of the proper magnitude and reflect the similarity in density of the various phases. The low densities of the β structures are due to the numerous cracks and voids at these compositions. The δ alloys are more dense than expected and this is partly due to a contraction of the BCC cell on the addition of rhenium atoms.

As mentioned earlier, the as-cast 1, 2 and 3 a/o Re alloys had numerous small cracks present. During cooling of these compositions, β forms at the low end of the temperature gradient and is accompanied by a volume decrease. The geometry of the as-cast button does not lend itself readily to a quantitative treatment, especially when unidirectional cooling is involved. A qualitative explanation is proposed. Consider a pieplate of β uranium supporting supercooled δ uranium. The δ will transform at this interface and in so doing wishes to contract. The contraction is restricted by the underlying β uranium, resulting in tangential and radial tension in the newly formed β phase. The δ at the interface will be in compression thus resulting in a longitudinal

tension in the newly formed β. The result of the near hydrostatic tension in the newly formed β will be to prevent plastic flow and when the residual stress exceeds the fracture stress, cracks will develop.

For alloys containing more than 3.5 a/o Re, the as-cast buttons were free of cracks. Had any β formed during the rapid cooling, cracks would be expected in the as-cast buttons. This is further evidence for the direct $\gamma \rightarrow \alpha'(\alpha'')$ transformation.

Hardness

The hardness-composition curves for either vacuum quenched or water quenched γ alloys were quite similar. The general shape of the curve is explained in the following manner. The initial α hardening is a combined solid solution and precipitation hardening effect. The early discontinuity is due to the higher inherent hardness of the β solid solution. The increase in β hardness with composition is a combined solid solution (due to supersaturation) and precipitation hardening effect.

The linear decrease in hardness with composition of the α' and α'' structures is puzzling. At first glance it might appear that the decrease is associated with the coarsening of the structure, i.e., the appearance of bands and large lenticular plates. However, comparison of vacuum quenched and water quenched microstructures disproves this and indicates

the softening is inherent in the transition structure. Another possibility is that as the rhenium content is increased, the tendency for precipitation is lessened (possibly due to the $\gamma \rightarrow \alpha', \alpha''$ reaction occurring at a lower temperature); and at the lower compositions an early stage of precipitation occurs which is undetectable by normal x-ray and metallographic techniques. It has been shown by others (33) that precipitated phases that are undetectable by normal x-ray and metallographic techniques are often found to markedly affect hardness. In any event, the continuous and gradual hardness change in passing from γ° to α'' to α' lends credence to the argument that γ°, α'' and α' are intermediate transition states in the formation of α from γ.

The hardness minimum of the γ quenched alloys is always associated with the first appearance of the ductile γ° structure. The increase in hardness at higher rhenium contents is due to the grain boundary network of ϵ phase.

Figure 49 contrasts the difference in hardness for the vacuum quenched, water quenched and slow cooled alloys. The anomaly at 1 a/o is due to retention of the β phase on water quenching from the γ field whereas vacuum quenching yielded α. The higher hardness of the 4 and 5 a/o Re alloys vacuum quenched from the γ region is due to the formation of a detectable second phase. Water quenching of these compositions from the γ field resulted in apparent single phase

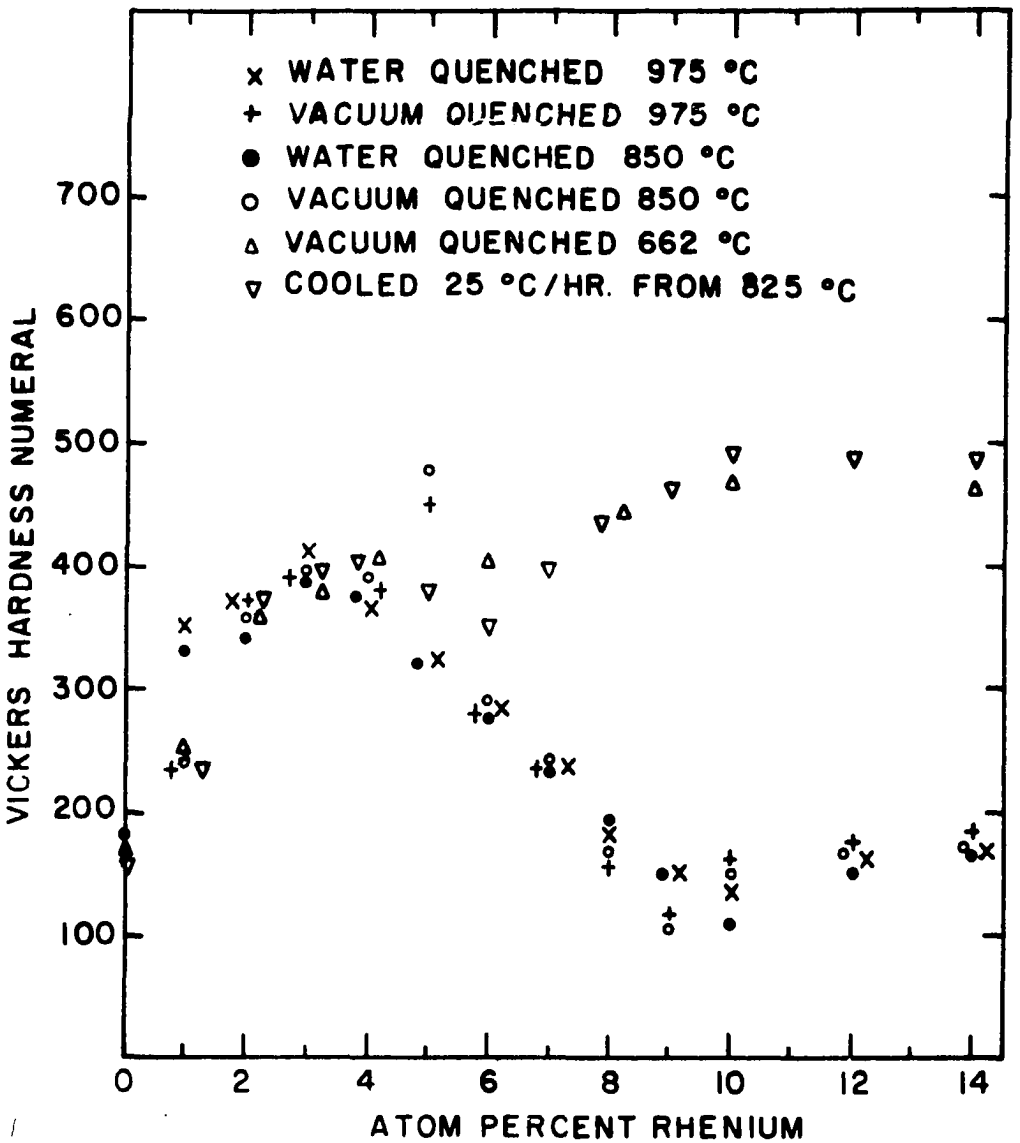

Figure 49. Comparison of hardness values after various thermal treatments

structures. The anomaly at the minimum for γ quenched alloys is due to the effect of cooling rate on structure produced, i.e., α'' or γ°. At higher rhenium contents, the slightly higher values for γ quenched alloys may be attributed to a precipitation hardening effect. The similarity in hardness at higher rhenium contents of the β quenched and slow cooled γ alloys is interesting. The uranium phase present was β in one case and α in the other, thus the hardness is probably governed by the δ phase distribution which was similar in both cases.

Grain size

The results of the grain size measurements are shown graphically in Figures 43 through 48. It is seen that all heat treatments used resulted in similar γ grain sizes that were quite large except at relatively high rhenium contents. The reason for the restricted grain growth at high rhenium contents is undoubtedly the grain boundary network of URe_2 particles.

An interesting grain size trend for retained β alloys obtained on γ quenching is also readily seen. The β grain size of water quenched alloys decreased with increasing rhenium content whereas on vacuum quenching the β grain size increased with increasing rhenium content. This effect is probably associated with the greater degree of supercooling of the $\gamma \rightarrow \beta$ reaction on water quenching and the resulting

larger number of nucleation sites.

Microstructures

Representative microstructures for vacuum quenched and water quenched γ alloys are shown in Figures 50 through 53.

The γ quenched pure uranium alloy (Figure 50a) was characterized by irregular grain boundaries and highly twinned grains. A similar microstructure was observed in the 1 a/o Re alloys vacuum quenched from 850° and 975°C (Figure 51a and 53a). The 1 a/o Re alloys water quenched from 850° or 975°C were retained β (Figure 52a). The retained β phase at these compositions, as shown earlier, decomposed at room temperature by the isothermal growth of martensitic α plates in the β matrix. The 2 and 3 a/o Re alloys either vacuum quenched or water quenched from 850° or 975°C were retained β (Figures 50b, 51b, 53b and 53c). The retained β at these compositions was quite stable and no decomposition at room temperature was detected. The grain boundaries in these alloys were often characterized by a sawtooth appearance.

For water quenched alloys containing 4 to 9 a/o Re, the M_s temperature for the direct $\gamma \rightarrow \alpha'(\alpha'')$ transformation lies above that for the $\gamma \rightarrow \beta$ transformation and only α' or α'' is observed in the microstructure of these alloys. These alloys were distinguished by smooth γ grain boundaries and coarse microstructures which at all compositions were banded and/or acicular in appearance. Figures 50c through 50g and

Figure 50. Representative microstructures of a series of alloys water quenched after 4 hours at 850°C

(a). The 100% U alloy showing twinned α grains. Polarized illumination. X150.

(b). The 3 a/o Re alloy showing retained γ microstructure. Polarized illumination. X100.

(c). The 4 a/o Re alloy showing banded α' phase. Polarized illumination. X100.

(d). The 6 a/o Re alloy showing large bands and fine bands or plates of α' microstructure. Polarized illumination. X100.

(e). The 7 a/o Re alloy showing acicular appearing α'' microstructure. Polarized illumination. X100.

(f). The 8 a/o Re alloy showing banded α'' microstructure. Polarized illumination. X150.

(g). The 9 a/o Re alloy showing banded α'' microstructure. Polarized illumination. X100.

(h). The 10 a/o Re alloy showing γ^{o} microstructure. Polarized illumination. X150.


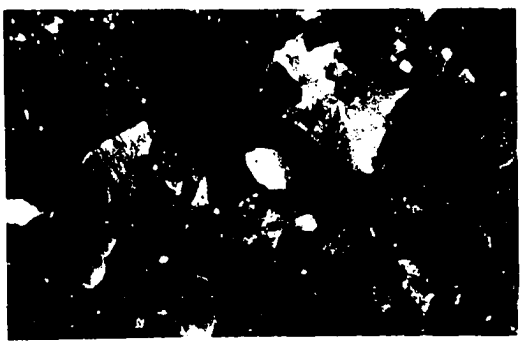
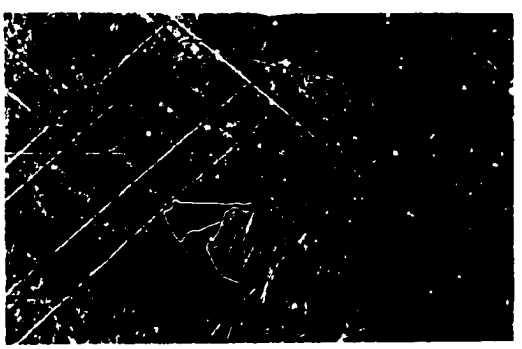
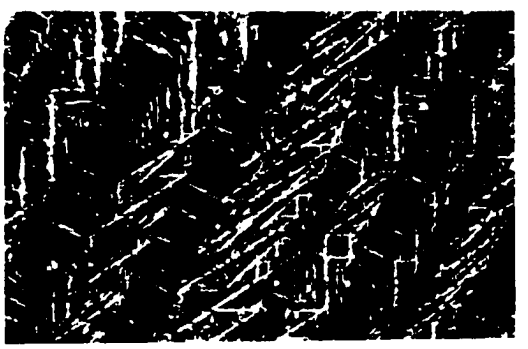
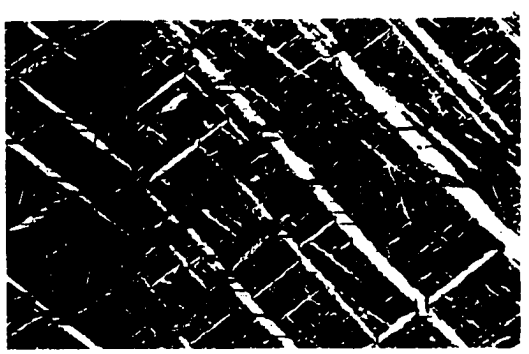


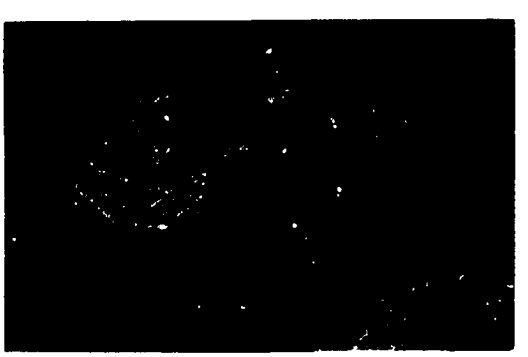

Figure 51. Representative microstructures of a series of alloys vacuum quenched after 4 hours at 850°C

(a). The 1 a/o Re alloy showing irregular and twinned α grains. Polarized illumination. X100.

(b). The 3 a/o Re alloy showing retained β microstructure. Note sawtooth appearance of β grain boundaries. Polarized illumination. X100.

(c). The 4 a/o Re alloy showing the granular appearing α' phase and small amounts of a second phase (white). Polarized illumination. X100.

(d). The 6 a/o Re alloy showing the mixed crosshatch and granular appearing α'' phase. Polarized illumination. X100.

(e). The 7 a/o Re alloy showing the coarse crosshatch α'' phase. Polarized illumination. X100.

(f). The 8 a/o Re alloy showing the crosshatch α'' microstructure. Polarized illumination. X100.

(g). The 9 a/o Re alloy showing the δ° microstructure. Polarized illumination. X100.

(h). The 14 a/o Re alloy showing δ° phase with grain boundary network of URe_2. Polarized illumination. X100.

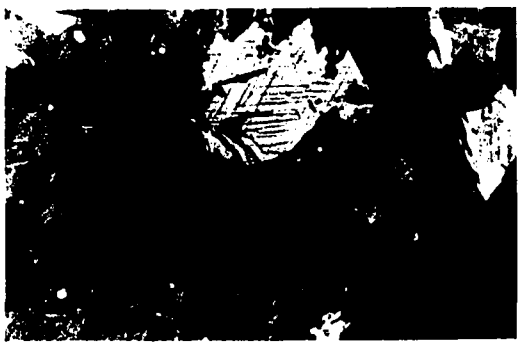


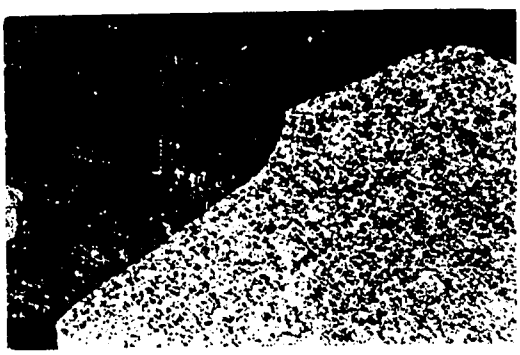
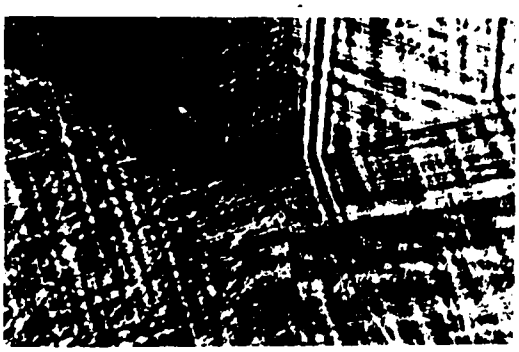
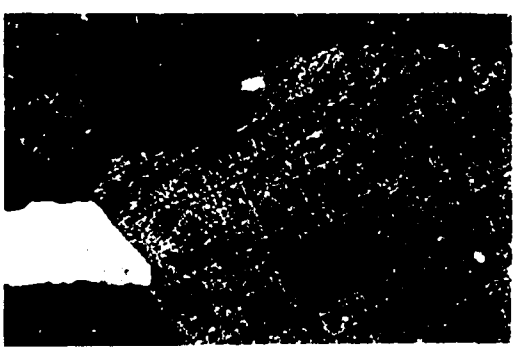

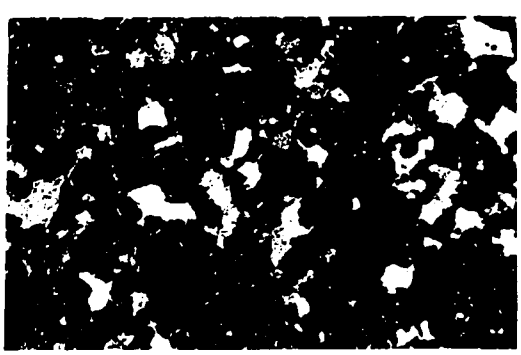

Figure 52. Representative microstructures of a series of alloys water quenched after ½ hour at 975°C

(a). The 1 a/o Re alloy showing retained β. Polarized illumination. X150.

(b). The 5 a/o Re alloy showing banded α'. Polarized illumination. X150.

(c). The 6 a/o Re alloy showing coarse bands of α'. Polarized illumination. X150.

(d). The 7 a/o Re alloy showing acicular appearing α' and a pinned "γ" grain boundary. Polarized illumination. X100.

(e). The 8 a/o Re alloy showing acicular appearing α'. Polarized illumination. X150.

(f). The 10 a/o Re alloy having "diffuse γ^o" structure. Polarized illumination. X100.

(g). The 12 a/o Re alloy showing equi-axed γ^o. Polarized illumination. X150.

(h). The 14 a/o Re alloy showing equi-axed γ^o. Polarized illumination. X150.

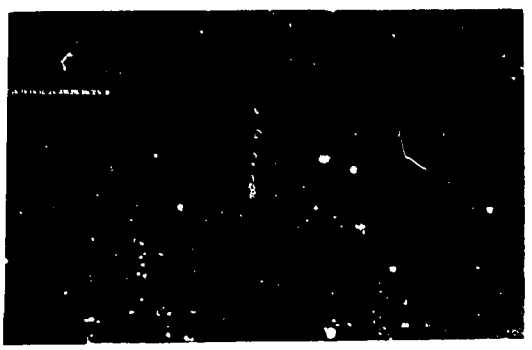

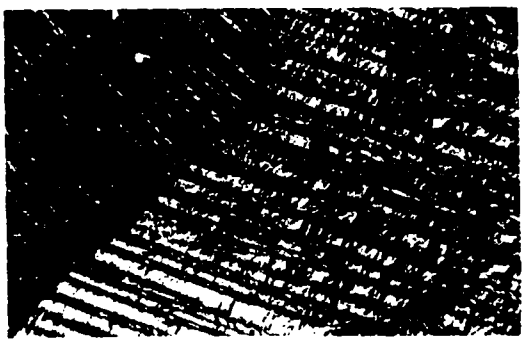

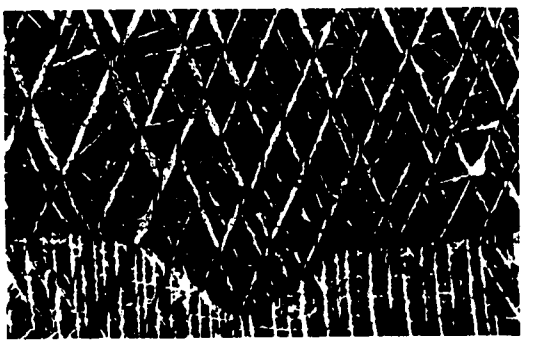

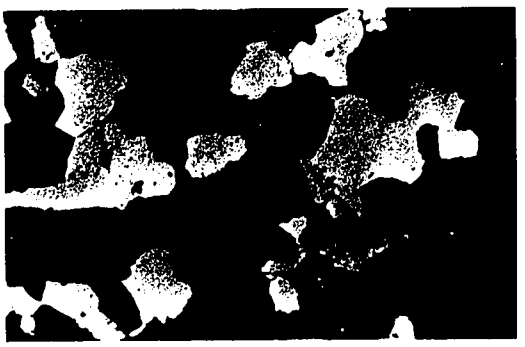

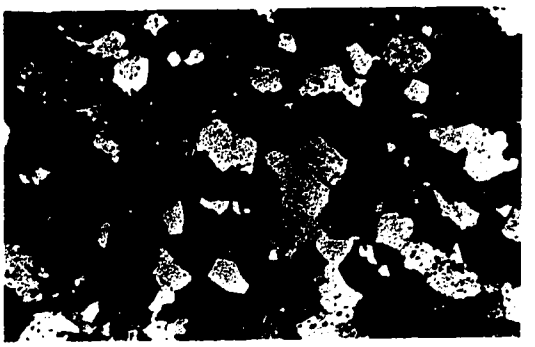

Figure 53. Representative microstructures of a series of alloys vacuum quenched after ½ hour at 975°C

(a). The 1 a/o Re alloy showing irregular and twinned α grains. Polarized illumination. X150.

(b). The 2 a/o Re alloy showing retained β microstructure. Polarized illumination. X150.

(c). The 3 a/o Re alloy showing retained β microstructure. Polarized illumination. X150.

(d). The 4 a/o Re alloy showing granular α' and a second phase (white material along grain boundary). Polarized illumination. X150.

(e). The 6 a/o Re alloy showing mixed granular and crosshatch appearing α" microstructure. Polarized illumination. X150.

(f). The 7 a/o Re alloy showing crosshatch α" microstructure. Polarized illumination. X150.

(g). The 8 a/o Re alloy showing crosshatch α" microstructure. Polarized illumination. X160.

(h). The 10 a/o Re alloy showing β° structure and discontinuous grain growth. Polarized illumination. X150.

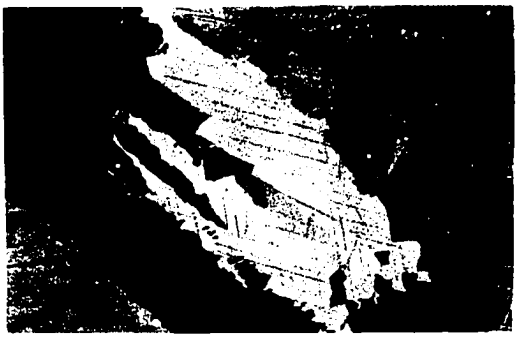
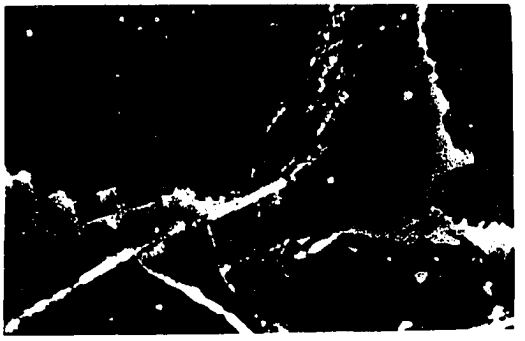

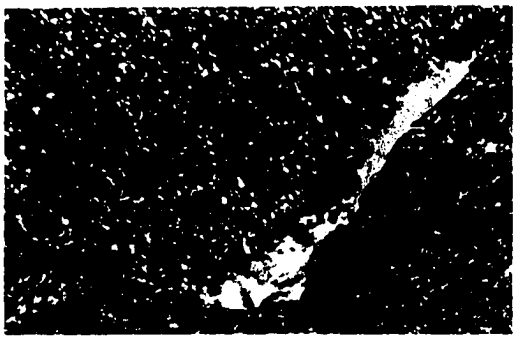
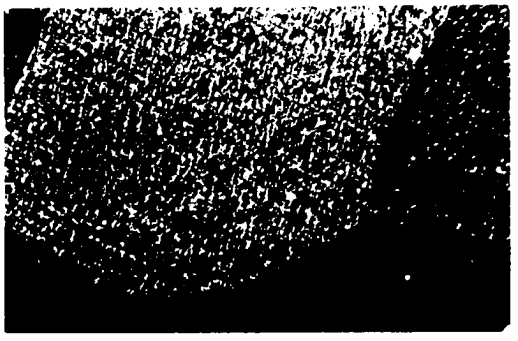
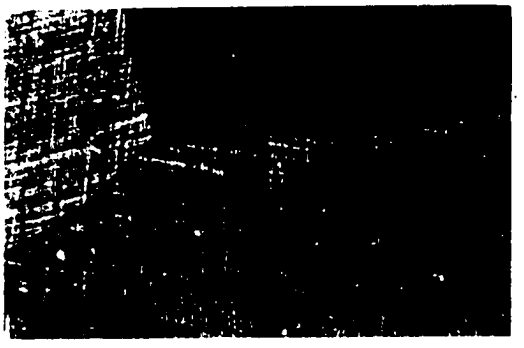
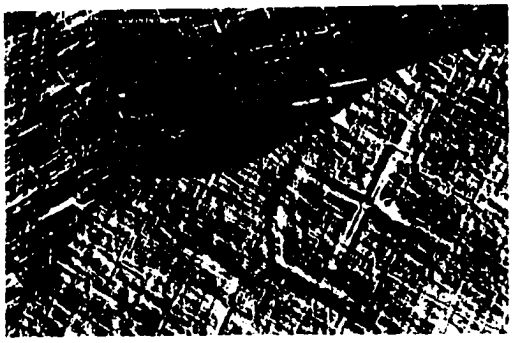


52b through 52e are representative of these microstructures.

For vacuum quenched alloys containing 4 to 8 a/o Re a similar direct $\gamma \rightarrow \alpha'(\alpha'')$ behavior was observed except for the 4 and 5 a/o alloys where a second phase was detectable. Vacuum quenching yielded microstructures which at low rhenium compositions were granular and which with increasing rhenium content developed a crosshatch structure. Representative microstructures of the vacuum quenched alloys are shown in Figures 51c through 51f and 53d through 53g.

The reason for the different appearing α' and α'' microstructures and their dependency on cooling rate and composition is not readily evident. An interpretation that explains the observed microstructures is as follows.

It was shown earlier that the ordered tetragonal γ_b° phase having a crosshatch microstructure formed low in the γ region and that this phase yielded a granular structure after transforming to α on aging. This behavior possibly explains the α' and α'' microstructures seen in the vacuum quenched alloys. Presumably, on vacuum quenching the cooling rate is slow enough that the alloys order to form γ_b° as an intermediate transition state. The characteristic crosshatch microstructure of the γ_b° phase is thus given to the resulting α' or α'' phase. The α' or α'' platelets would thus be too small to be resolved in the optical microscope due to the small size of the bands making up the γ_b° crosshatch

structure. The observed change from a crosshatch to a granular structure is due to the presence of a second phase which in the case of the 4 and 5 a/o alloys was detectable by normal x-ray techniques.

On water quenching from the γ region, there is not sufficient time for ordering and the γ°_{b} structure does not form. Also, the thermal gradient and quenching stresses developed on water quenching are more severe than during vacuum quenching. Hills et al. (59) and Butcher and Hatt (60) have shown that retained γ° alloys in the U-Mo system deform by twinning mechanisms which results in coarse-banded γ° microstructures. Thus, on water quenching, coarse twin bands may form followed by transformation to α' or α'' by the growth of lenticular plates. The size of the resulting α' or α'' platelets would be governed by the size of the twin bands, or if twinning was absent by the size of the parent γ grain. Thus in Figure 50d, the large bands would be twin bands and the smaller bands lenticular plates of α'. In Figure 50e, twinning of the γ phase was restricted resulting in the formation of large lenticular plates of α'' followed at a lower temperature by the necessarily smaller lenticular plates of α''. In Figures 52b and 52c, the coarse bands would be twin bands within which lenticular plates of α' form.

This scheme with some modification allows interpretation of all the observed α' and α'' microstructures. For example,

the microstructure of the 8 a/o Re alloy water quenched from 975°C shown in Figures 54 and 55 could be interpreted in the following manner. On cooling below the M_s temperature the large lenticular α'' plates (mainly at 45°) form a network in the supercooled γ matrix. The resulting transformation and quenching stresses cause the "boxed-off" γ to deform by twinning giving rise to the vertical bands (some horizontal). The vertical bands then transform to α'' and the resulting transformation stresses cause slip along the twinned surfaces. This results in deformation of the α'' plates (white) that were not part of the original α'' network. Figure 55 shows the fine structure of the vertical bands and a deformed α'' plate.

As the rhenium content increases, the M_s temperature falls below room temperature. Thus, for vacuum quenched alloys containing 9 a/o Re or more and for water quenched alloys containing 10 a/o Re or more the γ^o phase is stabilized at room temperature. Figures 50h, 51g, 51h, 52g, 52h and 53h show the characteristic equi-axed microstructure.

Representative microstructures of a series of alloys cooled at 25°C/hr after 4 days at 825°C are shown in Figure 56. The 1 a/o Re alloy (not shown) was characterized by twinned and very irregular α grains which would be expected from the double transformation ($\gamma \rightarrow \beta \rightarrow \alpha$). The 2 a/o alloy consisted of a matrix of β and α uranium and a discontinuous precipitate of δ. Figure 56a shows small equi-axed grains of

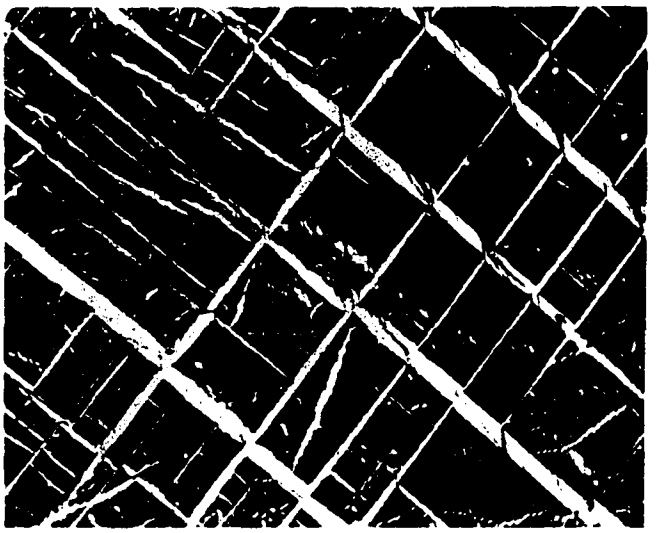

Figure 54. The 8 a/o Re alloy water quenched from 975°C showing coarse bands (white--mainly at 45°) and intermediate size vertical bands (some horizontal). Polarized illumination. X150.

Figure 55. Same alloy and orientation as in Figure 54, but showing the fine structure of the vertical bands and a deformed plate (white). Polarized illumination. X750.

Figure 56. Representative microstructures of the series of alloys cooled at 25°C/hr after 4 days at 825°C

(a). The 2 a/o Re alloy showing small "pseudo α" grains in β matrix. Polarized illumination. X150.

(b). The 3 a/o Re alloy showing discontinuous δ in unetched $\beta + \alpha$ matrix. Etchant: HNO_3, HAc. X925.

(c). The 4 a/o Re alloy showing nearly continuous δ precipitate (dark) in unetched $\alpha + \beta$ matrix (light). Electrolytic etch. X150.

(d). The 5 a/o Re alloy showing δ precipitate (dark) in α matrix (light). Etchant: HNO_3, HAc. X280.

(e). The 6 a/o Re alloy showing α (light) and δ (dark). Etchant: HNO_3, HAc. X280.

(f). The 7 a/o Re alloy showing acicular nature of α. Etchant: HNO_3, HAc. X200.

(g). The 8 a/o Re alloy showing decrease in acicular α. Polarized illumination. X150.

(h). The 9 a/o Re alloy showing irregular shaped regions of fine duplex $\alpha + \delta$ lamellar structure. Polarized illumination. X150.

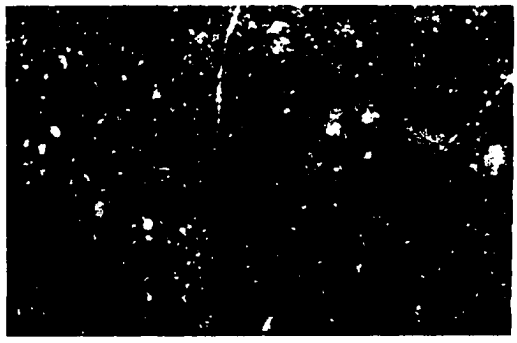

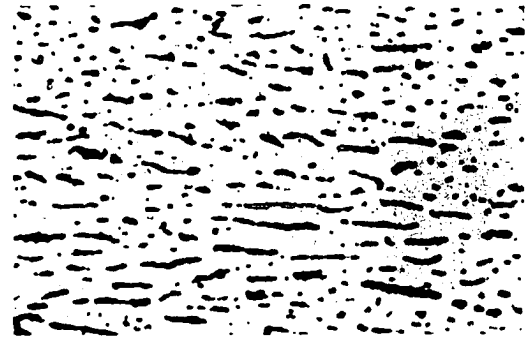

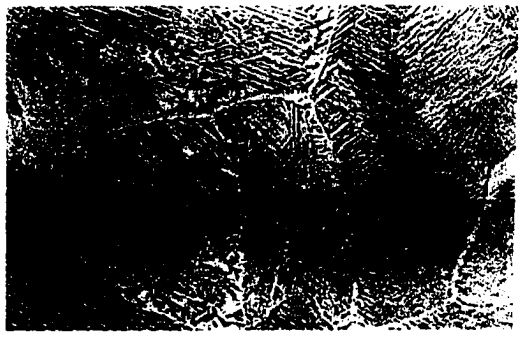

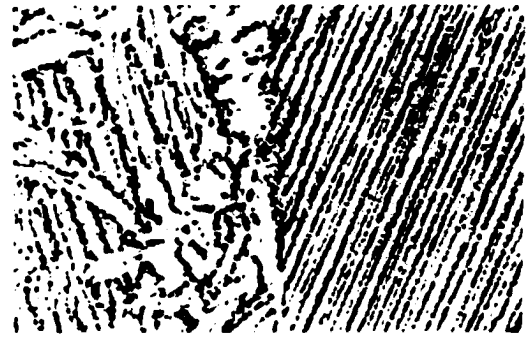

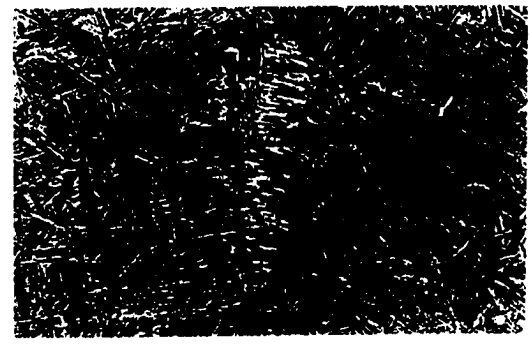

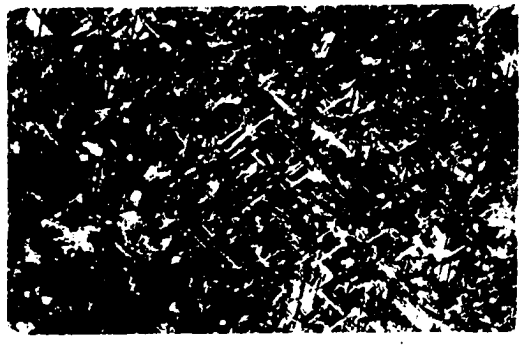

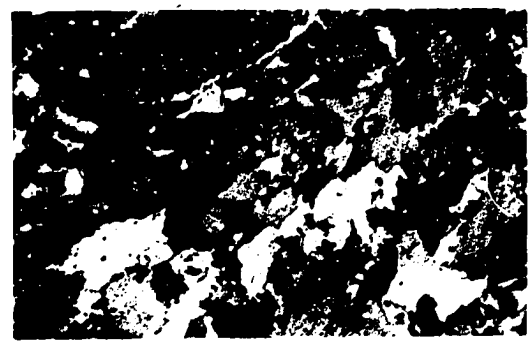

α in the coarse β matrix. This α structure is similar in appearance to a "psuedo α" structure reported by Hills et al. (61) for U-Mo alloys. They report that this phase forms in the high temperature α region and presumably consists of a duplex lamellar structure of $\alpha + \delta$ within the visible "psuedo α" grains. The discontinuous δ precipitate present in the 2 and 3 a/o alloy is illustrated in Figure 56b.

In the 4 and 5 a/o Re alloys the δ phase was present in the form of platelets (often parallel) which were nearly continuous as shown in Figure 56c and 56d. Figure 56c also shows a continuous β network outlining the prior γ grain boundaries. In the 4 a/o alloy, the matrix consisted mainly of β with some α present. Presumably the α-β boundaries are not visible due to the non-selectivity of the etchant. On cooling the hypoeutectoid alloys, uranium-rich β nucleates along γ grain boundaries. On further cooling, coring of the β phase results giving rise to concentration gradients within β. Precipitation of δ will occur at the rhenium-rich β interfaces. This retards lateral growth and gives rise to transverse growth of the β phase.

The regular decrease in the amount of retained β with increasing rhenium content is interesting. The 2 a/o alloy was heavily β, while only a small amount was present in the 5 a/o alloy. Possibly, the increasing amounts of δ promote formation of α from β by acting as nucleation sites.

Another possibility is that two reactions are competing for γ, i.e., the hypoeutectoid $\gamma \rightarrow \beta$ and the direct $\gamma \rightarrow \alpha$ reactions. The latter possibility seems the most plausible.

The 6 a/o Re alloy was free of retained β and its microstructure (Figure 56e) was more acicular in appearance than those of lesser rhenium contents. As the rhenium content increased further the acicular appearance lessened (Figures 56f and 56g) and was nearly absent in the 9 a/o alloy (Figure 56h). These were replaced by optically active irregularly shaped regions which appeared to consist of a duplex lamellar structure. An electron micrograph of this duplex lamellar structure of $\alpha + \delta$ present in the 10 a/o Re alloy is shown in Figure 57.

Relation to Other Systems

Metastable transition phases are found in a number of alloy systems in which the BCC structure is stable only at high temperature. The tendency towards metastable transition phase formation is most pronounced during the BCC→HCP transformation. This group is of particular interest in this investigation since the α-uranium structure is like hexagonal metals except that successive layers of atoms in the basal plane are skewed back and forth in the ⟨010⟩ direction (62). By comparing the α-uranium cell with the orthohexagonal cell for a HCP structure, one obtains b/a = 2.06 and c/a = 1.73

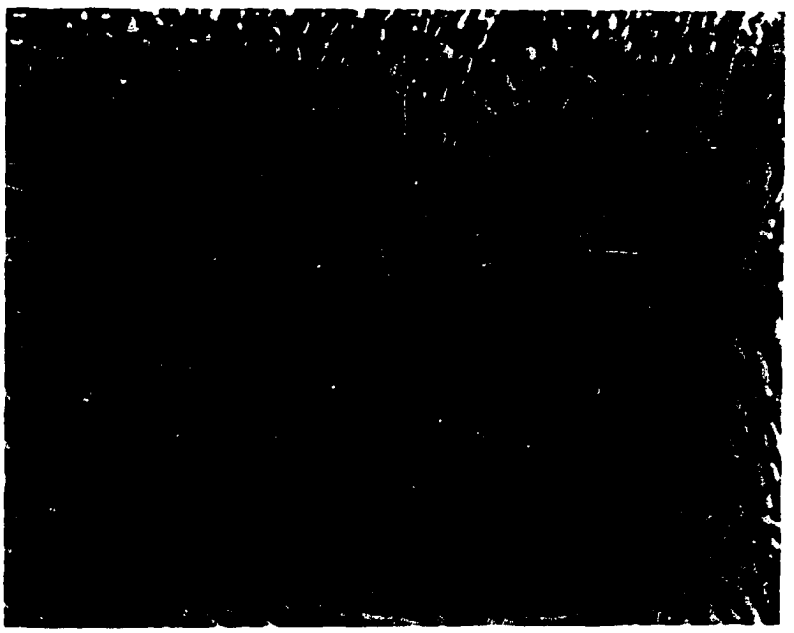

Figure 57. The 10 a/o Re alloy cooled at 25°C/hr after 4 days at 825°C showing duplex $\alpha + \delta$ lamellar structure. Etchant: HNO_3, HAc. Chromium shadowed carbon replica. X5600.

for α-uranium compared to b/a = 1.73 and c/a = 1.63 for a HCP structure. The addition of rhenium atoms to the α-uranium lattice has little effect on the c/a ratio while the b/a ratio decreases; thus, making α-uranium more "hexagonal like". It should also be pointed out that the shear mechanism proposed earlier for the U-Re system is merely an extension of Burgers' shear mechanism for the BCC→HCP transformation.

The nature of the metastable transition phases observed for the BCC→HCP transformation is shown in Table 21. At low solute concentration the transformation occurs β(BCC)→ α'(HCP) by Burgers' shear mechanism. The effect of increasing solute content is to stiffen the lattice making it more resistant to shear. This results in a transition phase further removed from the HCP structure. At medium solute concentrations a metastable transition phase forms via a mechanism that requires shorter atom movements. At higher solute concentrations the product may be diffuse ω (the x-ray reflections are diffuse; hence, the name diffuse ω) accompanied by a supersaturated β' or BCT β'' phase. The diffuse ω structure presumably arises from incomplete glide due to lattice stiffening resulting in a heavily faulted structure. At higher solute concentrations the β phase is stabilized and aging is required for the appearance of the metastable transition phases.

As mentioned earlier, metastable transition phases have

Table 21. Metastable transition phases and orientation relationships during the BCC→HCP transformation

Relative composition	Metastable phase	Orientation relationships
Low solute concentration	α'(HCP) (supersaturated α)	$\langle 0001\rangle_{HCP} \parallel \langle 110\rangle_{BCC}$ $\langle 11\bar{2}0\rangle_{HCP} \parallel \langle 111\rangle_{BCC}$
Medium solute concentration	ω(C32 hexagonal)	$\langle 0001\rangle_{hex} \parallel \langle 111\rangle_{BCC}$ $\langle 2110\rangle_{hex} \parallel \langle 101\rangle_{BCC}$
High solute concentration	diffuse ω(faulted ω structure) + β''(tetragonal c/a>1) or β'(solute rich)	$\langle 001\rangle_{BCT} \parallel \langle 001\rangle_{BCC}$ $\langle 100\rangle_{BCT} \parallel \langle 100\rangle_{BCC}$

Remarks: All found in Zr-Nb alloys (63).
α', ω, and diffuse ω in Zr-U alloys (52, 58).
α', ω found in Ti-V (64), Ti-Cr (65), Ti-Mn (66), Ti-Fe (66), Ti-Mo (66), Ti-Co (67) and Zr-Mo (68) alloys.
α' found in Ti-Cu (69) plus many other systems.

been observed in a number of uranium alloy systems. A summary of the formation conditions for these metastable transition phases and the orientation relationship when known is presented in Table 22.

Comparison of Tables 21 and 22 shows that the transition phases occurring during the BCC→HCP and BCC→α-uranium transformation are quite similar. Inspection of Table 22 alone shows that the behavior of the U-Re system is not unlike those of other highly γ-miscible uranium systems. The greatest similarity lies between U-Re and U-Mo alloys; the

Table 22. Metastable transition phases and orientation relationships during the BCC→orthorhombic (α-U) transformation

Relative composition	Metastable phase	Orientation relationships[a]
Very low solute concentration	α'(orthorhombic)	
Low solute concentration	β(tetragonal)	
Low solute concentration	α'_a(orthorhombic)	
Low solute concentration	α'_b(orthorhombic)	$\langle 100\rangle_\alpha \parallel \langle 1\bar{1}1\rangle_{BCC}$ $\langle 001\rangle_\alpha \parallel \langle \bar{1}01\rangle_{BCC}$
Medium solute concentration	α''_b(monoclinic)	Similar orientation to α'_b
High solute concentration	γ°_b(ordered tetragonal)	
High solute concentration	γ'(tetragonal c/a ≃ 1)	$\langle 001\rangle_{BCT} \parallel \langle 001\rangle_{BCC}$ $\langle 100\rangle_{BCT} \parallel \langle 100\rangle_{BCC}$

Remarks: All present in U-Mo system (53, 56).
All present in U-Re system (this investigation).
All except β in U-Nb system (70).
α', α'_a, α'_b, γ° in U-Ti system (33)
α', α'_b and possibly α''_b in U-Zr system (71).

[a]The orientation relations are those presented by Hatt and Roberts (52).

difference being the absence of the acicular α' microstructure at low rhenium contents. The sequence of phase changes for the two systems is in general the same. The U-Nb system is also quite similar except the β phase is not encountered.

Lattice parameters are available for the distorted α

structures in the U-Mo (53, 56), U-Nb (70) and U-Re systems. These lattice parameters along with the α'_b-α''_b and α''_b-γ° composition boundaries on water quenching are shown in Figure 58. If one compares the lattice parameters for the three systems, a correlation with size of the solute atom becomes obvious. As the solute size increased[1] the change in b parameter decreased as would be expected on the basis of substituting hard spheres for ellipsoidal uranium atoms.

Inspection of Figure 58 shows that the α'_b-α''_b composition boundary occurred at about b = 5.81 Å for all three systems. This finding indicates the monoclinic α'' phase corresponds to a given lattice distortion and that elements having a small atomic diameter favor the formation of the α''_b phase. Likewise, the α''_b-γ° composition boundary bears a similar relation for the three systems, i.e., at about b = 5.74 Å. This indicates that a given distortion is required to produce the double shear necessary for the generation of the γ° phase.

These size correlations are based on a limited number of observations, but do correlate most of the known data. They possibly could permit one to predict the extent of metastable phase regions on the basis of atomic size; the elements of small size decreasing the extent of the domains.

---

[1]The Goldschmidt metallic radii (CN = 12) for Re, Mo and Nb are 1.37, 1.40 and 1.47 Å, respectively (4). The Pauling metallic radii (CN = 12) for Re, Mo and Nb are 1.373, 1.386 and 1.456 Å, respectively (4).

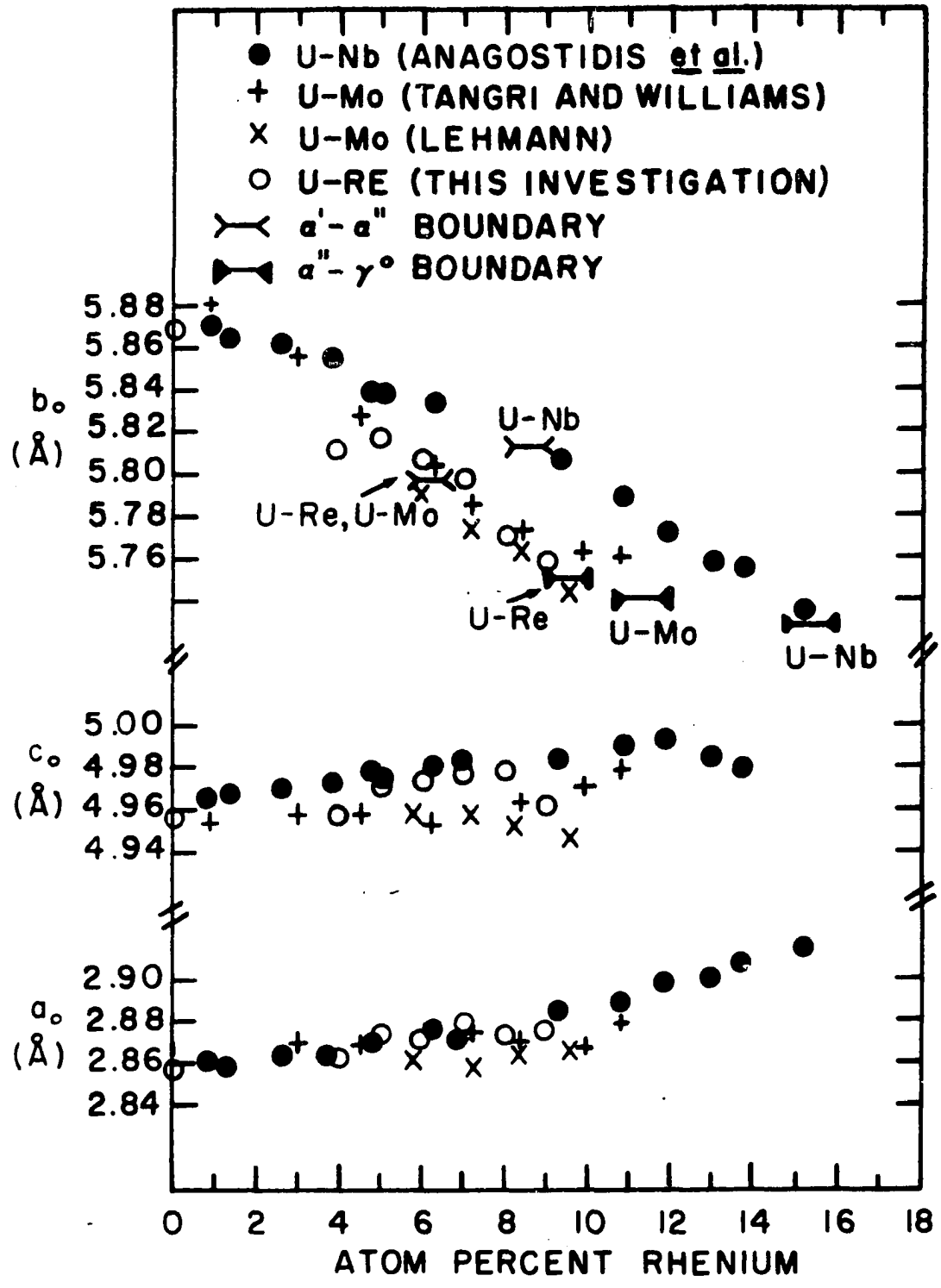

Figure 58. Variation of the α′ and α″ lattice parameters for the U-Mo, U-Nb and U-Re systems

SUMMARY

A study was made of the time-temperature-composition dependency of crystal structure and microstructure under non-equilibrium cooling conditions for uranium-rich alloys in the uranium-rhenium system.

Sluggish solid-state reactions of the stable phases led to nonequilibrium quantities of the equilibrium α, β, γ and δ phases. The principal causes for nonequilibrium quantities of stable phases were: (a) the slow rate of formation of the peritectoidally formed $\delta(U_2Re)$ phase; and (b) the ease with which the β and γ solid solutions were retained. The growth rate of the δ phase and the retention conditions for the β and γ phases were studied.

The $\beta \rightarrow \alpha$ transformation was found to proceed via an isothermal martensitic reaction or by a sluggish nucleation and growth process.

The γ phase under certain conditions was found to transform to α without passing through the intermediate β structure. Accompanying this transformation was a number of metastable transition states. Two transition states were modifications of the orthorhombic α-uranium structure. They were: (a) a supersaturated α structure showing a notable contraction of the b parameter with slight expansions along the a and c axes, and (b) a supersaturated α structure that had distorted to a monoclinic cell in addition to the

parameter changes noted above.

Two observed transition states were modifications of the normal BCC γ-uranium structure. They were: (a) a tetragonal ordered phase based on a block of 2 x 2 x 1 γ cells having a $c/a < 0.5$, and (b) a tetragonal disordered phase based on the same cell but with a $c/a \simeq 0.5$. The other observed transition state was an intermediate between the ordered tetragonal phase and the stable δ phase.

The compositional limits within which the stable and metastable phases form, and the effect of cooling rate and temperature on producing alternative structures were determined. From this was deduced the sequence of phase changes.

A crystallographic and microstructural model was developed to explain the observed crystal structures and microstructures and the effect of cooling rate and composition thereon.

Finally, the relation between metastability in uranium-rhenium alloys and other systems in which metastable states are observed was discussed.

BIBLIOGRAPHY

1. Holden, A. N. Physical metallurgy of uranium. Reading, Mass., Addison-Wesley Pub. Co., Inc. 1958.

2. Sims, C. T., Wyler, E. N., Gaines, G. B. and Rosenbaum, D. M. Survey of the literature of rhenium. U. S. Atomic Energy Commission Report WADC 56-319 [Wright Air Development Center, Dayton, Ohio]. 1956.

3. Klein, J. L. Uranium and its alloys. In Kaufmann, A. R., ed. Nuclear reactor fuel elements, metallurgy and fabrication. pp. 31-91. New York, N. Y., Interscience Pub., Inc. 1961.

4. Laves, F. Crystal structure and atomic size. In American Society for Metals. Theory of alloy phases. pp. 124-198. Cleveland, Ohio, Author. 1956.

5. Melaven, A. D. Rhenium. In Hampel, Clifford, ed. Rare metals handbook. 2nd ed. pp. 418-433. New York, N. Y., Reinhold Pub. Corp. 1961.

6. Klepfer, H. H. and Chiotti, P. Characteristics of the solid state transformations in uranium. U. S. Atomic Energy Commission Report ISC-893 [Ames Lab., Ames, Iowa]. 1957.

7. Sims, C., Craighead, C., and Jaffee, R. Physical and mechanical properties of rhenium. J. Metals 7: 168-179. 1955.

8. Chiswik, H. H. Advances in the physical metallurgy of uranium and its alloys. In Finniston, H. M. and Howe, J. P., eds. Progress in nuclear energy, series 5, metallurgy and fuels. Vol. 3. pp. 23-65. New York, N. Y., Pergamon Press, Ltd. 1961.

9. Wilkinson, W. D. Uranium metallurgy. Vol. 2. New York, N. Y., John Wiley and Sons, Inc. 1962.

10. Koch, L. J. Fast breeder power reactors. Nucleonics 16, No. 3: 68-73. 1958.

11. Nevitt, M. V. and Zegler, S. T. Transformation temperatures and structures in uranium-fissium alloys. J. Nuclear Materials 1: 6-12. 1959.

12. Kleinberg, J., Argersinger, W. J. and Griswold, E. Inorganic chemistry. Boston, Mass., D. C. Heath and Co. 1960.

13. Buzzard, R. W. Alloying theory. U. S. Atomic Energy Commission Report NBS-4032 [National Bureau of Standards, Washington, D. C.]. 1955.

14. Birchenall, C. E. Physical metallurgy. New York, N. Y., McGraw-Hill Book Co., Inc. 1959.

15. Rough, Frank A. and Bauer, Arthur A. Constitutional diagrams of uranium and thorium alloys. Reading, Mass., Addison-Wesley Pub. Co., Inc. 1958.

16. Darken, L. S. and Gurry, R. W. Physical chemistry of metals. New York, N. Y., McGraw-Hill Book Co., Inc. 1953.

17. Tucker, C. W. Crystal structure of metallic uranium. Trans. Am. Soc. Met. 42: 762-770. 1950.

18. Tucker, C. W. Crystal structure of the beta phase of uranium. Science 112: 448. 1951.

19. Pauling, L. Nature of the chemical bond. 2nd ed. Cornell University Press, Ithaca, N. Y. 1948.

20. Seybolt, A. U. [Title classified]. U. S. Atomic Energy Commission Report LA-68 [Los Alamos Scientific Lab., N. Mex.]. 1944.

21. Seybolt, A. U. [Title classified]. U. S. Atomic Energy Commission Report LA-96 [Los Alamos Scientific Lab., N. Mex.]. 1944.

22. Kulin, P. A., DeAvellar, J. and Jenkins, R. [Title classified]. U. S. Atomic Energy Commission Report AD-44620 [Armed Service Technical Information Agency, Dayton, Ohio]. 1954.

23. Hatt, B. A. Crystal structure of URe_2. Acta Cryst. 14: 119-123. 1961.

24. Jackson, R. J., Williams, D. E. and Larsen, W. L. Uranium-rhenium alloy system. J. Less-Common Metals 5: 443-461. 1963.

25. Hills, R. F., Butcher, B. R. and Heywood, J. A. Study of the effect of cooling rate on the decomposition of the gamma-phase alloys in uranium-low molybdenum alloys. J. Less-Common Metals 3: 155-169. 1961.

26. Kramer, D. and Rhodes, C. G. Precipitation of metastable alpha phase during the gamma to gamma prime transformation in uranium-16 wt pct molybdenum. Trans. Am. Inst. Mining Met. Engrs. 224: 1015-1020. 1962.

27. Harding, A. G. and Waldron, M. B. Transformations in uranium alloys with high solute solubility in the B.C.C. γ phase. Gt. Brit. Atomic Energy Research Establishment Report AERE M/R 2673 [Gt. Brit. Atomic Energy Research Establishment, Harwell, Berks, England]. 1958.

28. Thomas, D. E. and Lustman, B. Resume of uranium alloy data. U. S. Atomic Energy Commission Report WAPD-MM-413 [Westinghouse Atomic Power Div., Pittsburg, Penn.]. 1954.

29. Douglass, D. L. Structure and mechanical properties of uranium-titanium martensite. Trans. Am. Soc. Met. 53: 307-319. 1961.

30. Douglass, D. L., Marsh, L. L. and Manning, G. K. Transformation kinetics of zirconium-uranium alloys. Trans. Am. Soc. Met. 50: 305-322. 1958.

31. Hills, R. F., Harries, D. R., Hodkin, D. J. and Waldron, M. B. Transformation of metastable phases in the uranium-molybdenum alloy system. Gt. Brit. Atomic Energy Research Establishment Report AERE M/R 2840 [Gt. Brit. Atomic Energy Research Establishment, Harwell, Berks, England]. 1959.

32. Dwight, A. E. and Mueller, M. H. Constitution of the uranium-rich U-Nb and U-Nb-Zr systems. U. S. Atomic Energy Commission Report ANL-5581 [Argonne National Lab., Lemont, Ill.]. 1957.

33. Harding, A. G., Waldron, M. B. and Knight C. Transformations in uranium alloys with high solute solubility in the B.C.C. γ phase. Gt. Brit. Atomic Energy Research Establishment Report AERE M/R 2673A [Gt. Brit. Atomic Energy Research Establishment, Harwell, Berks, England]. 1958.

34. Geach, G. A. and Summers-Smith, D. Laboratory arc-furnace for melting alloys containing the refractory transition metals. Metallurgia 42: 153-156. 1950.

35. Williams, J. T. Vanadium-zirconium alloy system. Trans. Am. Inst. Mining Met. Engrs. 203: 345-350. 1955.

36. Carlson, A. J., Williams, J. T., Rogers, B. A. and Manthos, E. J. Etching metals by ionic bombardment. U. S. Atomic Energy Commission Report ISC-480 [Ames Lab., Ames, Iowa]. 1954.

37. Kehl, George L. Principles of metallographic laboratory practices. 3rd ed. New York, N. Y., McGraw-Hill Book Co., Inc. 1949.

38. Chiotti, P. Adaptation of a Geiger counter x-ray diffractometer for high temperature investigations. Rev. Sci. Instr. 25: 683-688. 1954.

39. Cullity, B. D. Elements of x-ray diffraction. Reading, Mass., Addison-Wesley Pub. Co., Inc. 1956.

40. Thewlis, J. X-ray powder study of beta uranium. Acta Cryst. 5: 790-794. 1952.

41. Mueller, M. H., Meyer, E. F. H. and Simonsen, S. H. Crystallographic d-space computer program. U. S. Atomic Energy Commission Report ANL-6519 [Argonne National Lab., Lemont, Ill.]. 1962.

42. American Society for Testing and Materials. Index to the powder diffraction file 1963. A.S.T.M. Special Technical Publication 48-M2. 1963.

43. Mueller, M. H. and Heaton, L. Determination of lattice parameters with the aid of a computer. U. S. Atomic Energy Commission Report ANL-6176 [Argonne National Lab., Lemont, Ill.]. 1961.

44. Hansen, David A. Structure of YNi. Unpublished M.S. thesis. Ames, Iowa, Library, Iowa State University of Science and Technology. 1964.

45. Halteman, E. K. Crystal structure of U_2Mo. Acta Cryst. 10: 166-169. 1957.

46. Holden, A. N. and Seymour, W. E. Intermediate phase in the uranium-zirconium system. J. Metals 8: 1312-1316. 1956.

47. White, D. W. Transformation kinetics in uranium-chromium alloys. Trans. Am. Inst. Mining Met. Engrs. 203: 1221-1224. 1955.

48. Holden, A. N. Isothermal transformation of metastable beta-uranium single crystals. Acta Met. 1: 617-619. 1953.

49. Tangri, K. Phases gamma metastables dans les alliages d'uranium contenant du molybdene. Memoires Scientifiques Rev. Metallurg. 58: 469-478. 1961.

50. Newkirk, J. E. General theory, mechanism and kinetics. In American Society for Metals. Precipitation from solid solution. pp. 6-149. Cleveland, Ohio, Author. 1959.

51. Foster, E. L. Study of the tensile fracture and microstructure of uranium. U. S. Atomic Energy Commission Report BMI-1664 [Battelle Memorial Institute, Columbus, Ohio]. 1964.

52. Hatt, B. A. and Roberts, J. A. Study of the omega phase in zirconium alloys. Gt. Brit. Atomic Energy Research Establishment Report AERE/X/PR 2558/9 [Gt. Brit. Atomic Energy Research Establishment, Harwell, Berks, England]. 1960.

53. Lehmann, J. Phases monocliniques dans les alliages uranium-molybdene. J. Nuclear Materials 4: 218-225. 1961.

54. Lehmann, J. and Hills, R. F. Proposed nomenclature for phases in uranium alloys. J. Nuclear Materials 2: 261-268. 1960.

55. Duwez, P. Effect of the rate of cooling on the allotropic transformation temperatures of uranium. J. Appl. Phys. 24: 152-156. 1953.

56. Tangri, K. and Williams, G. I. Metastable phases in the uranium-molybdenum system and their origin. J. Nuclear Materials 4: 226-233. 1961.

57. Gridnev, V. N., Trefilov, V. I. and Minakov, V. N. Martensitic transitions in the system titanium-zirconium. Soviet Physics Doklady 5: 1094-1096. 1961.

58. Hatt, B. A. and Roberts, J. A. Omega phase in zirconium base alloys. Acta Met. 8: 575-584. 1960.

59. Hills, R. F., Butcher, B. R. and Howlett, B. W. Mechanical properties of quenched uranium-molybdenum alloys. J. Nuclear Materials 11: 149-162. 1964.

60. Butcher, B. R. and Hatt, B. A. Mechanical properties of quenched uranium-molybdenum alloys. J. Nuclear Materials 11: 163-182. 1964.

61. Hills, R. F., Howlett, B. W. and Butcher, B. R. Further studies on the decomposition of the γ phase in uranium-low molybdenum alloys. J. Less-Common Metals 5: 369-373. 1963.

62. Jacob, C. W. and Warren, B. E. Crystalline structure of uranium. J. Am. Chem. Soc. 59: 2588-2591. 1937.

63. Stiegler, J. O., Houston, J. T. and Picklesimer, M. L. Transmission electron microscopy of omega phase in a Zr-15% Nb alloy. J. Nuclear Materials 11: 32-40. 1964.

64. Silcock, J. M., Davies, M. H. and Hardy, H. K. Structure of the ω precipitate in titanium-16% vanadium alloy. In Institute of Metals. Mechanism of phase transformation in metals. Institute of Metals Monograph and Report Series No. 18: 93-104. 1956.

65. Frost, P. D., Parris, W. M., Hirsch, L. L., Doig, J. R. and Schwartz, C. M. Isothermal transformations of titanium-chromium alloys. Trans. Am. Soc. Met. 46: 231-256. 1954.

66. Frost, P. D., Parris, W. M., Hirsch, L. L., Doig, J. R. and Schwartz, C. M. Isothermal transformation of titanium-manganese alloys. Trans. Am. Soc. Met. 46: 1056-1074. 1954.

67. Yakymyshyn, F. W., Purdy, G. R., Taggart, R. and Parr, J. G. Relationship between the constitution and mechanical properties of titanium-rich alloys of titanium and cobalt. Trans. Am. Soc. Met. 53: 283-294. 1961.

68. Domagala, R. F., Levinson, D. W. and McPherson, D. J. Transformation kinetics and mechanical properties of Zr-Mo alloys. Trans. Am. Inst. Mining Met. Engrs. 209: 1191-1196. 1957.

69. Gomez, M. P. and Polonis, D. H. Kinetics of decomposition of alpha prime in a titanium-copper alloy. Trans. Am. Soc. Met. 52: 201-220. 1960.

70. Anagnostidis, M., Colombie, M. and Monti, H. Phases metastables dans les alliages uranium-niobium. J. Nuclear Materials 11: 67-76. 1964.

71. Virot, A. Caracteristiques de l'alliage uranium-zirconium a 6% en poids de zirconium. J. Nuclear Materials 5: 109-119. 1962.

ACKNOWLEDGMENTS

The author wishes to express appreciation to Dr. W. L. Larsen for advice, counsel and helpful criticism during the course of the investigation. Acknowledgment is also made to Mr. D. M. Bailey and Mr. D. A. Hansen for aid in using the computer programs and to Mr. E. N. Hopkins and Mr. H. H. Baker for use of their photographic facilities and for doing the electron microscopy.